Transport and Proximity Effect in Unconventional Ferromagnet / Superconductor Heterostructures

Gaetano Annunziata

A Dissertation submitted to the

Dipartimento di Fisica "E. R. Caianiello"
Facoltà di Scienze Matematiche Fisiche e Naturali

in fulfillment of the requirements
for the Degree of

Philosophiæ Doctor in Physics

in the

Università degli Studi di Salerno

under the Supervision of

Prof. Canio Noce, Dr. Mario Cuoco

IX Ciclo II Serie (2007–2010)
Coordinator: Prof. G. Grella

Abstract

This dissertation collects results of my own work about heterostructures with unconventional ferromagnets and superconductors. It both introduces the matter by reviewing part of the existing literature and it includes original results. In particular charge and spin transport in ferromagnet/superconductor bilayer, Josephson effect in superconductor/ferromagnet/superconductor junctions, and proximity effect in ferromagnet/triplet superconductor stuctures are examined. All work has been supervised by Prof. Canio Noce and Dr. Cuoco from Dipartimento di Fisica "E. R. Caianiello", Università degli Studi di Salerno. I have also benefited from collaborations with Prof. Alfonso Romano and Dr. Paola Gentile from the same department. Part of the work has been supervised by Prof. Asle Sudbø and Prof. Jacob Linder from Department of Physics, Norwegian University of Science and Technology. I have also benefited from collaboration with Henrik Enoksen from the same department.

Contents

Part I

Preliminaries

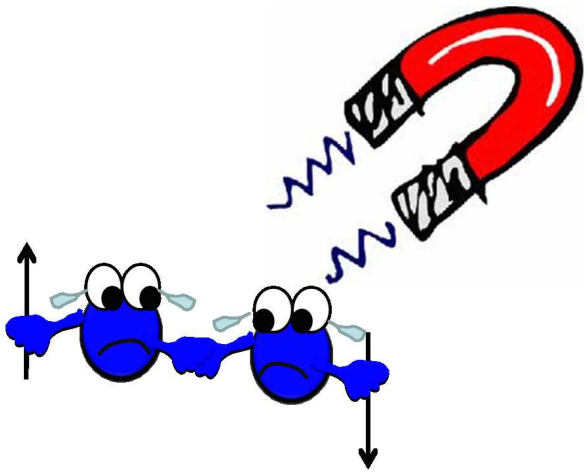

Introduction

Ferromagnetism and superconductivity are usually competing phenomena in solid state systems. In spatially homogeneous superconductors the application of an external magnetic, or the internal field associated with ferromagnetic order, are known to be detrimental to the stability of the superconducting phase. In most of the cases, orbital pair-breaking effects lead to the emergence of the Abrikosov vortex state, eventually making the system become fully normal as the upper critical field H_{c2} is exceeded. However, under very specific conditions a breaking-up of the translational invariance may allow the superconducting order to remain stable even in the presence of a polarizing field [1]. The most celebrated example of an inhomogeneous state where SU(2) and U(1) symmetries are simultaneously broken, can probably be considered the so-called Fulde-Ferrell-Larkin-Ovchinnikov (FFLO) state [2, 3, 4, 5]. In this state Cooper pairs acquire a finite center-of-mass momentum and, as a consequence, the superconducting order parameter and the magnetization both exhibit a modulation in space. A further peculiar feature of the FFLO state is that it tends to be stabilized by the mixing of even and odd parity pairings. Evidence for this behavior has been given by Shimahara [6] for a quasi-two-dimensional system where singlet pairing interactions coexist with relatively weak triplet ones. Moreover, an enhancement of the stability of the FFLO state due to the singlet-triplet mixing has also been demonstrated in recent studies on spin fluctuation-mediated superconductivity performed within the Hubbard model on a square lattice [7], as well as on two-leg ladders becoming superconducting away from half filling [8]. Little evidence, however, has so far been reported of the occurrence of the FFLO state in real systems. This is mostly due to the fact that the coupling of a magnetic field to the electron spin via Zeeman effect is required to break Cooper pairs more efficiently than orbital coupling does, a situation which is typically not encountered in most of the known type-II superconductors. Nonetheless, besides the case of systems such as $ErRh_4B_4$ [9], where aligned magnetic impurities generate a very strong internal exchange field, a spin paramagnetic effect dominating over the orbital one can in principle take place in quasi two-dimensional layered systems where an external magnetic field is applied parallel to the planes. In this case orbital effects can be small or even negligible due to the weakness of the interlayer coupling, and thus the Zeeman effect is expected to dominate. A further element hindering the formation of the FFLO state is that it is not robust against the presence of impurities and thus its occurrence requires very clean samples. Presently, these rather stringent conditions are likely to be satisfied in very few superconducting systems, essentially belonging to two classes of systems, the heavy-fermion compounds [10] and the organic superconductors [11]. Within the former, evidence of the FFLO state has been

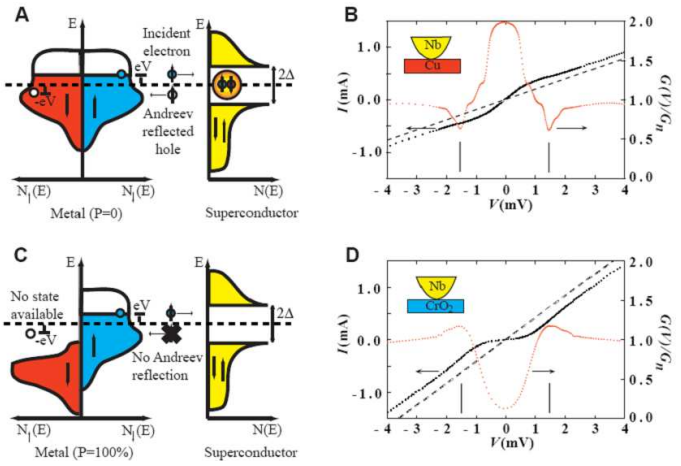

Figure 1. Supercurrent conversion at the superconductor/metal interface. (A) Schematic of the process for an unpolarized metal when the Andreev reflection is unhindered by a spin minority population at E_F. The solid circles denote electrons and open circles denote holes. (B) Experimental measurement of the $I-V$ and differential conductance dI/dV at $T = 1.6K$ via a superconducting Nb point contact on Cu. The vertical lines denote the bulk gap of Nb. (C) Schematic of process for a fully polarized metal when there is no supercurrent conversion at the interface. (D) Experimental $I-V$ and dI/dV at $T = 1.6K$ via the Nb point contact on CrO2. Taken from [16].

found in several measurements performed on the compound $CeCoIn_5$ [12], while in the latter a clearcut signature has been provided by specific heat measurements on κ-$(BEDT\text{-}TTF)_2Cu(NCS)_2$ [13] (though it is also conjectured that the FFLO state is realized in the quasi one-dimensional Bechgaard salts $(TMTSF)_2X$ with $X = PF_6$ [14] and ClO_4 [15]).

Even if coexistence of ferromagnetism and superconductivity is still an open issue, their interplay in heterostructures is a well established sub–field. Indeed their interplay in hybrid systems has been the foundation for developments of several novel experimental techniques over the last decade or so [16, 17, 139] and, besides the interest from a fundamental physics viewpoint, such systems hold potential in terms of electronics and spintronics applications [19]. Versatility of such systems stems from the fact that Andreev reflection [20, 21], the peculiar process taking place at the superconductor/non–superconductor interfaces converting quasiparticles into Cooper pairs, is strongly sensitive to spin polarization [134, 171] and consequently it is modified if non–superconducting layers is a ferromagnet rather than a normal metal. Andreev reflection process is the main responsible of all unconventional phenomena in hybrid structures involving superconductors. Charge transport, spin transport, proximity effect, Josephson effect, all can be understood in terms of Andreev reflections. In its simplest realization, this process can be explained as follows. An electron in the normal metal excited from the Fermi level, e.g. by an applied voltage, which is trying to entering the superconductor can undergo several scattering processes depending on its energy. It can be transmitted in the superconductor only if its energy is larger than the gap because accessible single particle states exist only above this threshold (typical density of states for a normal

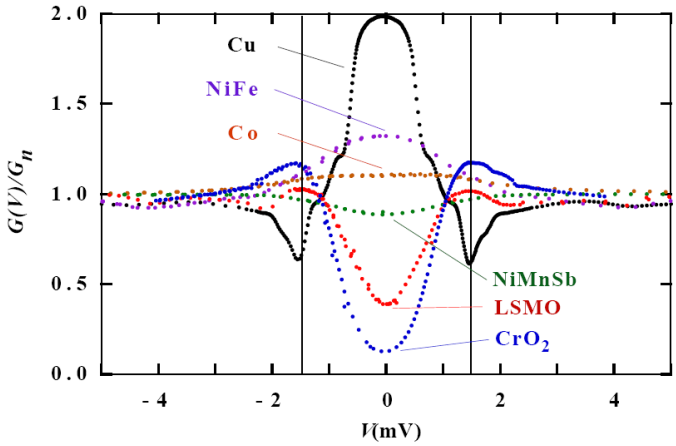

Figure 2. The differential conductance for several spin polarized metals showing the suppression of Andreev reflection with increasing polarization. Taken from [16].

metal and a superconductor are compared in panel A of Fig. 1). If its energy is smaller than the gap instead the electron cannot propagate in the superconductor as a single particle but only as a Cooper pair. In order to do so it pairs with another electron in the normal metal leaving beside an hole and the two electrons enter the superconductor as pair. Considering a singlet conventional superconductor, it is important to notice that the electron to which the incident one pairs with, must have opposite spin in order to form a singlet pair. The Andreev reflection process in which a superconductor reflects electrons as holes allows quasiparticle to supercurrent conversion. Thus in a normal metal/superconductor bilayer it is found that the low energy conductance is doubled with respect to same structure in which the two leads are both non superconducting (panel B of Fig. 1). This is because when Andreev reflection takes place for every injected unit of charge a Cooper pair, build up by two elementary charges, is obtained. When a ferromagnet/superconductor bilayer is considered this picture is modified. To understand why this is the case consider the extreme case of half metals, e.g. CrO_2 (ssee panel C of Fig. 1). In this case only one spin species exist at the Fermi level and Andreev reflections cannot take place simply because electrons cannot find an oppositely polarized partner to form a Cooper pair. As a result low energy conductance of half metal/superconductor structures is very low (see panel D of Fig. 1). From this extreme situation one can deduce that when there is spin polarization in a metal (that is the number of up and down electrons at the Fermi level is different) not all electrons can be Andreev reflected: the larger the spin polarization, the lower the probability for electrons to find an oppositely spin polarized partner to form a Cooper pair, the lower the conductance of the ferromagnet/superconductor structure. Fig. 2 shows how ferromagnets with increasing spin polarization (from top to bottom) lead to decreasing low energy conductance for the bilayer. This effects, together with their generalizations to unconventional superconductors and/or different geometries and setups, promise to be fundamental for future device applications in electronics, spintronics, information and communication technologies, and quantum computation (two examples are shown in Fig. 3). Their usefulness

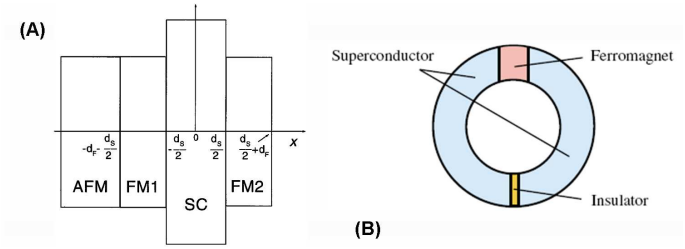

Figure 3. Two possible device applications involving F/S. (A) A superconducting spin valve. Taken from [25]. (B) A Josephson qubit. Taken from [72].

have been exploited in several experimental techniques like Point Contact Andreev Reflection Spectroscopy and Scanning Tunneling Microscopy. Besides an estimation of the degree of spin polarization in the ferromagnet [24], they can give insight about the amplitude and phase of superconducting order parameter, being Andreev reflection phase sensitive. This property has made this kind of measurements fundamental in finding clues about the symmetry of the new families of superconductors discovered, for which there is a general consensus that they cannot be considered as conventional. Over the last few decades, a remarkable set of unconventional superconductors has been found, including p-wave spin-triplet pairing in heavy fermions and He^3, d-wave spin-singlet pairing in superconducting high-temperature cuprates, and unusual forms of s-wave pairing in the recently discovered iron-pnictides, to mention a subset [27, 28, 29, 30, 31, 33, 34]. Pairing phenomena related to some of these have also been discussed in the context of particle physics and high-energy physics, such as pseudogap phases in the Nambu-Jona Lasinio model [35]. In all of the above cases, a major challenge is to determine the symmetry of the superconducting order parameter. This is generally believed to be the issue to address when searching for a fundamental understanding of these phenomena. To acquire information about the order parameter, it is often useful to study how the superconducting correlations behave in hybrid structures considering transport and proximity effect in order to look for unique signatures of the superconducting order parameter. When the non-superconducting material is not a simple normal metal featuring intrinsic properties, such as magnetism, then the heterostructure provide an arena for studying the interplay between superconductivity and different types of electronic ordering [36] which can give a deeper insight in underlying physics. For example, one of the strongest evidences supporting d-wave symmetry for high-T_c cuprates is the zero bias conductance peak (ZBCP) revealed in ab-plane tunneling conductance from normal metals [38]. In some cuprates, such as for instance $YBa_2Cu_3O_{7-\delta}$ [39, 40], the existence of a subdominant component in the order parameter possibly breaking time-reversal symmetry is still a matter of debate and, in this respect, exploiting the interplay between magnetism and superconductivity in tunneling experiments is one of the standard routes to investigate this issue. Generally, by using a ferromagnetic electrode in tunneling experiments it is possible to change the relative contributions of up and down electrons to the total density of states or, in the half-metal limit, to isolate a single spin channel. To interpret the large amount of tunneling experiments performed on ferromagnet/unconventional superconductor junctions [41, 42, 43, 44, 45, 46, 47, 48], fundamental theories of

transport, such as in particular the one by Blonder, Tinkham, and Klapwijk [141], have been suitably extended to take into account all possible symmetries of the superconducting order parameter. In this context, the ferromagnetic electrode has been predominantly described within the Stoner model, relying on the assumption that the bands associated with the two possible electron spin orientations have identical dispersion, but are rigidly shifted in energy by the exchange interaction. However, Stoner model may prove to be insufficient to describe real ferromagnets because many terms deriving from Coulomb repulsion are eliminated from the full Hamiltonian, although in some situations their contribution can be important [50, 51]. Indeed the complexity of ferromagnetism in metals is testified by the wide range of manifestations it exhibits in nature. As relevant examples of this variety, we mention the ferromagnetic transition metals Fe, Co, and Ni and their alloys [52], weak metallic ferromagnets such as $ZrZn_2$ [53, 54] and Sc_3In [55, 56], colossal magnetoresistance manganites such as $La_{1-x}Sr_xMnO_3$ [57], and rare earth hexaborides such as EuB_6 [58, 59]. Therefore, when theoretically modelling ferromagnet/superconductor hybrid structures, it may be important to assume for the magnetism microscopic scenarios other than the Stoner one. Among them, of peculiar interest is a form of itinerant ferromagnetism driven by a gain in kinetic energy deriving from a spin dependent bandwidth renormalization, or, equivalently, by an effective mass splitting between up- and down-spin carriers [60, 61, 62, 63, 64, 65]. The interplay of superconductivity with this kinetically driven ferromagnetism has been recently shown to originate different features compared to the Stoner case, concerning the phenomena of coexistence and proximity. More precisely, the occurrence of the coexistence of ferromagnetism and s-wave singlet superconductivity within a model where the magnetic moments are due to a kinetic exchange mechanism, has been studied and it has been shown that the depaired electrons play a crucial role in the energy balance, and that when their dynamical effect is such that to undress the effective mass of the carriers which participate in the pairing, a coexisting ferromagnet-superconducting phase can be stabilized [66]. Also an extended version of the reduced BCS model for particles that get paired in the presence of a polarization arising from spin dependent bandwidths has been solved and the ground-state phase diagram in the full parameter space of the pair coupling and the bandwidth asymmetry as a function of filling for different types of spectrum topologies has been calculated [67]. The two above-mentioned mechanisms for ferromagnetism have been shown to lead to different features of proximity effect in ferromagnet/superconductor bilayers as concerns the formation at the interface of dominant and sub-dominant superconducting components as well as their propagation in in the ferromagnetic side [68]. Part of this Dissertation is devoted to the analysis of the bandwidth asymmetry ferromagnetism effect in charge transport and spin transport in bilayers as well as its influence in Josephson effect in superconductor/ferromagnet/superconductor junctions. These are systems capable of sustaining a supercurrent carried by Cooper pairs in the superconducting leads and by quasiparticles in the ferromagnetic mid-layer. The unique interplay between ferromagnetic and superconducting orders provides quasiparticles with extra phase shifts absent in junctions with a non-magnetic mid-layer. This can give rise to the appearance of the so-called "$\pi-$phase" [69]. Under such circumstances, the energy minimum of the junction is reached at a phase difference of π across the junction, unlike the standard "$0-$phase" in junctions with a non-magnetic mid-layer. The

existence of the $\pi-$phase has been experimentally confirmed [70, 71] and promise to be important for applications. Indeed π-junctions are considered to be one of the best candidates for realizing solid state qubits [72].

We postpone to appropriate sections more detailed descriptions of ferromagnetism and superconductivity and their unconventional manifestations hoping that this discussion has been convincing about the richness of the physics resulting from the interplay between the two orders. We conclude wishing that results described in the following may provide a useful contribution to the comprehension of some relevant phenomena in these hybrid structures. We believe that this rapidly growing field can become a playground for a wealth of interesting quantum mechanical effects pertaining to the interplay between spin and charge degrees of freedom, given the increasing number of investigations and continuous refinements of experimental techniques allowing physicists to deal with new intriguing systems.

Outline

This Dissertation is organized as follows. In Part I itinerant ferromagnetism, superconductivity, and their interplay in heterostructures are introduced together with materials and theoretical models. Part II is devoted to the analysis of charge and spin transport in ballistic ferromagnet/superconductor bilayers. In Part III Josephson effect in ballistic superconductor/ferromagnet/superconductor junctions is analyzed. In Part IV proximity effect in heterostructures involving triplet superconductors and diffusive normal metals and ferromagnets is examined. Part V is devoted to conclusions, summary and discussion of the results, and analysis of future works. The last section at the end of the thesis is a List of Symbols and Acronyms. The reader which might feel confused with the notation is invited to consult it skipping to the last page of the thesis.

CHAPTER 1

Materials, frameworks, and models

This chapter introduces types of ferromagnets and superconductors which are analyzed in the Dissertation. We focus on materials and models for both type of orders and comment about role and description of interfaces in hybrid structures.

1.1. Superconductors and their symmetries

Superconductivity may be defined as conventional or unconventional depending on the properties of the pairing state and whether or not multiple broken symmetries are present in the system. In conventional superconductors, the pairing state belongs to the trivial representation of the point-group and the system ground state breaks the U(1) gauge symmetry. On the other hand, unconventional superconductors display pairing symmetries belonging to higher-dimensional representations of the point group and may also exhibit multiple broken symmetries in the ground state. Since 1970 at least 10 distinct families of superconductors (Ss) which could hardly be framed in the conventional scenario of electron-phonon BCS theory have been discovered [73], namely: (1) High-T_c cuprates, hole-doped (Y $Ba_2Cu_3O_7$) and electron-doped ($Nd_{1-x}Ce0_xCuO_{4-y}$); (2) Heavy fermions ($CeCu_2Si_2$, UBe_13, UPt_3); (3) Organics ($TMTSF_2PF_6$); (4) Strontium-ruthenate (Sr_2RuO_4); (5) Fullerenes (K_3C_60, Cs_3C_60); (6) Borocarbides ($LuNi_2B_2C$, YPd_2B_2C); (7) Bismuthates ($Ba_{1-x}K_xBiO_3$,$BaPb_{1-x}Bi_xO_3$); (8) Almost heavy fermions (U_6Fe, URu_2Si_2, UPd_2Al_3); (9) Iron arsenide compounds ($LaFeAsO_{1-x}F_x$, $La_{1-x}Sr_xFeAs$); (10) Ferromagnetic superconductors (UGe_2, $URhGe_2$). In all of the above cases, a major challenge is to determine the symmetry of the superconducting order parameter. This is generally believed to be *the* issue to address when searching for a fundamental understanding of these phenomena. Only for few of them there is a general consensus on the effectively realized form of superconductivity, e.g. the orbital and spin symmetries of the order parameter. The specification of mechanisms driving the superconducting states is even more puzzling. We do not deepen these points here but rather we describe only some particular forms of order parameters which will be analyzed in the following (see Fig. 1.1).

Cooper pairs can be in spin singlet ($S = 0$) or spin triplet ($S = 1$) states. To respect the overall antisymmetry under exchange of particles, they have to be associated with even ($L = 0, 2, \dots$) and odd ($L = 1, 3, \dots$) orbital states, respectively [1]. Conventional superconductors are in a singlet states characterized by an orbital gap function $\Delta(\mathbf{k})$, with $\mathbf{k}$ a unit vector on the fermi surface, with constant

[1] This is not true when time (energy) dependence is considered. In that case the overall antisymmetry can be obtained with equal parity of spin and orbital parts considering odd parity in the frequency part.

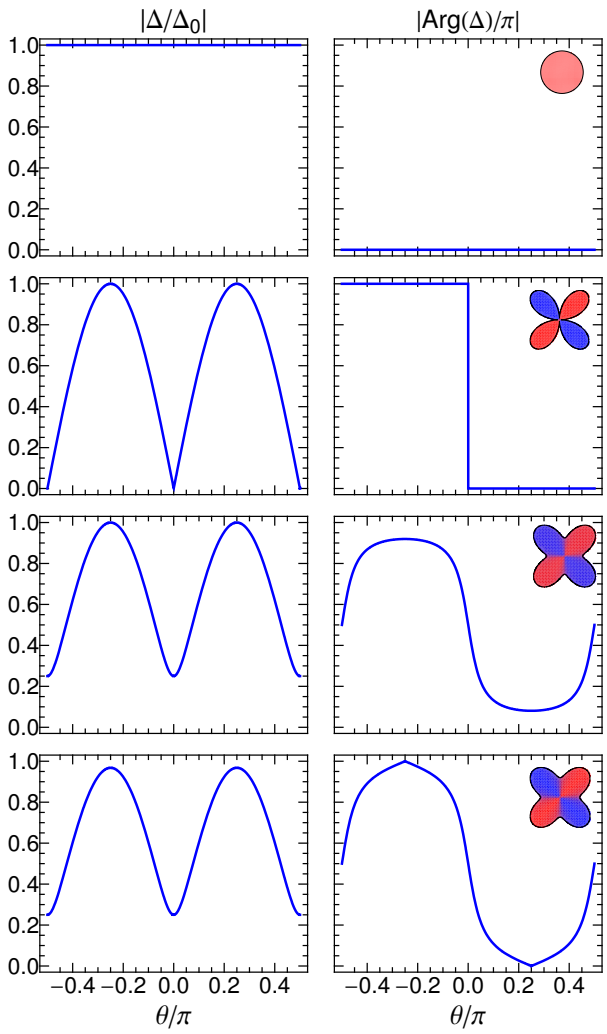

Figure 1.1. Modulus (left panels) and phase (right panels) of pair potential in several spin singlet superconductors: $s-$, $d_{x^2-y^2}+is-$, $d_{x^2-y^2}+is-$, $d_{x^2-y^2}+id_{xy}-$wave from top to bottom.

phase. Its magnitude can have directional dependence or be constant. In the latter case (s-wave) simply $\Delta^s(\mathbf{k}) = \Delta_0$. High-$T_c$ cuprates are singlet superconductors with line nodes and sign change in the orbital gap function $\Delta^d(\mathbf{k}) = \Delta_0(k_x^2 - k_y^2)$. This state ($d_{x^2-y^2}$-wave) is clearly distinguishable from the conventional case. Indeed line nodes existence can be catched by several thermodynamical properties, e.g. discontinuity of specific heat at superconducting transition, behavior of low temperature specific heat, London penetration depth, nuclear magnetic resonance. It is generally accepted that for many unconventional superconductors a subdominant component of the order parameter breaking time-reversal symmetry can be induced whenever translational symmetry is broken, e.g. near surfaces, interfaces

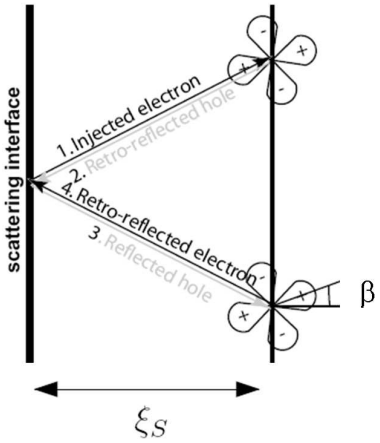

Figure 1.2. Depiction of coherent process giving rise to Andreev bound states.

and vortices [74, 75, 148]. For some materials, such as e.g. YBCO [40], there is controversy about the symmetry of the secondary component, namely if the order parameter is of the $d_{x^2-y^2} + is$- or $d_{x^2-y^2} + id_{xy}$-wave type. The subdominant components have the effect of removing the line nodes rendering the two possibilities hardly distinguishable through the same measurements which succeeding in discerning $d_{x^2-y^2}$-wave from s-wave.

The possibility of sign change in unconventional superconductors gap functions has deep implications in transport properties of hybrid structures. Consider the $d_{x^2-y^2}$-wave case. The sign change implies that electron-like and hole-like quasiparticles specularly reflected at the interface always find the "right" sign of the pair potential to be Andreev reflected (see Fig. 1.2). This resonant process opens mid gap surface states known as Andreev bound states [20, 77, 78] manifested as zero energy peak in the *ab*-plane tunneling conductance. If line nodes are perpendicular (parallel) to the interface all (none of the) trajectories contribute to the formation of the resonant state. The two broken time reversal states affect differently the sign change of pure d-wave: when the subdominant component is s-wave the sign change is eliminated while in the d_{xy}-wave the sign change is still there precisely along directions of maximum magnitude of superconducting gap. This point will be deepened in what follows aiming to discerning the two breaking time reversal states from transport properties. Transport properties and Josephson effect of hybrid structures with conventional and unconventional singlet superconductors will be analyzed in Part II and Part III.

Evidences for spin triplet unconventional superconductivity exist in some materials. Indeed, apart from the well-known case of superfluid ^{3}He, where the condensate is made of atomic pairs, strong evidences, mainly originating from Knight shift measurements, exists in favor of triplet superconductivity in the ferromagnetic compound $ZrZn_2$ [79], in the organic system $(TMTSF)_2PF_6$ [80], and in several heavy-fermion compounds which can be non-magnetic (UPt_3 [81, 82]), antiferromagnetic (UNi_2Al_3 [83, 82]), or ferromagnetic (UGe_2, [84] URhGe [85]). A further fundamental example of spin-triplet superconductor with a chiral p-wave order parameter

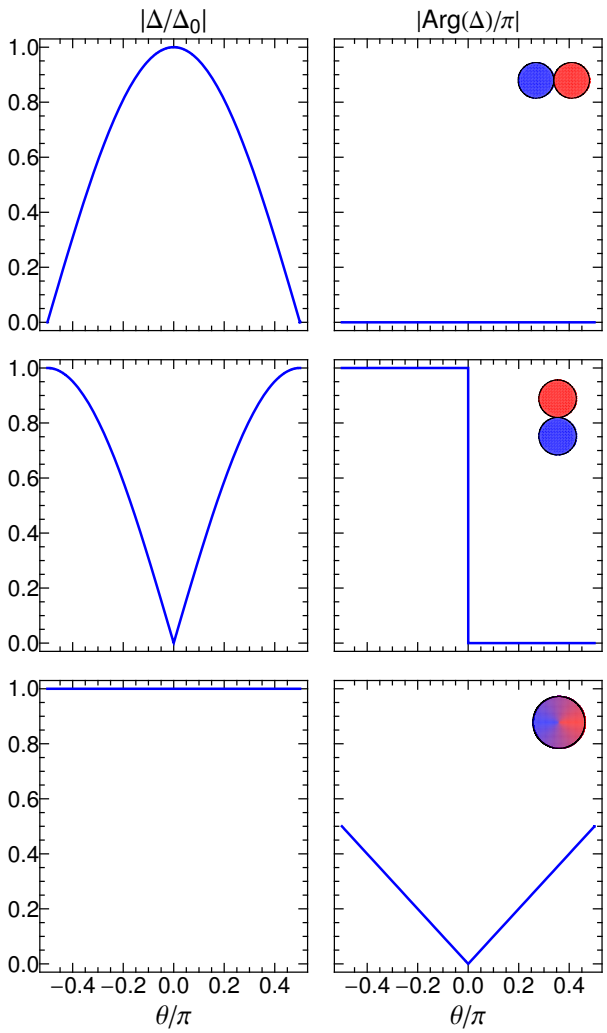

Figure 1.3. Modulus (left panels) and phase (right panels) of pair potential in several spin triplet superconductors: p_x-, p_y, chiral $p_x + ip_y-$wave, from top to bottom.

(See Fig. 1.3) is the layered perovskitic system Sr_2RuO_4 [86], which for its specific properties has probably offered in the last years the best opportunity to study the relevant features of spin triplet pairing. It is also worth mentioning that a peculiar modification of the superconducting behavior of this compound has been detected in two types of eutectic solidifications which contain it, i.e. Sr_2RuO_4/Ru and $Sr_3Ru_2O_7/Sr_2RuO_4$. In the case of Sr_2RuO_4/Ru, where the critical temperature is enhanced from $T_c = 1.5\,K$ of pure Sr_2RuO_4 to $T_c = 3\,K$ [87], lamellar microdomains of metallic ruthenium are embedded in the perovskitic oxide in such a way that a non-chiral spin triplet component may occur at the interface, or a spin-singlet pairing from the metallic ruthenium is mixed with the spin-triplet one of Sr_2RuO_4 [88]. On the other hand, for $Sr_3Ru_2O_7/Sr_2RuO_4$ an anomalous proximity effect as well

as multiple superconducting transitions have recently been observed [89, 90]. The behavior of both kinds of eutectic system underlines the subtle competition between spin-triplet pairing and translational and orbital symmetry breaking. The rich phenomenology of the classes of systems mentioned above is intimately related to the complex evolution of the superconducting state when extra symmetries other than the U(1) gauge invariance are spontaneously or explicitly broken. Indeed, time reversal symmetry breaking can lead to inhomogeneous superconducting states, and the removal of the crystal inversion symmetry opens the possibility of mixed parity pairings in which singlet and triplet correlations coexist. The interest in superconductors with parity mixing has rapidly increased in the last years also because of the discovery of superconductivity in several non-centrosymmetric heavy-fermion compounds. Its first observation in $CePt_3Si$ [91] at ambient pressure, and in $CeRhSi_3$ [93] and $CeIrSi_3$ [94] under pressure, has stimulated many experimental [95, 99, 100, 101, 102] and theoretical [103] studies motivated by the fact that this class of systems gives a unique opportunity of probing the effect of parity violation, which is otherwise hard to achieve by imposing specific external conditions to standard centrosymmetric compounds. When crystal structure lacks an inversion center, the corresponding asymmetry in the electric potential gives rise to an antisymmetric Rashba-type spin-orbit coupling. The minimal Hamiltonian to describe these systems is

$$H = H_{\rm N} + H_{\rm SC}, \tag{1.1}$$

where the normal-part Hamiltonian reads

$$H_{\rm N} = \sum_{\mathbf{k}\sigma} \varepsilon_{\mathbf{k}} c^{\dagger}_{\mathbf{k}\sigma} c_{\mathbf{k}\sigma} + \lambda \sum_{\mathbf{k}\alpha\beta} c^{\dagger}_{\mathbf{k}\alpha} (\hat{\mathbf{n}} \times \mathbf{k})_{\alpha\beta} c_{\mathbf{k}\beta}. \tag{1.2}$$

The antisymmetric Rashba spin-orbit coupling is

$$\mathbf{g}_{\mathbf{k}} = \lambda(\hat{\mathbf{n}} \times \mathbf{k}), \tag{1.3}$$

where λ denotes the strength of the spin-orbit interaction and $\hat{\mathbf{n}}$ denotes the axis of broken inversion symmetry. More specifically, the crystallographic structure of the material does not have a mirror plane with $\hat{\mathbf{n}}$ as normal vector. Above, $c_{\mathbf{k}\alpha}$ are fermion operators satisfying the equal-time anticommutation relation $\{c^{\dagger}_{\mathbf{k}\alpha}, c_{\mathbf{k}'\beta}\} = \delta_{\mathbf{k},\mathbf{k}'}\delta_{\alpha\beta}$ and all other anticommutators vanish. Moreover, the kinetic energy $\varepsilon_{\mathbf{k}} = \xi_{\mathbf{k}} - \mu$ is measured with respect to Fermi level μ. The long-lived excitations in the Fermi liquid picture are helicity eigenstates obtained by diagonalizing Eq. 1.2 as

$$H_{\rm N} = \sum_{\mathbf{k}\sigma} \mathscr{E}_{\mathbf{k}\sigma} \gamma^{\dagger}_{\mathbf{k}\sigma} \gamma_{\mathbf{k}\sigma}, \ \mathscr{E}_{\mathbf{k}\sigma} = \varepsilon_{\mathbf{k}} + \sigma|\mathbf{g}_{\mathbf{k}}|. \tag{1.4}$$

Usually is assumed that the superconducting pairing only occurs within the bands of these long-lived excitations. Interband pairing is neglected, since it would require Cooper pairs with a finite center-of-mass momentum. The superconducting part of the Hamiltonian may therefore be written as

$$H_{\rm SC} = \sum_{\mathbf{k}\mathbf{k}'\sigma} V_{\mathbf{k}\mathbf{k}'\sigma} \gamma^{\dagger}_{\mathbf{k}\sigma} \gamma^{\dagger}_{-\mathbf{k},-\sigma} \gamma_{-\mathbf{k}',\sigma} \gamma_{\mathbf{k}'\sigma}. \tag{1.5}$$

This may now be transformed back into the original fermion operators in the non-diagonalized basis. In general, one then finds that the superconducting order parameter in the original spin basis may be written as

$$\Delta_{\mathbf{k}} = \Delta_s i\sigma_y + \Delta_{t,\mathbf{k}} \frac{\mathbf{d}_{\mathbf{k}} \cdot \boldsymbol{\sigma}}{k_F} i\sigma_y,\ \mathbf{d}_{\mathbf{k}} \propto \mathbf{g}_{\mathbf{k}}, \tag{1.6}$$

where k_F is the Fermi wavevector and a singlet Δ_s and a triplet $\Delta_{t,\mathbf{k}}$ gap have been introduced with the vector $\mathbf{d}_{\mathbf{k}}$ describing its form as we discuss later. Indeed the lacking of inversion symmetry prevents the classification of Cooper pairs according to orbital parity. As a consequence, the superconducting phase is characterized by order parameters of mixed spin symmetry, consisting of an admixture of spin-singlet and spin-triplet pairing components [104, 105]. The mixed spin structure of the order parameter in superconducting non-centrosymmetric systems also leads to very specific features in the behavior close to interfaces, essentially because the presence of a strong spin-orbit interaction makes the interface scattering become spin active [106]. More exotic forms of mixed singlet-triplet superconductivity can be obtained when pairing time correlations lead to an even-frequency component in one of the spin symmetry channels and an odd-like frequency dependence in the other. The interest in this direction has been triggered by the observation of long-range proximity effect in junctions made of a spin-singlet superconductor interfaced with a half-metallic ferromagnet [107, 108]. A similar attention has also been devoted to other hybrid systems where due to interfaces, spin active sources of scattering or inhomogeneous profiles of the magnetization, a mixing of singlet and triplet pairing with a non-trivial time dependence may be generated [109, 110, 157, 111].

A triplet ($S = 1$) superconductor (TS) is described by a pair function like

$$|\psi\rangle = \Delta_{\uparrow\uparrow}|\uparrow\uparrow\rangle + \Delta_{\downarrow\downarrow}|\downarrow\downarrow\rangle + \Delta_0\left(|\uparrow\downarrow\rangle + |\downarrow\uparrow\rangle\right). \tag{1.7}$$

The gap can be described by matrix of functions or by a field $\mathbf{d}(\mathbf{k})$ [112] transforming like a vector in spin space as

$$\hat{\Delta}_{\mathbf{k}} = \begin{pmatrix} \Delta_{\uparrow\uparrow} & \Delta_{\uparrow\downarrow} \\ \Delta_{\downarrow\uparrow} & \Delta_{\downarrow\downarrow} \end{pmatrix} = \begin{pmatrix} -d_x + id_y & d_z \\ d_z & d_x + id_y \end{pmatrix}. \tag{1.8}$$

All the information about gap function (nodal, orbital, and spin structure) is coded in $\mathbf{d}(\mathbf{k})$. Quasiparticles excitation spectrum can be written as

$$E_k = \sqrt{\varepsilon_k + \mathbf{d}\cdot\mathbf{d}^* + |\mathbf{d}\times\mathbf{d}^*|}. \tag{1.9}$$

When $\mathbf{d}\times\mathbf{d}^* = 0$, the state "unitary", meaning that there is only one energy gap. In this case the energy gap magnitude

$$|\hat{\Delta}_{\mathbf{k}}|^2 = \frac{1}{2}\mathrm{Tr}\left(\hat{\Delta}^\dagger\hat{\Delta}\right), \tag{1.10}$$

becomes simply proportional to $\mathbf{d}\cdot\mathbf{d}^*$. For unitary states the direction of $\mathbf{d}(\mathbf{k})$ has immediate physical meaning. Its direction defines the normal to the plane in which the electrons are equal spin paired (along any quantization axes) and its magnitude is proportional to that of the energy gap. Part. IV is dedicated to analysis of two similar triplet superconductors with $\mathbf{d}(\mathbf{k}) \sim (0, 0, k_x + ik_y)$ and $\mathbf{d}(\mathbf{k}) \sim (-k_y, k_x, 0)$, that many experimental studies suggest to be effectively realized in superconducting phases of Sr_2RuO_4 and mixed parity non-centrosymmetric $CePt_3Si$, respectively.

They are both unitary and nodeless with equal gap magnitude $\sim (k_x^2 + k_y^2)$ but they point in different directions. We will show how these two possibilities can be discerned by an STM analysis of proximity effect modified density of states in a proximate ferromagnet. We also show that the interplay between the exchange field $\mathbf{h}$ and the $\mathbf{d}(\mathbf{k})$ vector can generate a spin-sensitive long-ranged proximity effect even without any magnetic inhomogeneity in the ferromagnetic layer.

1.2. Itinerant ferromagnets: Stoner exchange and spin bandwidth asymmetry

The origin of itinerant ferromagnetism is nowadays still a controversial question. Indeed, it is generally accepted that several distinct mechanisms have to be invoked to describe ferromagnetism in metals in the wide range of manifestations that it exhibits in nature. As relevant examples, we mention the ferromagnetic transition metals Fe, Co, and Ni and their alloys [52], the weak metallic ferromagnets such as $ZrZn_2$ and $ScIn_3$ [55], the colossal magnetoresistance manganites such as $La_{1-x}Sr_xMnO_3$ [57], and rare earth hexaborides such as EuB_6 [58]. The class of half-metals, defined by the property of having almost 100% transport spin polarization [24], is particularly important. As members of this class we cite CrO_2 [113], $La_{0.7}Sr_{0.3}MnO_3$ [114], Fe_3O_4 [115], and EuO [116], among others.

Commonly, metallic ferromagnetism has been understood as a competition between single particle kinetic energy, favoring the paramagnetic state, and the exchange energy originated by the Coulomb interaction, favoring the spin-polarized state [117]. It is argued that in ferromagnets the gain in exchange energy usually overcomes the cost in kinetic energy due to the Pauli principle that forbids double occupancy of low kinetic energy states for parallel spins, resulting in an energy split of the majority and minority spin bands. However, the interplay of Coulomb repulsion and the Pauli principle driving a metal into a ferromagnetic state [50], may induce a spin-dependent renormalization of the masses of charge carriers with opposite spins, i.e. a spin bandwidth asymmetry. A possible realization of this mechanism was first proposed to describe ferromagnetism in manganese oxides [60]. The origin of this effect may be ascribed to the Hund's rule interaction in degenerate orbitals that sustains the alignment between electrons in different orbitals. In this case, the ferromagnetic state does not result from the usual exchange interaction but rather is due to a kinetic effect [60]. A different mechanism not requiring a multi-orbital character may be also invoked as responsible for a kinetically driven ferromagnetism. This appears in microscopic approaches where off-diagonal terms of Coulomb repulsion, generally neglected in studies based on the Hubbard model, are taken into account. A mean-field treatment of these contributions in addition to the exchange and nearest-neighbor pair hopping terms shows that quasiparticle energies for the two spin species are not simply splitted but get different bandwidths, i.e. effective masses. The net effect of these interactions is to render the hopping integral in the kinetic term spin dependent through bond charge Coulomb repulsion factors which are different for spin up and down carriers [61]. For low enough temperature and depending on Hamiltonian parameters, ferromagnetic order can be established only through this spin bandwidth asymmetric renormalization [32, 62]. In this picture the ferromagnetism should be understood as kinetically driven, in the sense that it arises from a gain in kinetic energy rather than potential energy, unlike the usual Stoner scheme. It is worth

stressing that, in contrast to the double exchange model, the latter mechanism may develop within a single electronic band [92]. How it is possible to extract experimentally the contributions of the exchange splitting and spin dependent mass renormalization that emerge in the two types of ferromagnet mentioned above? One way is to look at the optical properties [63]; other useful information could be obtained from angle-resolved photoemission experiments, which can probe band renormalization effects as a function of temperature and magnetization [64], as well as from de Haas-van Alphen oscillation measurements [65]. All such experiments can yield insight on the mechanism behind the origin of ferromagnetism in metals.

Spin bandwidth asymmetry will substantially affect the coexistence of ferromagnetism and superconductivity [67], as well as the proximity effect [37] and transport in ferromagnet/superconductor bilayers [96, 98, 97], and Josephson effect in superconductor/ferromagnet/superconductor junction. It is also responsible for an extension of the regime in which FFLO phase can be stabilized in heavy-fermion systems. [118, 119].

Independently of mechanism generating bandwidth asymmetry ferromagnetism, see e.g. [61, 118, 119], it can be qualitatively understood as follows. Consider a tight binding framework on the lattice in its simplest form, i.e. single band of non interacting electrons in a 1D linear lattice with only nearest neighbor hopping. In this case band dispersion have the form

$$\varepsilon_k \sim -t\cos(ka) \tag{1.11}$$

being a the lattice constant, k the quasi-momentum, and t the hopping integral, i.e. the bandwidth. Note that this kind of band describe normal metals (ferromagnetic solutions can be obtained only from interacting electrons). Taking the continuum limit of this tight binding solution, i.e. $ka \ll 1$, one readily obtains a parabolic dispersion and applying definition of effective mass one can see that it is constant throughout the band, i.e. it has no k dependence, and its value its inversely proportional to the bandwidth, $m \sim 1/t$.

When considering interacting electrons, the simplest ferromagnetic solution, i.e. Stoner model, can be written as

$$\varepsilon_{k,\sigma} \sim -t\cos(ka) - \rho_\sigma U \tag{1.12}$$

where $\sigma = \uparrow, \downarrow$ is the spin index, $\rho_{\uparrow(\downarrow)} = +1(-1)$, and U the exchange energy. In this case the bands are rigidly shifted each other and the masses of oppositely polarized electron are the same (see top panel of Fig. 1.4).

Under certain circumstances [61] spin bandwidth asymmetric ferromagnetic solutions can be obtained. They have the form

$$\varepsilon_{k,\sigma} \sim -t_\sigma\cos(ka) \tag{1.13}$$

with $t_\uparrow \neq t_\downarrow$, i.e. up and down electrons bands have different bandwidth (see bottom panel of Fig. 1.4). This is different from Stoner solutions because splitting is absent even if a spin polarization exists (we calculate it below). Taking the continuum limit as explained before for a normal metal, one readily obtains that spin bandwidth asymmetric solutions correspond to two parabolic bands with different spin dependent effective masses, i.e. $m_\uparrow \neq m_\downarrow$. In general both contributions are present and dispersion take the form

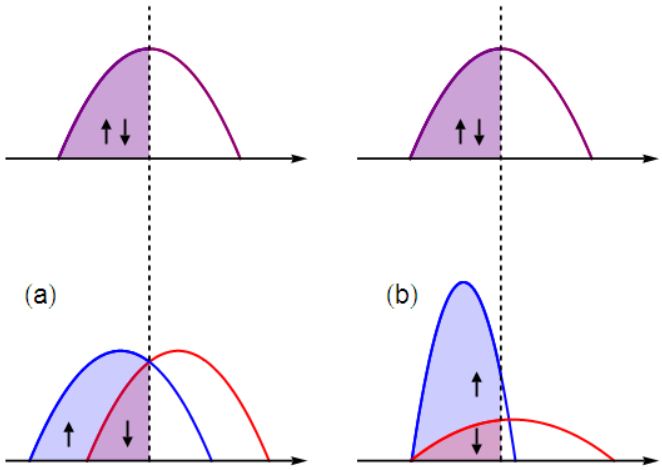

Figure 1.4. Comparison of Stoner (a) and spin bandwidth asymmetry (b) ferromagnets.

$$\varepsilon_{k,\sigma} \sim -t_\sigma \cos(ka) - \rho_\sigma U. \tag{1.14}$$

The dimensionless spin polarization or magnetization M can be defined as

$$M = P_\uparrow - P_\downarrow, \tag{1.15}$$

where P_σ is the fraction of carriers with spin σ, i.e.

$$P_\sigma = \frac{n_\sigma}{n_\uparrow + n_\downarrow}, \tag{1.16}$$

where n_σ is the thermal average of number operator for particles with spin σ. Magnetization takes value in the range $[0, 1]$ with extremes corresponding to a normal metal and an half-metal, respectively. A generic ferromagnet (F) including both exchange energy and mass splitting will be characterized by two magnetic parameters, namely the ratio of exchange energy and Fermi energy $X = U/E_F \in [0, 1]$, and $Y = m_\uparrow/m_\downarrow \in [0, \infty[$. At T=0 and for one-, two- and three-dimensional F one has

$$M_{1D} = \frac{\sqrt{\frac{(X+1)Y}{1-X}} - 1}{\sqrt{\frac{(X+1)Y}{1-X}} + 1}, \tag{1.17}$$

$$M_{2D} = \frac{X + (X+1)Y - 1}{X(Y-1) + Y + 1}, \tag{1.18}$$

$$M_{3D} = \frac{\sqrt{(X+1)^3 Y^3} - \sqrt{(1-X)^3}}{-\sqrt{(1-X)^3} - \sqrt{(X+1)^3 Y^3}}. \tag{1.19}$$

These expressions correctly reduce to known results for a pure Stoner ferromagnet when $Y \to 1$. On the other hand, for any fixed value of X, when $Y \to \infty(0)$ we precisely reproduce the half-metal limit $M \to 1(-1)$. For any $0 \leq X < 1$, the mass mismatch enhances the net polarization when the up electrons band has a

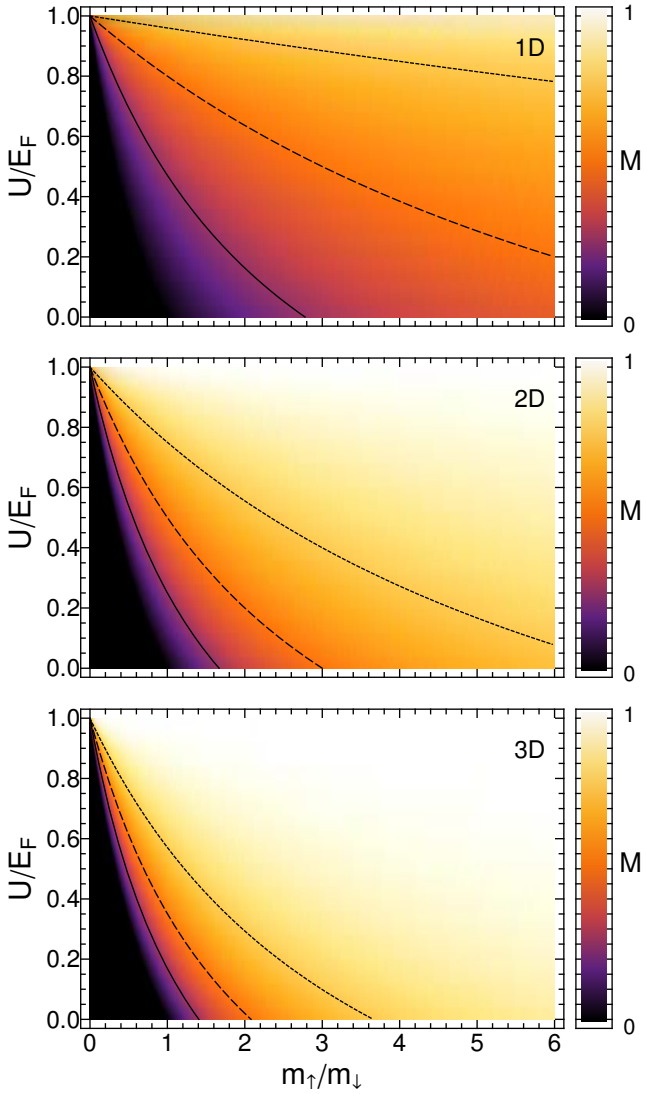

Figure 1.5. Density plot of the ground state magnetization as a function of the mass mismatch and the normalized exchange interaction, for one-, two- and three-dimensional ferromagnetic electrodes. As shown in the legend on the right, lighter color regions are associated with larger values of the magnetization. For clarity, only three iso-magnetization curves are plotted in all panels, corresponding to $M = 0.25$ (solid line), $M = 0.50$ (dashed line), and $M = 0.75$ (dotted line).

smaller bandwidth than the down electrons one (corresponding to $Y > 1$ and up electrons "heavier" than down electrons, i.e. $m_\uparrow > m_\downarrow$) and hinders it the other way around ($Y < 1$). The situation is illustrated in Fig. 1.5, where a density plot of the magnetization at $T = 0$ in the $(m_\uparrow/m_\downarrow,\, U/E_F)$ parameter space is shown

for one-, two- and three-dimensional ferromagnets, together with three isomagnetization curves plotted to clarify the magnetization trend. Each colored point on plots corresponds to a different realization of the ferromagnetic order in the sense that the relative weights of the exchange splitting and the mass mismatch are determined by the coordinates of that point, while the value of M is fixed along any isomagnetization curves, e.g. the solid, dashed and dotted lines of Fig. 1.5. Regions corresponding to $M < 0$ (indicated in black in Fig. 1.5) are excluded since they are mirror images of those with positive M. It is clear that in order to obtain a fixed magnetization the values of exchange and/or mass mismatch needed are larger for lower dimensionalities. Indeed we see that though the qualitative behavior is independent on the dimensionality, for the chosen band dispersion in F, one always finds $M_{3D} > M_{2D} > M_{1D}$ when evaluated for the same $m_\uparrow/m_\downarrow$ and U/E_F values. These are simply consequences of the fact that the number of levels in the $k-$space at a certain energy grows with dimensionality.

1.3. Modelling interfaces

The quality of interfaces has a dramatic influence on physics of heterostructures. Complicated details of interfaces which depend on materials constituting the samples and synthesis technique are usually not included in standard theoretical models simply because they would render the problem intractable. A possible model of interface is to consider it as a positive potential energy term in the Hamiltonian different from zero only around the interface plane working as a barrier on particles, i.e. a scattering potential. The simplest case of a constant potential which is non zero only in the interface plane representing an infinitely thin insulator is usually employed. Within this assumption a ferromagnetic insulator (FI) can easily be included in the model by using different potential values for up and down particles along a certain quantization axis. Spin flip scattering at the interface can also be included introducing a matrix of potentials in spin space with non zero "off-diagonal" terms describing scattering accompanied by a flipping of the spin. Interface roughness can be simulated by random sampling of both the location and the height of the scattering potential in given ranges. In lattice tight binding models interfaces can be modelled including in the boundary planes hopping terms in the Hamiltonian which have a different values from the one taken in the surroundings, e.g. in the bulk. Even in this case one can "spread" the interface on more planes with position dependent hopping values, and describe a ferromagnetic insulator by assigning different hopping values for up and down particles. In what follows we will make use of this simplified models assuming thin interfaces and neglecting any roughness. This are usual assumptions in the literature and are considered to be able to reproduce the features of heterostructures whenever the quality of interfaces is good.

1.4. Bogoliubov–de Gennes equations

Bogoliubov-de Gennes equations (BdG) describe quasiparticle excitations in clean, i.e. without impurities, superconductors [120]. They can also describe non superconducting materials, e.g. a normal metal (N) or a ferromagnet (F), so they can be used to model any component of heterostructures we are interested in. We derive them here for a 2D F/I/S junction (the interface lies in the y direction

at $x = 0$) where F is a general ferromagnet possessing both exchange and spin bandwidth asymmetry, I is a infinitely thin insulating barrier, and S a generic superconductor.

The real-space Hamiltonian written in terms of canonical field operators $\psi(\mathbf{r},t), \psi^\dagger(\mathbf{r},t)$ in the Heisenberg picture reads

$$\begin{aligned} H = &\sum_{\alpha,\beta} \int \mathrm{d}\mathbf{r} \psi^\dagger_\alpha(\mathbf{r},t) H^0_{\alpha,\beta}(\mathbf{r},\mathbf{p}) \psi_\beta(\mathbf{r},t) \\ &+ \frac{1}{2} \sum_{\alpha\beta} \int\int \mathrm{d}\mathbf{r}\mathrm{d}\mathbf{r}' V_{\alpha\beta}(|\mathbf{r}-\mathbf{r}'|) \psi^\dagger_\alpha(\mathbf{r},t) \psi^\dagger_\beta(\mathbf{r}',t) \psi_\beta(\mathbf{r}',t) \psi_\alpha(\mathbf{r},t), \end{aligned} \tag{1.20}$$

where α, β are spin index, $H^0_{\alpha,\beta}(\mathbf{r},\mathbf{p})$ is the single particle Hamiltonian ($\mathbf{p} = -i\hbar\nabla_\mathbf{r}$) and $V_{\alpha\beta}(|\mathbf{r}-\mathbf{r}'|)$ is the attractive interaction responsible for superconductivity (here all spin paring channel are assumed to be open). In order to describe a F/I/S junction superconducting pairing and single particle Hamiltonian in Eq. 1.20 have to be considered "piecewise". The superconducting term pairs electron only on the right side of the junction

$$V_{\alpha\beta}(|\mathbf{r}-\mathbf{r}'|) = \Theta(x) \widetilde{V}_{\alpha\beta}(|\mathbf{r}-\mathbf{r}'|), \tag{1.21}$$

being Θ the Heaviside step function. Choosing the magnetization in F along the spin quantization axis [2] the single-particle Hamiltonian is

$$H^0_{\alpha,\beta}(\mathbf{r},\mathbf{p}) = \delta_{\alpha\beta} \left[H^F_\alpha \Theta(-x) + H^I \delta(x) + H^S \Theta(x) \right], \tag{1.22}$$

where δ is the Dirac delta function and

$$\begin{aligned} H^F_\alpha &= -\hbar^2\nabla^2/2m_\alpha - \rho_\alpha U - E^F_F \\ H^I &= V \\ H^S &= -\hbar^2\nabla^2/2m - E^S_F, \end{aligned} \tag{1.23}$$

where V is the scattering potential at interface and in F both exchange term and mass mismatch have been included.

Mean field approximation is employed

$$\psi^\dagger_\alpha(\mathbf{r},t)\psi^\dagger_\beta(\mathbf{r}') = \langle \psi^\dagger_\alpha(\mathbf{r},t)\psi^\dagger_\beta(\mathbf{r}',t)\rangle + \delta\psi^\dagger_{\alpha\beta}, \tag{1.24}$$

where the last term describes the fluctuations around the average field. Neglecting time (energy) dependence, i.e. in the weak coupling limit, the superconducting order parameter is defined as

$$\Delta_{\alpha\beta}(\mathbf{r},\mathbf{r}') = V_{\alpha\beta}(|\mathbf{r}-\mathbf{r}'|)\langle \psi_\beta(\mathbf{r}',t)\psi_\alpha(\mathbf{r},t)\rangle. \tag{1.25}$$

The Hamiltonian within these approximation becomes

$$\begin{aligned} H = &\sum_{\alpha\beta} \int \mathrm{d}\mathbf{r} \psi^\dagger_\alpha(\mathbf{r},t) H^0_{\alpha,\beta}(\mathbf{r},\mathbf{p}) \psi_\beta(\mathbf{r},t) \\ &+ \frac{1}{2} \sum_{\alpha\beta} \int\int \mathrm{d}\mathbf{r}\mathrm{d}\mathbf{r}' [\Delta^\dagger_{\alpha\beta}(\mathbf{r},\mathbf{r}') \psi_\beta(\mathbf{r}',t) \psi_\alpha(\mathbf{r},t) \\ &\quad + \Delta_{\alpha\beta}(\mathbf{r},\mathbf{r}') \psi^\dagger_\alpha(\mathbf{r},t) \psi^\dagger_\beta(\mathbf{r}',t)]. \end{aligned} \tag{1.26}$$

[2] This assumption makes the calculation less general when S is a triplet superconductor but in what follows we will apply BdG only to singlet superconductors.

where $(\delta\psi)^2$ term has been neglected and a constant term dropped. The equation of motion for field operators $\psi(\mathbf{r},t) = \mathrm{e}^{i\frac{Ht}{\hbar}}\psi(\mathbf{r})\mathrm{e}^{-i\frac{Ht}{\hbar}}$ are

$$\begin{aligned}
i\hbar\partial_t\psi_\alpha(\mathbf{r},t) &= [\psi_\alpha(\mathbf{r},t), H] \\
&= \sum_\beta \int \mathrm{d}\mathbf{r}'\delta(\mathbf{r}-\mathbf{r}')H^0_{\alpha\beta}(\mathbf{r}',\mathbf{p})\psi_\beta(\mathbf{r}',t) \\
&+ \sum_\beta \int \mathrm{d}\mathbf{r}'\Delta_{\alpha\beta}(\mathbf{r},\mathbf{r}')\psi^\dagger_\beta(\mathbf{r}',t), \\
i\hbar\partial_t\psi^\dagger_\alpha(\mathbf{r},t) &= [\psi^\dagger_\alpha(\mathbf{r},t), H] \\
&= \sum_\beta \int \mathrm{d}\mathbf{r}'\delta(\mathbf{r}-\mathbf{r}')[-H^0(\mathbf{r}',-\mathbf{p})]^{\mathrm{T}}_{\alpha\beta}\psi^\dagger_\beta(\mathbf{r}',t) \\
&+ \sum_\beta \int \mathrm{d}\mathbf{r}'\Delta^\dagger_{\alpha\beta}(\mathbf{r},\mathbf{r}')\psi_\beta(\mathbf{r}',t).
\end{aligned} \tag{1.27}$$

The equations can be written in a matrix form introducing a vector of field operators as follows

$$\begin{aligned}
i\hbar\partial_t\Psi(\mathbf{r},t) &= \int \mathrm{d}\mathbf{r}'\mathscr{H}(\mathbf{r},\mathbf{r}')\Psi(\mathbf{r}',t), \\
\Psi(\mathbf{r},t) &= [\psi_\uparrow(\mathbf{r},t), \psi_\downarrow(\mathbf{r},t), \psi^\dagger_\uparrow(\mathbf{r},t), \psi^\dagger_\downarrow(\mathbf{r},t)]^{\mathrm{T}}, \\
\mathscr{H}(\mathbf{r},\mathbf{r}') &= \begin{pmatrix} \hat{H}^0(\mathbf{r}',\mathbf{p})\delta_{\mathbf{r}\mathbf{r}'} & \hat{\mathbf{\Delta}}(\mathbf{r},\mathbf{r}') \\ -\hat{\mathbf{\Delta}}^*(\mathbf{r},\mathbf{r}') & [-\hat{H}^0(\mathbf{r}',-\mathbf{p})]^{\mathrm{T}}\delta_{\mathbf{r}\mathbf{r}'} \end{pmatrix},
\end{aligned} \tag{1.28}$$

with gap matrix

$$\hat{\mathbf{\Delta}}(\mathbf{r},\mathbf{r}') = \begin{pmatrix} \Delta_{\uparrow\uparrow}(\mathbf{r},\mathbf{r}') & \Delta_{\uparrow\downarrow}(\mathbf{r},\mathbf{r}') \\ \Delta_{\downarrow\uparrow}(\mathbf{r},\mathbf{r}') & \Delta_{\downarrow\downarrow}(\mathbf{r},\mathbf{r}') \end{pmatrix}. \tag{1.29}$$

Stationary solutions $\Psi(\mathbf{r},t) = \Psi(\mathbf{r})\mathrm{e}^{-i\frac{Et}{\hbar}}$ with E as the wavefunction energy are solution of

$$E\Psi(\mathbf{r}) = \int \mathrm{d}\mathbf{r}'\mathscr{H}(\mathbf{r},\mathbf{r}')\Psi(\mathbf{r}'). \tag{1.30}$$

Assuming plane-wave-like solutions and dividing out the fast oscillations on Fermi wavelength scale the usual form of BdG is obtained

$$\begin{pmatrix} \hat{H}^0(\mathbf{r},\mathbf{p}) & \hat{\mathbf{\Delta}}(\mathbf{k},\mathbf{r}) \\ \hat{\mathbf{\Delta}}^\dagger(\mathbf{k},\mathbf{r}) & [-\hat{H}^0(\mathbf{r},-\mathbf{p})]^{\mathrm{T}} \end{pmatrix}\Psi(\mathbf{r}) = E\Psi(\mathbf{r}), \tag{1.31}$$

where the quasiparticle momentum $\mathbf{k}$ is the Fourier conjugate of the relative coordinate $\mathbf{s} = (\mathbf{r}-\mathbf{r}')/2$. Its modulus is fixed on the Fermi surface, and only its direction enters in Eq. 1.31, $\mathbf{k} \to k_F\hat{\mathbf{k}}$.

In order to solve BdG for a heterostructure boundary conditions at any interface have to be employed. Precise form of these equations are different depending on the particular junction. They will be listed in the following for every setup analyzed. The general recipe is that eigenfunctions have to be continuous at any interface. The matching of derivatives depends on scattering potential at interfaces and the right equation have to be obtained demanding consistency when BdG are integrated in a finite interval around interface which is successively taken to zero. This procedure gives continuity of derivatives unless the scattering potential

is infinite and/or different effective masses are assumed in different layers as in our case.

1.5. Eilenberger and Usadel equations

Eilenberger [121] and Usadel [122] equations provide quasiclassical Green's functions in clean and dirty superconductors, respectively. As BdG they can describe also a normal metal (N) or a ferromagnet (F) so they are applicable to systems here considered. Being their derivation quite long, we simply report them here after a brief introduction in which the formalism of quasiclassical theory of superconductivity is introduced. We will use units such that $\hbar = c = 1$ and use $\underline{\ldots}$ for 2×2 matrices in spin space and $\hat{\ldots}$ for 4×4 matrices in spin $\otimes$ Nambu (electron-hole) space. Using the simplified notation $(\mathbf{r}_1, t_1) = 1$, $(\mathbf{r}_2, t_2) = 2$, the retarded, advanced, and Keldysh Green's functions are defined as

$$
\begin{aligned}
G^R_{\sigma,\sigma'}(1,2) &= -i\Theta(t_1 - t_2)\left\langle \left\{ \psi_\sigma(1), \psi^\dagger_{\sigma'}(2) \right\} \right\rangle, \\
G^A_{\sigma,\sigma'}(1,2) &= i\Theta(t_2 - t_1)\left\langle \left\{ \psi_\sigma(1), \psi^\dagger_{\sigma'}(2) \right\} \right\rangle, \\
G^K_{\sigma,\sigma'}(1,2) &= -i\left\langle \left[\psi_\sigma(1), \psi^\dagger_{\sigma'}(2) \right] \right\rangle.
\end{aligned}
$$

Superconducting correlations are coded in "anomalous" Green's functions

$$
\begin{aligned}
F^R_{\sigma,\sigma'}(1,2) &= -i\Theta(t_1 - t_2)\left\langle \{ \psi_\sigma(1), \psi_{\sigma'}(2) \} \right\rangle, \\
F^A_{\sigma,\sigma'}(1,2) &= i\Theta(t_2 - t_1)\left\langle \{ \psi_\sigma(1), \psi_{\sigma'}(2) \} \right\rangle, \\
F^K_{\sigma,\sigma'}(1,2) &= -i\left\langle [\psi_\sigma(1), \psi_{\sigma'}(2)] \right\rangle.
\end{aligned}
$$

Both kind of functions are collected in the following matrices

$$
\begin{aligned}
\hat{G}^R(1,2) &= \begin{pmatrix} \underline{G}^R(1,2) & \underline{F}^R(1,2) \\ (\underline{F}^R)^*(1,2) & (\underline{G}^R)^*(1,2) \end{pmatrix}, \\
\hat{G}^A(1,2) &= \begin{pmatrix} \underline{G}^A(1,2) & \underline{F}^A(1,2) \\ (\underline{F}^A)^*(1,2) & (\underline{G}^A)^*(1,2) \end{pmatrix}, \\
\hat{G}^K(1,2) &= \begin{pmatrix} \underline{G}^K(1,2) & \underline{F}^K(1,2) \\ -(\underline{F}^K)^*(1,2) & -(\underline{G}^K)^*(1,2) \end{pmatrix}.
\end{aligned}
$$

Retarded and advanced Green's function matrices are not independent. Indeed

$$
\hat{G}^A(1,2) = \left[\hat{\rho}_3 \hat{G}^R(2,1) \hat{\rho}_3 \right]^\dagger, \tag{1.32}
$$

where

$$
\hat{\rho}_3 = \begin{pmatrix} 1 & 0 & 0 & 0 \\ 0 & 1 & 0 & 0 \\ 0 & 0 & -1 & 0 \\ 0 & 0 & 0 & -1 \end{pmatrix}. \tag{1.33}
$$

By passing to center of mass and relative coordinates (both in space and time) quasiclassical Green's functions can be introduced. By considering an equilibrium system, e.g. with no explicit time dependence in the Hamiltonian in the Schrödinger picture, they are defined as

$$\hat{g}(\mathbf{r},\mathbf{p}_F,\varepsilon)=\frac{i}{\pi}\int_{-\infty}^{\infty}\mathrm{d}\xi_{\mathbf{p}}\hat{G}(\mathbf{r},\mathbf{p},\varepsilon), \tag{1.34}$$

where $\xi_{\mathbf{p}}=\mathbf{p}^2/2m$, and $\hat{G}(\mathbf{r},\mathbf{p},\varepsilon)$ is the partial Fourier transform of $\hat{G}(1,2)$ after coordinates change, i.e. $\mathbf{p}$ and ε are conjugate variables of $\mathbf{r}_1-\mathbf{r}_2$ and t_1-t_2, respectively, and $\mathbf{r}$ is the center of mass position. This definition applies to both retarded, advanced, and Keldysh Green's functions. Their quasiclassical version has the following structure

$$\begin{aligned}
\hat{g}^R&=\begin{pmatrix}\underline{g}^R & \underline{f}^R\\ -\underline{\widetilde{f}}^R & -\underline{\widetilde{g}}^R\end{pmatrix},\\
\hat{g}^A&=\begin{pmatrix}\underline{g}^A & \underline{f}^A\\ -\underline{\widetilde{f}}^A & -\underline{\widetilde{g}}^A\end{pmatrix},\\
\hat{g}^K&=\begin{pmatrix}\underline{g}^K & \underline{f}^K\\ \underline{\widetilde{f}}^K & \underline{\widetilde{g}}^K\end{pmatrix},
\end{aligned} \tag{1.35}$$

where

$$\begin{aligned}
\underline{\widetilde{g}}(\mathbf{r},\mathbf{p}_F,\varepsilon)&=[\underline{g}(\mathbf{r},-\mathbf{p}_F,-\varepsilon)]^*,\\
\underline{\widetilde{f}}(\mathbf{r},\mathbf{p}_F,\varepsilon)&=[\underline{f}(\mathbf{r},-\mathbf{p}_F,-\varepsilon)]^*.
\end{aligned} \tag{1.36}$$

The three types of functions are not independent as

$$\hat{g}^A=-\left[\hat{\rho}_3\hat{g}^R\hat{\rho}_3\right]^\dagger, \tag{1.37}$$

$$\hat{g}^K=(\hat{g}^R-\hat{g}^A)\tanh\left(\frac{\beta\varepsilon}{2}\right). \tag{1.38}$$

From now on we choose to use only retarded Green's function and it will be simply denoted by $\hat{g}$. In clean systems it can be calculated by solving Eilenberger equation

$$i\mathbf{v}_F\cdot\nabla\hat{g}+[\varepsilon\hat{\rho}_3-\hat{\Sigma},\hat{g}]=\hat{0}, \tag{1.39}$$

where $\hat{\Sigma}$ includes all potential energies, e.g. exchange field and superconducting pairing.

If impurities exist, and self energy associated with elastic scattering is much larger than any other, i.e. the dirty limit, the Green's function is mainly isotropic depending weakly on direction of Fermi momentum. In this case from Eilenberger equation the simpler Usadel equation can be obtained which describe the angular average on Fermi surface of Green's functions $\langle\hat{g}\rangle$. It reads

$$D\nabla(\langle\hat{g}\rangle\nabla\langle\hat{g}\rangle)+i[\varepsilon\hat{\rho}_3-\hat{\Sigma}],\langle\hat{g}\rangle]=0, \tag{1.40}$$

where $D=v_F^2\tau/3$ is the diffusion constant and

$$\frac{1}{\tau}=\frac{1}{2}nN_0\int\mathrm{d}\mathbf{e}_F|v(\mathbf{p}_F-\mathbf{q})|^2, \tag{1.41}$$

where n is the impurity concentration, N_0 the density of states at the Fermi level, and v the Fourier transform of impurity potential in real space.

In order to solve Eilenberger or Usadel equations for heterostructures boundary conditions for quasiclassical Green's functions are necessary. They were derived by Zaitsev for conventional S/N bilayers [185] while Kuprianov and Lukichev [186] specialized them for the case of tunneling interfaces. They were generalized to the case of unconventional superconductors by Tanaka [125]. In diffusive media they are found to depend on resistance of electrodes and not only on properties of the interface. Their derivation is extremely long and complicated [125] and we will simply discuss their particular structure when applied to an heterostructure build up by a diffusive ferromagnet and a triplet superconductor in Part IV.

Part II

Transport in F/S

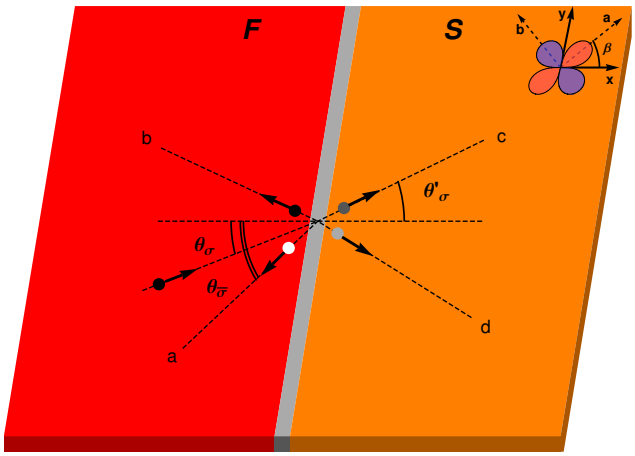

Abstract

This part of the dissertation is devoted to the analysis of transport in ferromagnet/superconductor ballistic junction. For the ferromagnetic side we assume that ferromagnetism may be driven by an unequal mass renormalization of oppositely polarized carriers, i.e. a spin bandwidth asymmetry, and/or by a rigid splitting of up-and down-spin electron bands, as in a standard Stoner ferromagnet, whereas the superconducting side is assumed to exhibit a s-wave and d-wave symmetry of the order parameter. The latter case is also considered accompanied by a minority component breaking time-reversal symmetry. The study is performed within the Blonder-Tinkham-Klapwijk approach and by solving the corresponding Bogoliubov-de Gennes equations. Chapter 2 focuses on charge transport, Chapter 3 on spin filtering effects, and Chapter 4 on spin transport. Results are summarized and discussed in the last section of this part at p. 55.

CHAPTER 2

Charge transport in F/S

This Chapter is devoted to analysis of charge transport in ballistic 2D F/S junctions. In particular we focus on differences deriving from a different magnetic mechanism in F. We will consider both a Stoner ferromagnet (STF) and spin bandwidth asymmetry ferromagnet (SBAF) with mass mismatch of oppositely polarized carriers (see Sec. 1.2). We will consider different symmetries in S, namely conventional s-wave, $d_{x^2-y^2}$-wave with line nodes perpendicular to the interface, and broken time-reversal states (BTRSs) with s- or d_{xy}-wave minority component, e. g. $d_{x^2-y^2}+is$-wave and $d_{x^2-y^2}+id_{xy}$-wave (see Sec. 1.1).

The system under study is built up of two semi-infinite layers connected by an infinitely thin non magnetic insulator barrier (I) resulting in an interfacial scattering potential of the form $V(\mathbf{r}) = H\delta(x)$. We choose an interface lying along the y direction at $x = 0$ (see Fig. 2.1) so that the region $x < 0$ (from now on the F side) is occupied by an itinerant ferromagnet (a Stoner or a spin bandwidth asymmetry ferromagnet, or a combination of the two), while the region $x > 0$ (from now on the S side) is occupied by a singlet superconductor (so there is no need to specify the spin quantization axis). Both conventional and unconventional symmetries will be considered in the S side.

We describe the excitations propagating through the junction by means of the single-particle Hamiltonian

$$\begin{aligned} H_0^\sigma &= \left[-\hbar^2\nabla^2/2m_\sigma - \rho_\sigma U - E_F\right]\Theta(-x) \\ &\quad + \left[-\hbar^2\nabla^2/2m' - E_F\right]\Theta(x) + V(\mathbf{r})\,, \end{aligned} \tag{2.1}$$

where $\sigma = \uparrow, \downarrow$, m_σ is the effective mass for σ-polarized electrons in the F side, $\rho_{\uparrow(\downarrow)} = +1(-1)$, U is the exchange interaction, E_F is the Fermi energy of the ferromagnet, $\Theta(x)$ is the unit step function, m' is quasiparticles effective mass in the superconductor. When there are no spin flip scattering processes at the interface and/or a singlet superconductor is considered, it is enough to solve 2×2 BdG equations

$$\begin{pmatrix} H_0^\sigma & \Delta \\ \Delta^* & -H_0^{\bar\sigma} \end{pmatrix}\begin{pmatrix} u_\sigma \\ v_{\bar\sigma} \end{pmatrix} = \varepsilon\begin{pmatrix} u_\sigma \\ v_{\bar\sigma} \end{pmatrix},\ \sigma = \uparrow,\downarrow \quad , \tag{2.2}$$

where $\bar\sigma = -\sigma$ and $(u_\sigma, v_{\bar\sigma}) \equiv \Psi_\sigma$ is the energy eigenstate in the electron-hole space associated with the eigenvalue ε (excitation energies are measured from the Fermi level). Eqs. 2.2 admit an analytical solution in the approximation of a rigid superconducting pair potential, i.e. $\Delta(\mathbf{r}) = \Delta(\theta')\Theta(x)$, where θ' is the angular variable for the S side (see Fig. 2.1). The Hamiltonian invariance under y-directed translations permits to factorize the part of the eigenstate parallel to the interface, i.e. $\Psi_\sigma(\mathbf{r}) = e^{i\mathbf{k}_\parallel\cdot\mathbf{r}}\psi_\sigma(x)$, reducing the effective dimensionality of the problem.

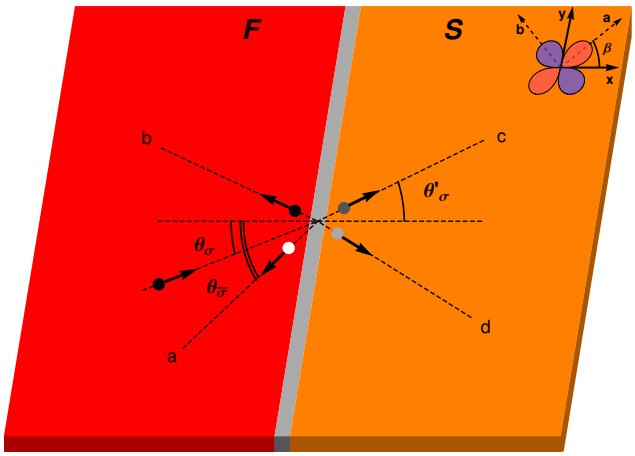

Figure 2.1. Scheme of the planar F/I/S junction. Here, θ_σ, $\theta_{\bar\sigma}$, and θ'_σ are injection, Andreev reflection, and transmission angles, respectively, for electrons and quasiparticles with spin σ. β is the angle formed by the crystallographic a axis of a d-wave superconductor with the x axis.

2.1. Scattering processes at the interface

At the interface four scattering processes are possible for an electron injected from the F side with spin σ and momentum $\mathbf{k}_\sigma^+$ ($k_\sigma^+ = \left[\left(2m_\sigma/\hbar^2\right)\left(E_F + \rho_\sigma U + \varepsilon\right)\right]^{1/2}$). They are qualitatively depicted in Fig. 2.1: *a*) Andreev reflection (AR) resulting in a hole with momentum $\mathbf{k}_{\bar\sigma}^-$ ($k_{\bar\sigma}^- = \left[\left(2m_{\bar\sigma}/\hbar^2\right)\left(E_F + \rho_{\bar\sigma} U - \varepsilon\right)\right]^{1/2}$) belonging to the opposite spin band and a Cooper pair transmitted in the superconductor; *b*) normal reflection; *c*) transmission as electron–like quasiparticle (ELQ) with momentum $\mathbf{k}'^+_\sigma$ ($k'^+_\sigma = \left[\left(2m'/\hbar^2\right)\left(E_F + \sqrt{\varepsilon^2 - |\Delta_{\sigma+}|^2}\right)\right]^{1/2}$); *d*) transmission as hole–like quasiparticle (HLQ) with momentum $\mathbf{k}'^-_\sigma$ ($k'^-_\sigma = \left[\left(2m'/\hbar^2\right)\left(E_F - \sqrt{\varepsilon^2 - |\Delta_{\sigma-}|^2}\right)\right]^{1/2}$), where $\Delta_{\sigma\pm} = |\Delta_{\sigma\pm}|\, e^{i\phi^\pm_\sigma}$ is the pair potential felt by electron-like (+) and hole-like (−) quasiparticles. We notice that the spin dependence of $\Delta_{\sigma\pm}$ comes out from the different trajectories followed by up- and down-spin quasiparticles. Which of these processes actually takes place depends on the energy, momentum and spin orientation of the incoming electrons, as well as on the interfacial barrier strength, the spin polarization in the F side and the symmetry of the superconducting order parameter in the S side. Interestingly there can be also a dependence on magnetic mechanism in F as we will show.

2.1.1. Snell's law and critical angles

Angles associates to every scattering processes can be determined by conservation of parallel momentum. For standard low-biased F/S junctions, one has $E_F \gg (\varepsilon, |\Delta|)$, so that one can apply the Andreev approximation [20] and fix the momenta on the Fermi surfaces, e.g. $k^\pm_{\sigma(\bar\sigma)} \to k^F_{\sigma(\bar\sigma)}$ and $k'^\pm_\sigma \to k'^F_\sigma$. We will employ this approximation in what follows. In this case it is well known that in N/S junction all outgoing angles are equals to incoming angle. In particular this is true for

AR angle (this feature is known as "retroreflection"). This property is lost in F/S in which only normal reflection angle is equal to incoming angle. Andreev reflection and transmission angles can be determined by

$$k_\sigma^F \sin\theta = k_{\bar\sigma}^F \sin\theta_{\bar\sigma} = k'^F \sin\theta'_\sigma \,, \tag{2.3}$$

where $\theta_{\bar\sigma}$ and θ'_σ are AR and the transmission angles, respectively, for electrons with spin σ incoming from an angle θ. From this equation it is easy to verify the existence of critical angles above which these processes are no more possible, resulting in virtual AR [126] and normal reflection.

2.2. Solution of Bogoliubov–de Gennes equations

The solutions of Eq. 2.2 can be found by a plane wake like ansatz. In F and S they read

$$\psi_\sigma^F(x) = e^{ik_{\sigma,x}^F x}\begin{pmatrix}1\\0\end{pmatrix} + a_\sigma e^{ik_{\bar\sigma,x}^F x}\begin{pmatrix}0\\1\end{pmatrix} + b_\sigma e^{-ik_{\sigma,x}^F x}\begin{pmatrix}1\\0\end{pmatrix} \tag{2.4}$$

$$\psi_\sigma^S(x) = c_\sigma e^{ik_{\sigma,x}'^F x}\begin{pmatrix}u_+\\ e^{-i\phi_\sigma^+} v_+\end{pmatrix} + d_\sigma e^{-ik_{\sigma,x}'^F x}\begin{pmatrix}e^{i\phi_\sigma^-} u_-\\ v_-\end{pmatrix} \tag{2.5}$$

where

$$\begin{aligned} u_\pm &= \sqrt{\frac{\varepsilon \pm \sqrt{\varepsilon^2 - |\Delta_{\sigma\pm}|^2}}{2\varepsilon}} \\ v_\pm &= \sqrt{\frac{\varepsilon \mp \sqrt{\varepsilon^2 - |\Delta_{\sigma\pm}|^2}}{2\varepsilon}} \,, \end{aligned} \tag{2.6}$$

the superscript F in the wave-vectors denotes that they are taken on the Fermi surfaces, and $e^{i\phi_\sigma^\pm} = \Delta_{\sigma\pm}/|\Delta_{\sigma\pm}|$. The coefficients a_σ, b_σ, c_σ, and d_σ are probability amplitudes for an electron with spin σ to undergo AR, normal reflection, transmission as ELQ, and transmission as HLQ, respectively. They are functions of dynamical variables ε and θ besides depending on all junction parameters.

2.2.1. Boundary conditions

The boundary conditions at the interface allow for the calculation of the probability amplitude coefficients a_σ, b_σ, c_σ, d_σ for the four scattering processes. The solutions of BdG (Eq. 2.4) in F and S have to be matched at the interface ($x = 0$). The general recipe is that eigenfunctions have to be continuous at any interface. The matching of derivatives depends on scattering potential at the interface and the right equation has to be obtained demanding consistency when BdG are integrated in a finite interval around $x = 0$ which is successively taken to zero. This procedure gives continuity of derivatives unless the scattering potential is infinite and/or different effective masses are assumed in different layers as in our case. The fact that different effective masses are assumed in F for up and down quasiparticles implies that it is not possible to match the derivatives of the full wavefunction doublet but their electron σ and hole $\bar\sigma$ components obey separated equations. The boundary conditions read

$$\psi_\sigma^F(0) = \psi_\sigma^S(0) \tag{2.7a}$$

$$\frac{m_\sigma}{m'}\frac{du_\sigma^S}{dx}\bigg|_{x=0} - \frac{du_\sigma^F}{dx}\bigg|_{x=0} = \frac{2H\ m_\sigma}{\hbar^2}u_\sigma^S(0) \tag{2.7b}$$

$$\frac{m_{\bar\sigma}}{m'}\frac{dv_{\bar\sigma}^S}{dx}\bigg|_{x=0} - \frac{dv_{\bar\sigma}^F}{dx}\bigg|_{x=0} = \frac{2H\ m_{\bar\sigma}}{\hbar^2}v_{\bar\sigma}^S(0)\ . \tag{2.7c}$$

Eq. 2.7 show that the mass asymmetry explicitly renormalizes the interface barrier strength H, giving rise to a dependence of this quantity on the spin of the carriers. This effect, which under suitable conditions leads to a different behavior of these carriers across the barrier, allows to infer that the presence of spin dependent electron masses in Eq. 2.7 may mimic a spin active barrier, in the sense that electrons with opposite spin feel different values of the barrier height. A junction with a mass mismatch ferromagnet can thus induce an effective spin-active interfacial effect, which for specific choices of H will produce spin filtering effects as we will show in Chap. 3. This is analogous to the situation where the insulating barriers are polarized with magnetic moment parallel to the one in the F layer and thus act with different strength on particles with opposite spin. When only exchange splitting is present, i.e. $m_\sigma = m_{\bar\sigma} = m'$, the usual form of the boundary conditions is recovered [126]. The dimensionless parameter $Z = 2m'H\pi^2/(\hbar^2 k'_F)$ in what follows will conveniently characterize the strength of the interfacial scattering.

2.3. Generalized BTK model and charge differential conductance

Once probability amplitudes are calculated by solving the linear system obtained by imposing Eq. 2.7, the charge differential conductance can be estimated within an extended Blonder-Tinkham-Klapwijk approach (BTK), here formulated for a two-dimensional F/S junction. This formalism has been generalized in the last years to take into account higher dimensionalities, unconventional forms of the superconducting order parameter, different Fermi energies for the two sides of the junction, and a spin–flip interfacial scattering [127, 126, 128, 129, 130, 131, 132, 133, 134, 135, 136, 137, 138].

The charge differential conductances at $T = 0$ and energy ε, i.e. at bias voltage $V = \varepsilon/e$, e being the electron charge, are calculated from the ratio between the charge flux across the junction and the incident flux at that bias. It can be easily obtained from the probabilities associated with the four processes listed above [126], and for each spin channel it can be written as

$$G_\sigma(\varepsilon,\theta) = P_\sigma\left(1 + \frac{k^F_{\bar\sigma,x}}{k^F_{\sigma,x}}\,|a_\sigma(\varepsilon,\theta)|^2 - |b_\sigma(\varepsilon,\theta)|^2\right), \tag{2.8}$$

where θ is the angle formed by the momentum of the electrons propagating from the F side with respect to the normal to the interface (see Fig. 2.1), and the partial polarization $P_\sigma = n_\sigma/(n_\uparrow + n_\downarrow)$ is the fraction of electrons occupying the σ-spin band of the metallic ferromagnet. In our case

$$P_\uparrow = 1 - P_\downarrow = \frac{(X+1)Y}{X(Y-1)+Y+1}, \tag{2.9}$$

where $X = U/E_F$ and $Y = m_\uparrow/m_\downarrow$. The scalar part of the ratio of Fermi wavevectors in Eq. 2.8 can be shown to be in a one to one correspondence with spin polarization M and has the effect of suppressing the ARs for increasing magnetization. The sign in front of AR probability shows that whenever ARs take place there is an enhancement in charge conductance because the Andreev reflected holes has opposite charge and velocity sign than injected electrons thus their contributions to charge transport sums up. The junction conductance takes contributions from a range of angles determined by the experimental conditions. This range is limited from above due to the conservation of the momentum parallel component as shown in Eq. 2.3. From this equation it is easy to verify the existence of critical angles above which these processes are no more possible, resulting in virtual AR [126] and normal reflection. This implies that depending on spin polarization and effective masses in F, σ polarized electrons can be Andreev reflected or transmitted only if their trajectory is not too far from the normal injection. The angularly averaged differential conductances for given spin orientation are then defined as [126]

$$\langle G_\sigma(\varepsilon)\rangle = \int_{-\theta_C^\sigma}^{\theta_C^\sigma} d\theta \ \cos\theta \ G_\sigma(\varepsilon,\theta) / \int_{-\theta_C^\sigma}^{\theta_C^\sigma} d\theta \ \cos\theta \tag{2.10}$$

where θ_C^σ is the critical angle for the transmission of σ-spin electrons. In what follows we will consider the same Fermi energy in F and S and whenever mass mismatch will be considered it will be for $m_\uparrow/m_\downarrow > 1$ which corresponds to the usual situation where lowest band is narrower than highest band. Under these conditions critical angles exist only for majority $\sigma =\uparrow$ electrons. The measured net averaged charge conductance is defined as

$$\langle G(\varepsilon)\rangle \quad = \quad \langle G_\uparrow(\varepsilon)\rangle + \langle G_\downarrow(\varepsilon)\rangle. \tag{2.11}$$

This quantity has been defined dimensionless (we have omitted the $2e^2/h$ factor) and normalized in the range $[0, 2]$. For a particular energy the minimum is realized when ARs and transmission probabilities are both zero, e.g. in the tunneling regime $Z \gg 1$ and far from the energy gap when S is s-wave or far from Fermi energy when S is d-wave. The maximum is reached when only ARs take place, e.g. for $Z = 0$ and subgap energy when S is s-wave assuming only normal injection. In the literature the conductance of F/S expressed in Eqs. 2.8, and 2.11 sometimes is divided out with the conductance of F/N. This amounts to multiply our equations for a voltage independent factor proportional to $1 + Z^2$. This would extend the range of conductance values to infinity in the tunneling regime. We do not employ this choice because otherwise some of the effects that we will show could appear less clearly. Being the factor independent of the voltage our choice is just a matter of convention.

2.4. Probing spin bandwidth asymmetry

Degree of spin polarization of F can be estimated by fitting conductance experimental data taken with Point Contact Andreev Reflection Spectroscopy [16] or Scanning Tunneling Microscopy [17, 139] with superconducting counter electrodes. This procedure could in general be used to discriminate existence of spin bandwidth asymmetry in F (see Sec. 1.2) and to give an estimation of this parameter when fitting of experimental data is performed using both exchange splitting and mass mismatch rather than the degree of spin polarization alone.

However a junction setup in which is possible to focus the current in a particular direction which in turn can be manipulated, permits to directly measure both the spin polarization and mass asymmetry, if they exist. This effect could be obtained in a 2D junctions through the application of three tunable gates on the top of the structure [140]. In this way one can probe the angular dependence of conductance, and in particular of AR and transmission probabilities which are the main contributions for $|eV| \ll \Delta_0$ and $|eV| \gg \Delta_0$ being Δ_0 the gap amplitude in S. In N/S junctions it is well known that conductance decreases continuously increasing angle of injection with respect to the normal to the interface. Indeed $G(\varepsilon, \theta)$ depends on Z through a term $\sim Z/\cos\theta$. This can be explained simply by noticing that the length to travel in the insulating layer is minimum for normally injected quasiparticles and increases for more sloping trajectories. In F/S structures this mechanism is still present but it is overcome by a stronger effect deriving from existence of critical angles which can be calculated from the equation

$$k_\sigma^F \sin\theta = k_{\bar{\sigma}}^F \sin\theta_{\bar{\sigma}} = k'^F \sin\theta'_\sigma \,, \tag{2.12}$$

by determining injection angle θ values such that AR $\theta_{\bar{\sigma}}$ and transmission θ'_σ become $\pi/2$. By inspection of equation 2.12 it can be seen that such critical angles exist only for majority $\sigma = \uparrow$ electrons. As a consequence the up channel of the conductance becomes zero when θ overcomes critical angles. This effect is clearly distinguishable from the continuous decrease as a function of Z in N/S previously described appearing it as an abrupt drop in conductance because as soon as critical angle is reached only the minority channel survives, i.e. $G_\uparrow(\theta_c) = 0, G_\downarrow(\theta_c) \neq 0$. What is more this effect exist even for perfectly transparent interface $Z = 0$. As seen by Eq. 2.8 the drop in the total conductance when critical angle is overcome is related to the partial polarization P_σ and consequently to M. By measuring the angle at which this drop takes place in the ranges $|eV| \ll \Delta_0$ and $|eV| \gg \Delta_0$ one can determine AR and transmission critical angles, respectively. A closer look to Eq. 2.12 reveals that critical angle for AR contains the information about the spin polarization M. Using expression for spin polarization in 2D (Eq. 1.18) a little algebra shows that

$$\theta_c^{AR} = \arcsin\sqrt{\frac{1-M}{1+M}}, \tag{2.13}$$

where θ_c^{AR} is the critical angles over which AR is no more possible for majority electrons, and M the spin polarization in F. However existence of bandwidth asymmetry in F cannot be discriminated, or in general the weight of exchange splitting and mass mismatch in building up M cannot be separated when critical angle for AR is measured.

On the other hand critical angle for transmission is sensible to the relative weights of the magnetization sources. Fig. 2.2 shows the critical angle for the transmission of up electrons in the superconductor along three iso–magnetization curves as plotted in the mid panel of Fig. 1.5. These curves are plotted as a function of the mass mismatch ratio whereas the exchange energy U is varied in such a way to keep the magnetization constant. If the value of M in F lead is known, e.g. with spin resolved photoelectron spectroscopy or by measuring the critical angle for AR as explained before, than it is possible to directly estimate mass mismatch by measuring the critical angle for transmission. As an example consider that F has spin polarization $M = 0.50$ and the critical angles is $\pi/4$. Than from red curve

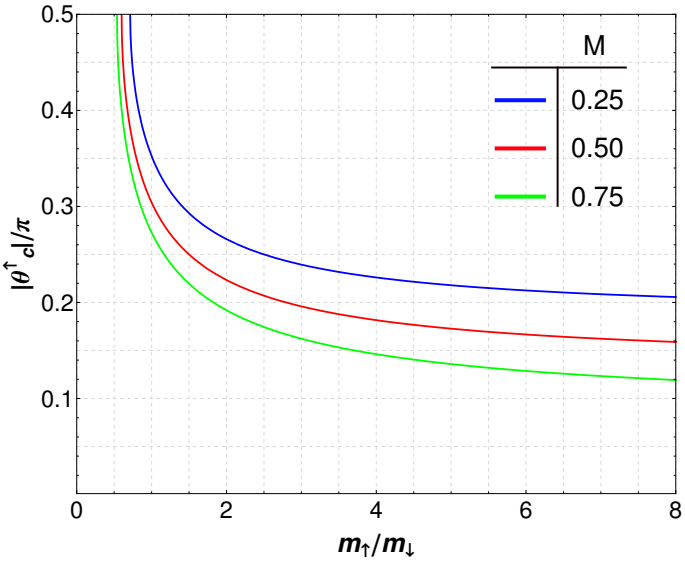

Figure 2.2. Critical angles for the transmission of spin up electrons in S as a function of mass mismatch for three different M values.

in Fig. 2.2 it is easy to see that there is mass mismatch and $m_{\uparrow}/m_{\downarrow} = 1.5$. In the general case one can derive the relation between critical angle for transmission and mass mismatch for arbitrary M from Eq. 2.12.

2.5. SBAF/S vs. STF/S

In this section charge transport through two kinds of F/S junctions differing only in the magnetic mechanism in F (see Sec. 1.2) will be compared. Our model enable us to analyze a generic F including both exchange energy and mass splitting. However in the following subsections we discuss the results only for the six representative points highlighted in the mid panel of Fig. 2.3, which correspond to a pure Stoner ferromagnet (STF), i.e. $m_{\uparrow}/m_{\downarrow} = 1$, and a pure spin bandwidth asymmetry ferromagnet (SBAF), i.e. U/E_F=0, for three different values of the magnetization $M = 0.25, 0.50, 0.75$ (the corresponding values of $m_{\uparrow}/m_{\downarrow}$ and U/E_F are reported in Table 2.I). We exclude the regions corresponding to $M < 0$ (indicated in black in Fig. 2.3) since they are mirror images of those with positive M, and assume that $m_{\uparrow}/m' = m'/m_{\downarrow}$, $m_{\uparrow}/m_{\downarrow} \geq 1$, and $U \geq 0$. These are just conventions that do not affect our results. F/S conductance spectra will be shown for various symmetries of the superconducting order parameter, emphasizing the differences in transport between STF/S and SBAF/S junctions. We notice that spectra change continuously as one moves along an isomagnetization curve from a point corresponding to a STF to a point corresponding to a SBAF (see Fig. 2.3) so that the case of F with both contributions can be recovered interpolating the two extreme cases.

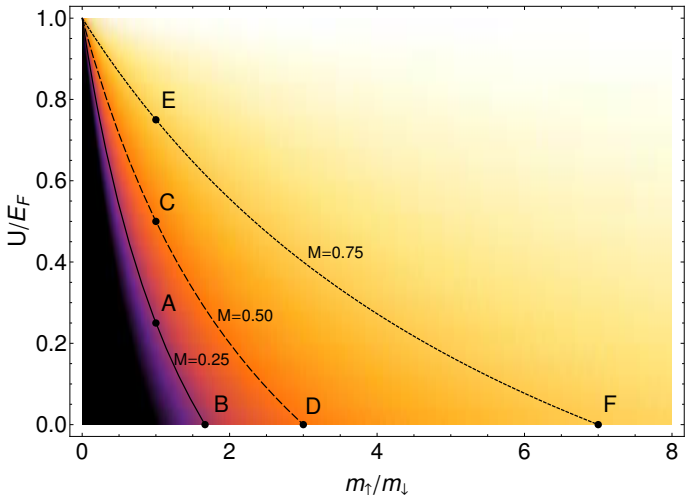

Figure 2.3. Density plot of the ground state magnetization as a function of the mass mismatch and the normalized exchange interaction for a two-dimensional ferromagnetic electrode. Lighter color regions are associated with higher values of the magnetization $M \in [0,1]$. For clarity, only three iso-magnetization curves are plotted, corresponding to $M = 0.25$ (solid line), $M = 0.50$ (dashed line), and $M = 0.75$ (dotted line). We depict six representative points: A and B correspond to two different microscopic states with the same macroscopic magnetization M = 0.25, A representing a standard Stoner ferromagnet ($m_\uparrow/m_\downarrow = 1$), and B a purely spin bandwidth asymmetry ferromagnet ($U/E_F = 0$). The same holds for the (C,D) and (E,F) couples of points, referring to higher values of the magnetization ($M = 0.50$ and $M = 0.75$, respectively). The values assumed by the microscopic parameters in the above mentioned six states are summarized in Table 2.I.

		M	U/E_F	$m_\uparrow/m_\downarrow$
A	STF	0.25	0.25	1
B	SBAF		0	5/3
C	STF	0.50	0.50	1
D	SBAF		0	3
E	STF	0.75	0.75	1
F	SBAF		0	7

Table 2.I. Values of the normalized exchange interaction U/E_F, the mass mismatch $m_\uparrow/m_\downarrow$ and the magnetization M for the six illustrative points displayed in the middle panel of Fig. 2.3.

2.5.1. s-wave superconducting electrode

We fix as a reference energy the maximum magnitude of energy gap in S $\Delta_0 > 0$. For s-wave superconducting electrode the pair potential can be chosen simply as $\Delta_{\sigma,\pm} = \Delta_0$. Then the charge conductance can be obtain by using this choice when evaluating coherence factors of Eq. 2.6. Before we move on to analyze the F/S case, for comparison we will briefly discuss the N/S case in 1D as calculated

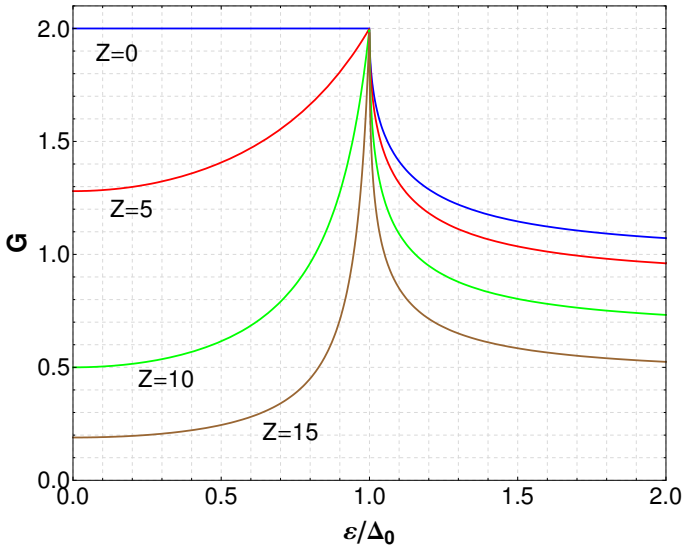

Figure 2.4. Differential conductance spectra in 1D N/S for a junction with a s-wave superconducting electrode, for different dimensionless interface barrier strength Z.

in BTK [141]. As discussed previously we prefer to analyze conductance without dividing it for the bias independent conductance of the N/N junction. This would amount to simply multiply our conductance for a factor $\sim (1+Z^2)$. The reader can also notice that our definition $Z = 2m'H\pi^2/(\hbar^2 k'_F)$ include a π^2 factor which is absent in BTK paper [141] so in order to compare our results with others one has to take into account that our values of Z are approximately ten times the ones in BTK when the same interfacial scattering is considered.

The N/S case in 1D is shown in Fig. 2.4 where conductance as a function of ε/Δ_0 is shown. Here ε is the quasiparticle energy with respect to Fermi energy and is related to bias voltage, i.e. $\varepsilon = eV$. As clear form the $Z = 0$ curve in Fig. 2.4 for subgap energies only AR is possible and $G = 2$ while for larger energies single particle transmission as electron-like quasiparticle (ELQ) and hole-like quasiparticle (HLQ) are possible and they become the only processes for sufficiently large voltages, i.e. $G \to 1$ for $\varepsilon \gg \Delta_0$. The effect of a finite Z is to suppress conductance everywhere (so it hinders both ARs for subgap energies and single particle transmission for energies above the gap) except at the gap edge, i.e. $G(\varepsilon = \Delta_0) = 2$, $\forall\, Z$. The last properties in no more true in 2D or 3D because angular average lowers the conductance being more sloping trajectories more sensitive to Z as explained before.

We move on to analyze the total angle averaged conductance $\langle G\rangle = \langle G_\uparrow\rangle + \langle G_\downarrow\rangle$ in F/S. This is plotted in Fig. 2.5 in the limit of full transparency of the barrier (left panel) and for an intermediate value of Z (right panel). Three values of magnetization M and both magnetic mechanisms are considered as shown in the legend which refers to the six points highlighted in Fig. 2.3 and listed in Table 2.I. Blue curves are for $M = 0.25$ (solid lines for a Stoner ferromagnet (STF) and dashed for a spin bandwidth asymmetry ferromagnet (SBAF)) and so on. Comparing the behavior of a SBAF/S and a STF/S junction, we find qualitative deviations in the

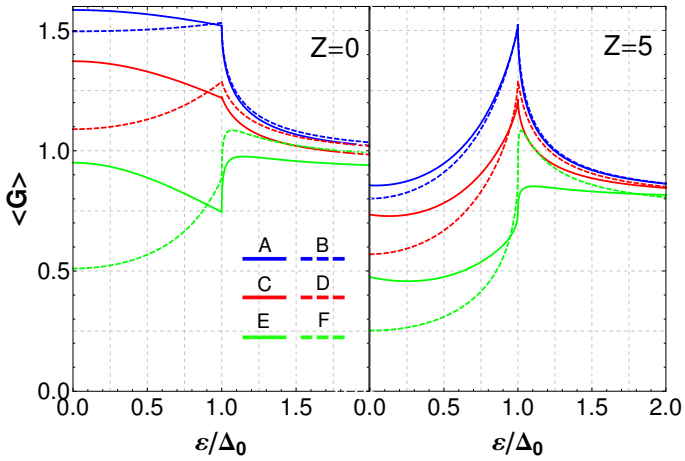

Figure 2.5. Averaged differential conductance spectra for a junction with a s-wave superconducting electrode, evaluated in the states corresponding to the six points indicated in Fig. 2.3 and listed in Table 2.I, in the metallic limit $Z = 0$ (left panel) and for intermediate barrier transparency $Z = 5$ (right panel).

subgap charge conductance which become more and more significant as increasing values of the magnetization and high barrier transparency is considered. Indeed, in this case the averaged differential conductance is a monotonically increasing function when the F-side is a SBAF, whereas the same quantity in the STF case an opposite behavior being a decreasing function of ε/Δ_0. In general one sees that both the first and second derivatives of the subgap conductance spectra have opposite signs for a standard STF and for a SBAF when $Z = 0$. The net effect of bandwidth asymmetry is to move the junction towards the tunneling regime, e.g. the junction behaves as if $Z \neq 0$, as can be clearly seen by a comparison with the right panel or with Fig. 2.4. This implies that one can in principle use a F/S junction, in the metallic limit, as an efficient tool to discriminate the existence of a mass asymmetry contribution in the F-side of the junction because spectra associated with it should appear more "tunneling-like" with respect to the case of Stoner exchange. This kind of consideration is supported from looking at the $Z = 5$ case in Fig. 2.5 where it is shown that even if now the spectra associated with the two magnetic mechanism are qualitatively similar, when a bandwidth asymmetry ferromagnet is considered the conductance is always lower that the one corresponding to a Stoner ferromagnet as if the former was referring to a stronger interface scattering. This is indeed the case because when a mass mismatch is introduced the Fermi velocities in the two leads are different and this renormalizes the interface scattering Z [140]. Larger Z values can give rise to spin filtering effects which will be analyzed in Chap. 3.

2.5.2. d-wave superconducting electrode

It is well known [142, 143] that in N/S junctions involving a normal metal and a d-wave superconductor with line nodes perpendicular to the interface, a zero-bias conductance peak (ZBCP) develops in the tunneling limit, this peak becoming narrower and narrower as increasing values of the interfacial barrier strength are

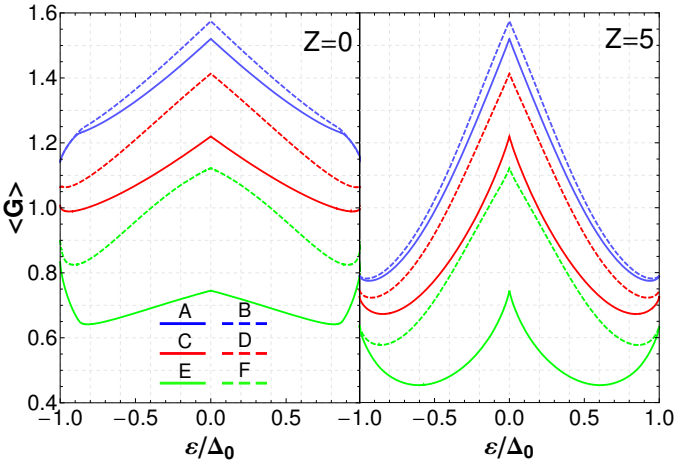

Figure 2.6. Averaged differential conductance spectra for a junction with a $d_{x^2-y^2}$-wave superconducting electrode, evaluated in the states corresponding to the six points indicated in Fig. 2.3 and listed in Table 2.I, in the metallic limit $Z = 0$ (left panel) and for intermediate barrier transparency $Z = 5$ (right panel).

considered. This ZBCP is the consequence of the presence of an Andreev bound state [144] (ABS) at the Fermi energy, induced by the change in sign of the pair potential across line nodes. It implies that electron-like and hole-like quasiparticles specularly reflected at the interface always find the "right" sign of the pair potential to be Andreev reflected. In this case the ABS is at the same energy for every quasiparticle trajectory, i.e. for every angle θ. When the normal metal in the junction is replaced by a ferromagnet, the ZBCP is lowered because of the presence of spin polarization which inhibits ARs and can be splitted in two sub-peaks developing symmetrically at finite energies, [128, 129] depending on interfacial scattering strength. [3] The splitting of the ZBCP is clearly visible in the angle-resolved charge conductance, while in the angle-averaged one it is distinguishable only in particular cases (see Chap. 3). When the interface barrier strength Z is reduced, this structure becomes better defined since the two peaks get more separated, though less pronounced. We remind that, when the superconducting electrode has d-wave symmetry, the pair potential felt by electrons (+) and holes (−) is $\Delta_{\sigma,\pm} = \Delta_0 \cos[2(\theta'_\sigma \mp \beta)]$, where β is the angle formed by the crystallographic a axis of the superconductor with the x axis (see Fig. 2.1). We here fix $\beta = \pi/4$ to analyze a $d_{x^2-y^2}$-wave superconductor with line nodes perpendicular to the interface. In Fig. 2.6 we show the averaged differential conductance spectra evaluated at the six points highlighted in Fig. 2.3 and listed in Table 2.I, in the limit of full transparency of the barrier (left panel) and for an intermediate value of Z (right panel). Comparing the behavior of a SBAF/$d_{x^2-y^2}$ and a STF/$\mathrm{d}_{x^2-y^2}$ junction, we find deviations in the charge conductance which become more and more significant as increasing values of the magnetization and of the barrier strength are considered. It is found that

[3] Other causes for peak splitting that do not involve magnetism are line nodes not perpendicular to the interface or presence of secondary component in superconducting order parameter breaking time reversal symmetry.

with the increase of the magnetization the ZBCP is lowered rapidly and eventually smeared out in the STF case, whereas in the SBAF case the ZBCP is more robust against the polarization of the F-side and appears more narrow. The drop of the zero bias conductance may be understood considering that the ARs probability amplitude decreases with increasing spin polarization (the AR processes for the incident majority electrons is suppressed while the AR for minority electrons still contributes to the ZBCP). This is represented in BTK-type models by a suppression in the Andreev term coefficient of conductance with increasing polarization. This picture is slightly modified when a SBAF is considered, since in this case the barrier, according to Eq. 2.7, is renormalized and can assist the conductance of the two spin channels in a different way. This effect results into a charge conductance always larger than the one obtained in the corresponding STF case with the same magnetization M. Finally, we notice that with increasing Z, i.e. when we move from the metallic limit towards the tunneling one, the averaged charge conductance here obtained reproduces the well-known behavior previously reported in the literature [127, 126].

2.5.3. Time reversal breaking superconducting electrodes

It is generally accepted that for many unconventional superconductors a subdominant component of the order parameter breaking time-reversal symmetry can be induced whenever translational symmetry is broken, e.g. near surfaces, interfaces and vortices [74, 75, 148]. For some materials, such as e.g. YBCO [40], there is controversy about the symmetry of the secondary component, namely if the order parameter is of the $d_{x^2-y^2} + is$- or $d_{x^2-y^2} + id_{xy}$-wave type. Furthermore, the splitting of the ZBCP, leading to the formation of symmetric peaks at finite bias, has been interpreted [39, 145, 146] as a signature of the admixture of an imaginary pair potential component with the dominant $d_{x^2-y^2}$-wave one, corresponding to a time-reversal broken symmetry state [74, 147]. The peak splitting reflects the fact that the zero-energy states are shifted by a positive or negative amount due to the Doppler shift of a finite vector potential, and the good agreement between theory and experiments suggests that the existence of broken time reversal states (BTRSs) is a plausible explanation for the origin of the peak splitting of the charge conductance. Thus, motivated by the fact that charge transport in junctions with a superconducting electrode could be a valuable probe of the order parameter symmetry, we compare here transport through F/S junctions having $d_{x^2-y^2} + is$ or $d_{x^2-y^2} + id_{xy}$ BTRS states in the S side and a SBAF or a STF in the F side. When the superconducting electrode has $d_{x^2-y^2} + is$- or $d_{x^2-y^2} + id_{xy}$-wave symmetry, the pair potential felt by electrons $(+)$ and holes $(-)$ is $\Delta^s_{\sigma,\pm} = \Delta_1 \cos[2(\theta'_\sigma \mp \pi/4)] + i\Delta_2$ and $\Delta^d_{\sigma,\pm} = \Delta_1 \cos[2(\theta'_\sigma \mp \pi/4)] + i\Delta_2 \sin[2(\theta'_\sigma \mp \pi/4)]$, respectively. We have analyzed spectra for several values of Δ_1 and Δ_2 but for brevity we show here the results only for $\Delta_1 \approx 0.968\Delta_0$ and $\Delta_2 = 0.25\Delta_0$. We notice that for this choice of Δ_1 and Δ_2 the gap amplitude is Δ_0 for $\theta' = \pi/4$. In Fig. 2.7 the averaged charge conductance is plotted considering the two above-mentioned BTRS superconductors for a F/S junction with a STF (left panel) and a SBAF (right panel), for two representative values of the barrier strength Z and for a magnetization M equal to 0.5 such that the panels refers to C and D points of Fig. 2.3 listed in Table 2.I. An inspection of this figure suggests that, for high Z, the junction exhibits for both kinds of ferromagnet a zero-bias charge response different for the

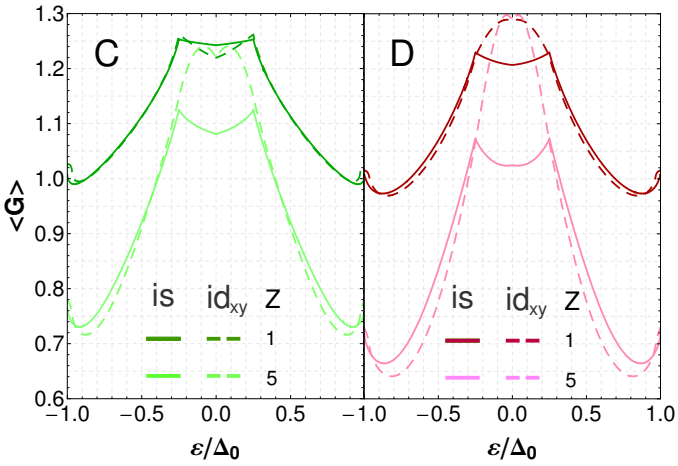

Figure 2.7. Averaged differential conductance spectra for a junction with a $d_{x^2-y^2}+is$ (solid lines) and a $d_{x^2-y^2}+id_{xy}$ (dashed lines) superconducting electrode, evaluated at the points C (STF, left panel) and D (SBAF, right panel) indicated in Fig. 2.3, in the intermediate (Z=5) and high transparency (Z=1) regime. We recall that the magnetization is M=0.5 for both panels.

two BTRS states, implying that STF/S or SBAF/S junctions are equally useful to discriminate between BTRS order parameters involved in the S-side. In the low-barrier limit, the spectra for the two BTRS states almost coincide for a STF, while for a SBAF they are clearly more distinguishable. Therefore, we can state that in the high transparency limit a SBAF/S junction may be seen as a more powerful tool than a STF/S one to discriminate between the two BTRSs. The origin of the different behavior of the conductance at zero bias for STF and SBAF electrodes lies in an ABS at zero energy which is present in the case of $d_{x^2-y^2}+id_{xy}$-wave symmetry (only for particular angles [149]), but not in the $d_{x^2-y^2}+is$ one. As explained In Sec. 2.5.1, this effect is clearly visible for a SBAF, because this kind of ferromagnetic electrode introduces an extra effective barrier which affects the charge transport of the hybrid structure, and pushing actually the junction toward the tunneling regime where ABSs become the dominant channel for transport.

CHAPTER 3

Spin filtering effects in SBAF/S

This Chapter is devoted to analysis of spin filtering effect in ballistic 2D F/S junctions. In particular we show that when F is a spin bandwidth asymmetry ferromagnet (SBAF) these effects exist even if the interface is non magnetic. In this Chapter we focus on conventional s-wave and unconventional d-wave superconducting order parameter symmetry in S.

3.1. Physical origin of spin active interface behavior

The physical origin of spin filtering effects in SBAF/S junctions can be seen in the boundary conditions obeyed by wavefunctions at the interface

$$\psi_\sigma^F(0) = \psi_\sigma^S(0) \tag{3.1a}$$

$$\frac{m_\sigma}{m'}\frac{du_\sigma^S}{dx}\bigg|_{x=0} - \frac{du_\sigma^F}{dx}\bigg|_{x=0} = \frac{2H\ m_\sigma}{\hbar^2}u_\sigma^S(0) \tag{3.1b}$$

$$\frac{m_{\bar\sigma}}{m'}\frac{dv_{\bar\sigma}^S}{dx}\bigg|_{x=0} - \frac{dv_{\bar\sigma}^F}{dx}\bigg|_{x=0} = \frac{2H\ m_{\bar\sigma}}{\hbar^2}v_{\bar\sigma}^S(0)\ , \tag{3.1c}$$

where H is the Hamiltonian parameter quantifying scattering strength at the interface. These equations are a generalization to a spin polarized scenario of boundary conditions in semicondutor/N and semicondutor/S junctions [140] in which effective masses, i.e. Fermi velocities, are assumed to be different in the two leads. The net effect of this mismatch ia a renormalization of interfacial scattering. If the first electrode manifests spin polarization and it is a Stoner ferromagnet (STF) this effect is absent while if it is a partial of pure spin bandwidth asymmetry ferromagnet (SBAF) this effect is doubled in the sense that there are two renormalizations of interfacial scattering which are different for up and down quasiparticles. This case is analogous to a junction without mass mismatch but with a ferromagnetic insulator (FI) with spin splitted interfacial scattering potentials, i.e. $H \to \{H_\uparrow, H_\downarrow\}$. Consequently mass mismatch may mimic a spin active barrier, in the sense that electrons with opposite spin feel different values of the barrier height values. While in a STF spin polarization and spin sensitive interfacial scattering are separated phenomena, in SBAF they are intimately connected since considering a mass mismatch turns on both features. Indeed a junction with a mass mismatch ferromagnet can induce an effective spin active interface, which for specific choices of H will produce spin filtering effects. The dimensionless parameter $Z = 2m'H\pi^2/(\hbar^2 k'_F)$ in what follows will conveniently characterize the strength of the interfacial scattering.

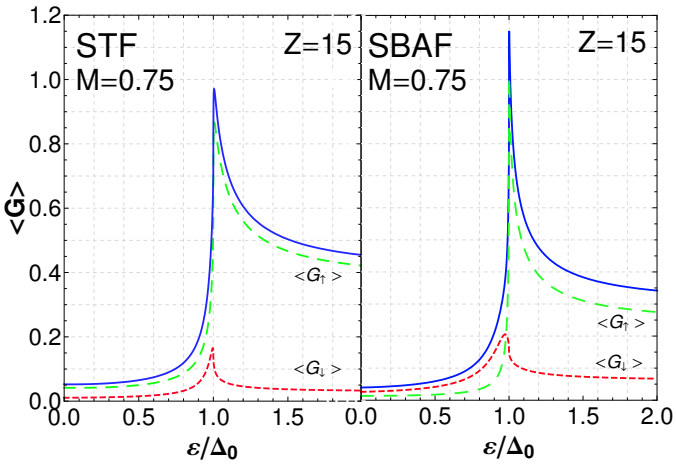

Figure 3.1. Spin-dependent charge conductance spectra and total averaged conductance spectrum (full lines) for a F/S junction. The left and the right figures refer to the cases of a Stoner-like ferromagnet ($U/E_F = 0.75, m_\uparrow/m_\downarrow = 1$) and of a spin bandwidth asymmetry ferromagnet ($U/E_F = 0, m_\uparrow/m_\downarrow = 7$), respectively. In both cases we have fixed $Z = 15$ and $M = 0.75$.

3.2. Spin filtering in junction with conventional superconductors

We start by considering the case of an isotropic s-wave superconductor, i.e. $\Delta_{\sigma\pm} = \Delta_0$, coupled to a STF or a SBAF, assuming a moderately large value of the interface barrier strength Z (=15) and a fixed value of the magnetization $M = 0.75$. From the behavior of the averaged charge conductance, reported in Fig. 3.1 together with its two spin-resolved contributions, we see that in the SBAF case (right panel) for energies lower than the energy gap value Δ_0, the component $\langle G_\downarrow \rangle$ associated with the minority down-spin carriers is larger than the component $\langle G_\uparrow \rangle$ associated with the majority up-spin ones, this order relation being reversed for ε larger than Δ_0, approximately. This behavior strongly contrasts with the one observed for the STF case (left panel), where $\langle G_\downarrow \rangle$ is always lower than $\langle G_\uparrow \rangle$. The fact that minority channel can contributes more than majority one to the the conductance as seen for SBAF/S can be counterintuitive being the number of carriers in the majority band larger than the one in minority band. However conductance depends on Fermi velocities and not only on number of carriers this apparently anomalous behavior can readily be interpreted by noticing that in the SBAF case the barrier acquires a spin active character and thus the majority electrons, although larger in number than the minority ones, feel a stronger value of the barrier height, i.e. have a lower Fermi velocity, resulting in a correspondingly reduced charge conductance. We point out that the manifestation of this behavior depends on the actual values of Z and the masses ratio $m_\uparrow/m_\downarrow$. To clarify this point, in Fig. 3.2 we report a density plot for the quantity

$$\Delta I = \frac{\langle I_\downarrow \rangle - \langle I_\uparrow \rangle}{\langle I_\uparrow \rangle}, \tag{3.2}$$

where

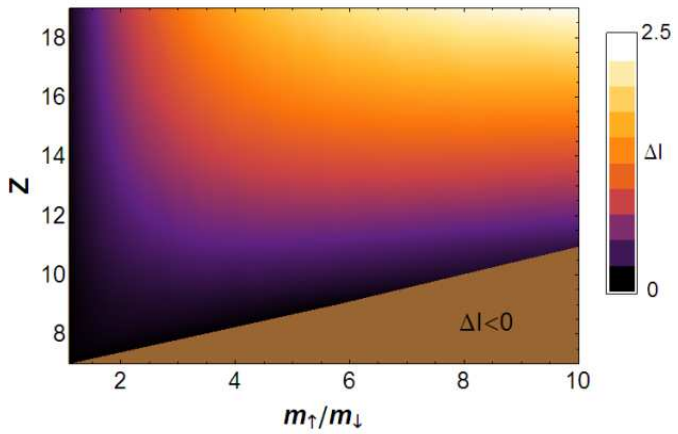

Figure 3.2. Density plot showing the quantity ΔI, defined in Eq. 3.2, as a function of the barrier height Z and the mass ratio $m_\uparrow/m_\downarrow$. Positive values of ΔI correspond to values of the minority spin integrated conductance, i. e. up to Δ_0, larger than the corresponding majority ones. Negative values of ΔI indicate that minority down-spin electrons contribute to the current less than majority up-spin ones (standard case without spin filtering). Colors are associated with the values taken by the quantity ΔI.

$$\langle I_\sigma \rangle = \int_0^{\Delta_0} \langle G_\sigma(\varepsilon) \rangle d\varepsilon \,, \tag{3.3}$$

is the current in the σ channel evaluated at $\varepsilon = \Delta_0$. The quantity ΔI represents the relative gain of minority charge current with respect to majority one. This quantity is always negative, i.e. the standard relation $\langle I_\uparrow \rangle > \langle I_\downarrow \rangle$ holds, for STF/S while it can be positive for SBAF/S, i.e. the "anomalous" relation $\langle I_\uparrow \rangle < \langle I_\downarrow \rangle$ holds. Fig. 3.2 depicts the values of Z and the masses ratio $m_\uparrow/m_\downarrow$ for which the spin filtering effect exists. The brighter the color the larger ΔI. We deduce that above moderately high values of the bare barrier height Z, a low degree of the mass mismatch is already sufficient to give rise to a charge current contribution from minority carriers larger than the one produced by majority ones. The effect being more pronounced for large Z and $m_\uparrow/m_\downarrow$ values. This effects can be effectively probed in F/S junctions being possible to measure the majority and minority channels separately [139].

3.3. Spin filtering in junction with unconventional superconductor

When an unconventional d-wave superconductor is considered in the junction spin filtering effect can be seen yet in the total conductance and there is no necessity to isolate the up and down channels. Indeed it has been shown [127] that in the case of a d-wave superconducting electrode with line nodes perpendicular to the interface, a spin filtering insulating barrier can split the zero bias conductance peak (ZBCP) that characterize the total charge conductance when a non magnetic interface is considered (see Sec. 2.5.2). This splitting is symmetrical in N/S and asymmetrical in F/S and it is created by a downwards (upwards) shifting of ZBCP for majority (minority) carriers.

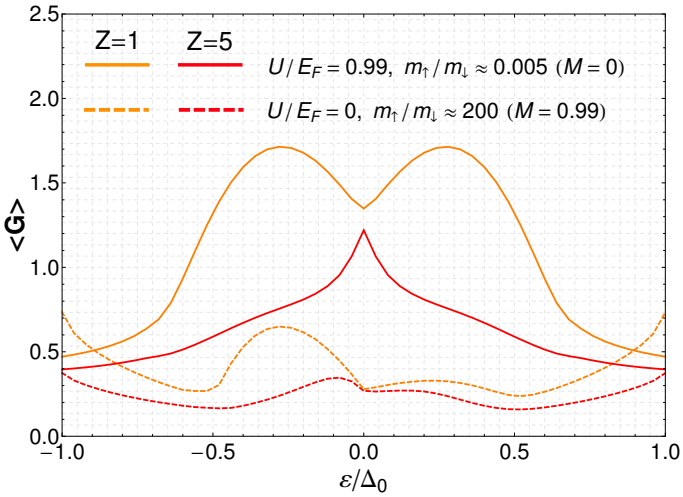

Figure 3.3. Averaged charge conductance curves plotted as a function of the normalized energy (ε/Δ_0) for two values of the barrier height Z, namely Z=1 (orange curves) and Z=5 (red curves). The full lines refer to a N/I/S junction, where the magnetization M=0, whereas the dotted ones correspond to a F/I/S junction with a strong mass mismatch effect and a very large magnetization M=0.99. In both cases we consider a $d_{x^2-y^2}$-symmetry superconductor.

The results obtained in the case of a $d_{x^2-y^2}$-wave superconductor, i. e. $\Delta_{\sigma,\pm} = \Delta_0 \cos[2(\theta'_\sigma \mp \beta)]$ with $\beta = \pi/4$, are presented in Fig. 3.3. The full lines correspond to the case where the F-side is normal, i.e. the magnetization in the ferromagnet is zero as a consequence of the combined counteracting effect of the two microscopic mechanisms, realized here with a suitable combination of the exchange interaction and a vanishingly small value of the mass spin asymmetry ratio. From this figure we observe a symmetric splitting with respect to zero bias of the averaged charge conductance as a consequence of the energy gain for majority spin, and the energy loss for minority ones, produced by the spin sensitive tunneling processes, with the peak splitting disappearing as the barrier height is increased. This is consistent with the results obtained in [127] for N/S with magnetic interface even if in our case insulator is non magnetic and spin filtering effects are exclusively a consequence of mass mismatch. The case of an SBAF/S junction is analyzed here assuming a value of $m_\uparrow/m_\downarrow$ large enough to make the ferromagnet behave almost like an half-metal. In this case the charge conductance profile that we observe (dotted lines in Fig. 3.3) is characterized by peaks of different heights, which moreover are not symmetrically shifted with respect to zero energy. Also in this case the splitting is reduced for larger Z. These results show remarkable similarities to the ones reported in Ref. [127], and thus support our conjecture that a mass mismatch ferromagnet produces effects which are qualitatively similar to the ones obtained with spin active barriers. We also stress that the large value of $m_\uparrow/m_\downarrow$ ($\sim 10^2$) required to get a clear spin active behavior in the 2D case analyzed here, gets considerably reduced in three dimensions. Actually, we have verified that for the same case of large magnetization considered in Fig. 3.3, it becomes lower by about one order of magnitude ($m_\uparrow/m_\downarrow \simeq 30$).

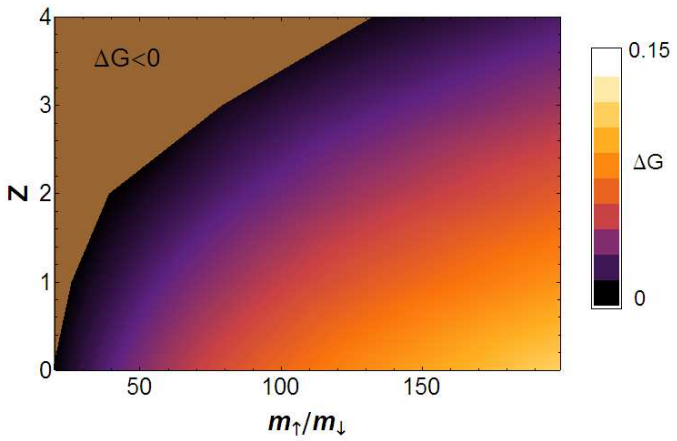

Figure 3.4. Density plot showing the values of Z and $m_\uparrow/m_\downarrow$ for which in a SBAF/I/S junction an asymmetric splitting of zero bias peak appear as a signature of spin–active interface. Colors are associated with the values taken by the discrete right relative increment $\Delta G = (\langle G(\varepsilon = 0.1\Delta_0)\rangle - \langle G(0)\rangle)/\langle G(0)\rangle$.

We remark that also in the case of a $d_{x^2-y^2}$-wave superconductor, the results depend on the choice of the microscopic parameters of the model. To clarify this point in Fig. 3.4 we draw a density plot giving the values assumed by the discrete right increment of the averaged charge conductance at the origin, namely $\Delta G = (\langle G(\varepsilon = 0.1\Delta_0)\rangle - \langle G(0)\rangle)/\langle G(0)\rangle$, as a function of Z and $m_\uparrow/m_\downarrow$. The quantity ΔG being positive only when ZBCP splitting takes place. We infer that in the limit of low transparency of the barrier ($Z \geq 3.5$), ΔG is always negative until the masses ratio is as large as ~ 100 indicating that the peak in the averaged conductance is easily located at zero bias. On the other hand, for high barrier transparency, the subtle interplay between Z and $m_\uparrow/m_\downarrow$ gives rise to the peak splitting discussed above, which is here signalled by a positive value of ΔG. As a final consideration, we note that the features observed when a $d_{x^2-y^2}$-wave superconductor is considered, differently from the s-wave case, are visible especially in the limit of high transparency because in the tunneling limit only zero-energy Andreev bound states contribute to transport and this is unaffected by magnetization and/or spin active scattering at the interface, as pointed out in Ref. [127].

CHAPTER 4

Spin transport in F/S

This Chapter is devoted to analysis of spin transport in ballistic 2D F/S junctions. In particular we focus on differences deriving from a different magnetic mechanism in F. We will consider both a Stoner ferromagnet (STF) and spin bandwidth asymmetry ferromagnet (SBAF) with mass mismatch of oppositely polarized carriers (see Sec. 1.2). We will consider different symmetries in S, namely conventional s-wave, $d_{x^2-y^2}$-wave with line nodes perpendicular to the interface, and broken time-reversal states (BTRSs) with s- or d_{xy}-wave minority component, e. g. $d_{x^2-y^2}+is$-wave and $d_{x^2-y^2}+id_{xy}$-wave (see Sec. 1.1). System, formalism and notation is the same of Chapter. 2

4.1. Spin differential conductance

The spin conductance in F/S can be estimated similarly to the charge conductance when BTK approach is used. Once probability amplitudes a_σ, b_σ, c_σ, and d_σ for an electron with spin σ to undergo AR, normal reflection, transmission as ELQ, and transmission as HLQ, respectively, are calculated, the spin differential conductance at $T=0$ for spin orientation can be expressed as

$$\Sigma_\sigma(\varepsilon,\theta)=P_\sigma\left(1-\frac{k^F_{\bar\sigma,x}}{k^F_{\sigma,x}}\,|a_\sigma(\varepsilon,\theta)|^2-|b_\sigma(\varepsilon,\theta)|^2\right), \tag{4.1}$$

where θ is the angle formed by the momentum of the electrons propagating from the F side with respect to the normal to the interface (see Fig. 2.1), and the partial polarization $P_\sigma=n_\sigma/(n_\uparrow+n_\downarrow)$ is the fraction of electrons occupying the σ spin band of the metallic ferromagnet. Differently from charge conductance (see Eq. 2.8) AR contribution has a negative sign, i.e. ARs hinder spin current. This can be understood as follows: when ARs take place Cooper pairs in S are transmitted and they are in a singlet state. The situation could appear paradoxical from the point of view of F because when there is AR spin σ electrons propagating in one direction results in $\bar\sigma$ holes propagating in the opposite direction and the two contributions should sum up rather than cancel out each other. Indeed this is the case if one consider that $\bar\sigma$ holes have spin σ, e.g. destroying an electron in the $\bar\sigma$ band has the same effect of creating it in σ band. This can be demonstrated as follows: consider a polarized state $|M\rangle$ in F

$$S_z|M\rangle=\hbar M|M\rangle. \tag{4.2}$$

From the commutation relations

$$[S_z, c^\dagger_{k,\sigma}] = \sigma \frac{\hbar}{2} c^\dagger_{k,\sigma}, \tag{4.3}$$

$$[S_z, c_{k,\sigma}] = -\sigma \frac{\hbar}{2} c_{k,\sigma}, \tag{4.4}$$

it follows that the states $c^\dagger_{k,\sigma}|M\rangle$ and $c_{k,\bar{\sigma}}|M\rangle$ which represents states with a spin σ electron and a spin $\bar{\sigma}$ hole are still eigenstates of S_z with *the same* eigenvalue

$$S_z\left(c^\dagger_{k,\sigma}|M\rangle\right) = S_z\left(c_{k,\bar{\sigma}}|M\rangle\right) = \hbar\left(M + \frac{1}{2}\right)|M\rangle. \tag{4.5}$$

The total net spin conductance is defined as

$$\langle\Sigma(\varepsilon)\rangle \quad = \quad \langle\Sigma_\uparrow(\varepsilon)\rangle - \langle\Sigma_\downarrow(\varepsilon)\rangle \tag{4.6}$$

where

$$\langle\Sigma_\sigma(\varepsilon)\rangle = \int_{-\theta_C^\sigma}^{\theta_C^\sigma} d\theta \ \cos\theta \ \Sigma_\sigma(\varepsilon,\theta) / \int_{-\theta_C^\sigma}^{\theta_C^\sigma} d\theta \ \cos\theta, \tag{4.7}$$

and θ_C^σ is the critical angle for the transmission of σ-spin electrons.

The spin conductance here defined is dimensionless and normalized in the range $[0, 1]$. The maximum values is reached for a fully polarized F, i.e. an half metal, no interfacial scattering, i.e. $Z = 0$, and energies much larger than the superconducting gap $\varepsilon \gg \Delta_0$. For a generic F with spin polarization M the range of possible values for spin conductance is $[0, M]$ as can be seen by Eq. 4.6. The spin current in our setup is a quasiparticles current and not a spin supercurrent because in a singlet superconductor only single particle states can be spin polarized having Cooper pairs zero spin. This is different from charge transport where conversion from quasiparticles current to supercurrent can take place at the interface and the charge conductance of F/S is enhanced by S presence with respect to a F/N junction. Spin conductance in F/S instead is hindered by S with respect to a F/N. Indeed maximum value of spin conductance in F/S is reached in the limit $\varepsilon \gg \Delta_0$ where S behaves mostly like N. Spin supercurrent can be present in junctions with triplet superconductors and/or spin flip scattering at the interface, the two favoring the propagation of triplet Cooper pairs in S. Nonetheless the analysis of spin conductance in F/S with singlet superconductor is important both as an analysis of possible unconventional symmetries in S and for device applications as spin current switches which can turn on and off a spin current through the junction without modifying charge conductance.

4.2. SBAF/S vs. STF/S

We have analyzed the averaged spin conductance defined in Eq. 4.6, for different symmetries in S, namely s-wave, $d_{x^2-y^2}$-wave with line nodes perpendicular to the interface, and broken time-reversal states (BTRSs) with s- or d_{xy}-wave minority component, e. g. $d_{x^2-y^2} + is$-wave and $d_{x^2-y^2} + id_{xy}$-wave (see Sec. 1.1). The amplitudes of majority and minority components are fixed as explained in Sec. 2.5.3. Although several choices of the magnetization M in the F electrode and of the barrier strength Z have been considered, in Fig. 4.1 we limit ourselves to the presentation of the spin conductance curves in the case $M = 0.75$ and $Z = 5$. From

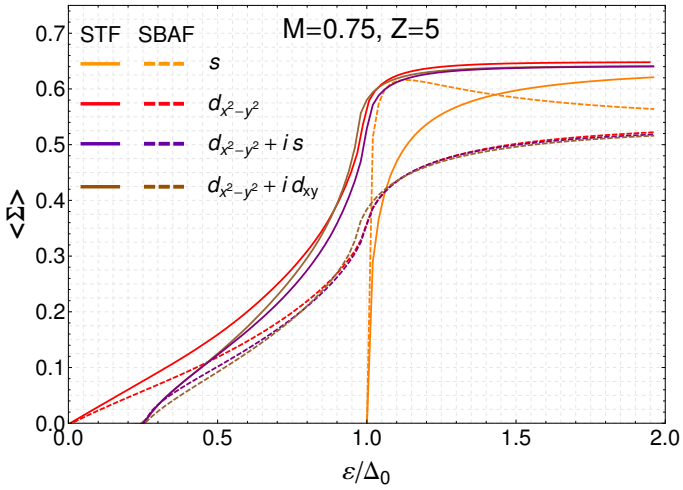

Figure 4.1. Averaged differential spin conductance spectra evaluated at $M = 0.75$ and $Z = 5$ for different type of F electrodes. Solid lines are for STF and dashed lines for SBAF. Conventional and unconventional superconducting electrodes are considered.

previous discussion it can be easily understood that larger Z (M) values lower (enhance) spin conductance. In this figure solid and dashed lines refer to the case of a junction with a Stoner ferromagnet (STF) and with a spin bandwidth asymmetry ferromagnet (SBAF), respectively, the different colors being associated with different superconducting order parameter symmetries. The averaged differential spin conductance for a junction with an s-wave superconductor (orange curves) shows that $\langle\Sigma(\varepsilon)\rangle$ is always zero below the energy gap; indeed in such a situation the electrons cannot enter the S side as quasiparticles because there are no quasiparticles states in the gap. Nevertheless, by Andreev reflection, they can cross the interface and decay into the singlet Cooper pair condensate, thus preventing a spin current flow. For $d_{x^2-y^2}$-wave pairing (red curves), the spin conductance is non-vanishing at every finite bias and its profile exhibits, at low biases, the well-known V-shaped behavior typically produced by the gapless excitations associated with nodes of the order parameter. On the other hand, for the two BTRSs considered here (purple and brown curves) the spin conductance starts being non-zero at a finite bias, corresponding to the energy of the time reversal breaking minority component of the superconducting pair potential. This feature can be exploited to determine if a d-wave superconductor has minority component breaking time reversal symmetry. We see that BTRSs behave as s-wave and pure d-wave for voltages smaller and larger than minority component, respectively. The spin conductance of two BTRS states is very similar even if only one of them has zero energy Andreev bound state (ABS). Even in the d-wave case there is no trace of the zero energy peak seen in charge conductance deriving from ABS. Indeed ABS has no effect on spin conductance being it related to Andreev reflections which are detrimental for spin transport in singlet superconductors. For the three kinds of unconventional pairing symmetries considered here, the spin conductance is always larger for a junction with a STF than for a junction with a SBAF. Above Δ_0 this difference in magnitude gets appreciably larger, and for a given kind of ferromagnet $\langle\Sigma(\varepsilon)\rangle$ becomes practically

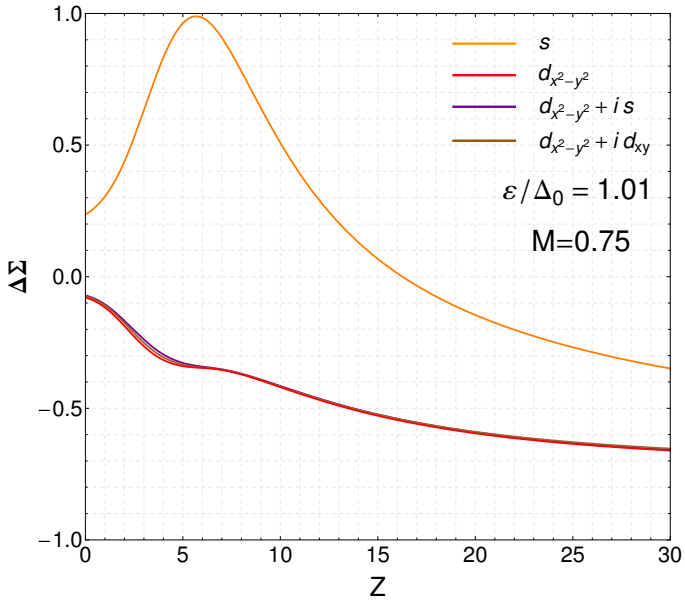

Figure 4.2. Relative gain in spin conductance of a SBAF with respect to a STF, $\Delta\Sigma = (\langle\Sigma(SBAF)\rangle - \langle\Sigma(STF)\rangle)/\langle\Sigma(STF)\rangle$, as a function of the barrier height Z, at a bias value immediately above the energy gap Δ_0, i. e. $\varepsilon = 1.01\Delta_0$ and $M = 0.75$.

independent on the specific unconventional pairing symmetry. For conventional S instead in a limited range of voltages immediately above the energy gap a junction with a SBAF can support a larger spin current than a junction with a STF. This point is deepened in Fig. 4.2. It shows the relative gain in the spin conductance of the SBAF spin conductance $\langle\Sigma(SBAF)\rangle$ with respect to the STF one $\langle\Sigma(STF)\rangle$, defined as $\Delta\Sigma = (\langle\Sigma(SBAF)\rangle - \langle\Sigma(STF)\rangle)/\langle\Sigma(STF)\rangle$, as a function of the barrier height at a fixed bias ε/Δ_0=1.01 immediately above the energy gap Δ_0, and for $M = 0.75$. We see that for a barrier height Z lower than approximately 15 the gain is positive, i.e. spin current in SBAF/S is larger than the one in F/S, only for an s-wave superconductor and it can be as high as 100%. We have checked that this peculiar effect is related to the presence of the superconducting electrode. Indeed, analyzing the spin conductance in STF/N and SBAF/N junctions, i.e. junctions where the superconductor is replaced by a normal metal, we have found that in the STF case the spin current is always greater than in the SBAF one. Looking separately at Andreev and normal reflection probabilities, we have verified that this extra spin current can be ascribed to the fact that majority electrons coming from a SBAF have a lower probability of being normally reflected at the gap edge, while electrons coming from a STF have a finite residual probability to undergo the same process. Being this probabilities a continuous function of energy, the probability of transmission immediately above the gap for electrons coming form a SBAF is larger.

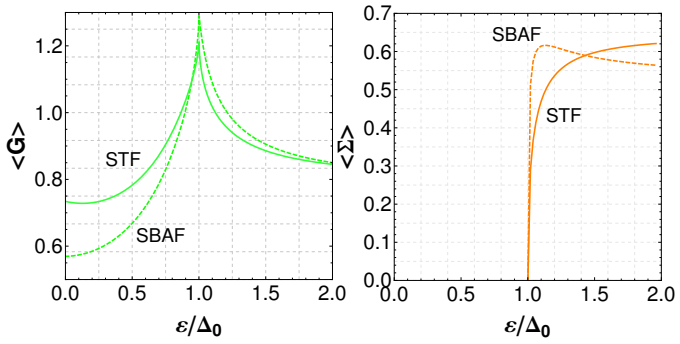

Figure 4.3. Comparison of charge and spin conductances for *s*-wave superconducting electrode suggesting that such a junction can work as a spin current switch. See Section 4.3 for more details. Same parameters values of Fig. 4.1 are adopted.

4.3. Spin current switch

For spintronics applications, the ability to perform operations acting on spin currents but not on charge currents is in general highly desirable. The results presented above allow to individuate a particular situation where this is possible using F/S junctions. For an *s*-wave superconductor in the case of a finite barrier strength, it has been recognized that the charge conductance is peaked around the gap edge [96, 131, 126]. On the other hand, we have previously shown that the spin current is zero below the energy gap Δ_0 and rises abruptly just above it. The charge and spin conductance for the same parameters are compared in Fig. 4.3. Being the charge conductance peaked around gap edge, it is possible to find two bias values $\varepsilon_{\text{off}} < \Delta_0$ and $\varepsilon_{\text{on}} > \Delta_0$ such that charge conductance is the same when the junction bias is switched between the two values. This bias values are in principle different for SBAF and STF but they will always be very close to the gap edge from the left (ε_{off}) and the right (ε_{on}). Right panel of Fig. 4.3 shows that spin conductance instead is zero below the gap and finite above the gap so by switching between ε_{off} and ε_{on} one activate a spin current while the charge conductance remains unaffected. Since the upper bias ε_{on} corresponding to the "on" state of the switch falls only slightly above Δ_0, we expect that the spin current through the device will be much larger if it is generated by a SBAF rather than by a STF, given the appreciable difference between the two cases visible in Fig. 4.2.

Part II results summary and discussion

In this Part of the dissertation we have investigated the charge and spin transport in F/S junctions for different types of itinerant ferromagnets and superconductors. Such kind of system may be easily realized using well consolidated fabrication procedures and standard measurements can be performed on it. We have considered both a Stoner ferromagnet (STF) and a spin bandwidth asymmetry ferromagnet (SBAF) as F lead and conventional s-wave, $d_{x^2-y^2}$-wave with line nodes perpendicular to the interface, and broken time-reversal states (BTRSs) with s- or d_{xy}-wave minority component, e.g. $d_{x^2-y^2}+is$-wave and $d_{x^2-y^2}+id_{xy}$-wave, order parameter symmetries in S. The analysis has been performed developing an extension of the standard BTK approach to the case of a ferromagnetic electrode exhibiting either a standard Stoner exchange mechanism or a mass mismatch-driven ferromagnetism and solving the corresponding BdG equations. A special emphasis has been devoted to the different roles played by the exchange splitting and spin dependent mass asymmetry in F. Our analysis has revealed several differences between the two cases. Our results suggest that the junction with conventional S can be considered an efficient device to probe mechanism behind the itinerant ferromagnetism. Moreover we have explained how a direct measurement of spin polarization in F and of its mass mismatch contribution is possible without a fitting procedure by measuring with focused currents critical angles for Andreev reflection (AR) and transmission. When $d_{x^2-y^2}$-wave S is considered, we have found that the zero bias conductance peak (ZBCP) in charge conductance is narrower and higher when the F lead is SBAF rather than STF. This finding being potentially useful for the experimental detection of a mass mismatch contribution to the magnetization. Since AR is phase sensitive, the onset and amplitude of Andreev bound states (ABSs), manifesting themselves in the ZBCP, is a signature of the symmetry of the order parameter. For this reason, we have also investigated the transport properties of a junction with a superconductor exhibiting a broken time-reversal symmetry of $d_{x^2-y^2}+is$ or $d_{x^2-y^2}+id_{xy}$ type motivated by the fact that such realizations can characterize several high-T_c cuprates. In the high transparency limit, we have found a different behavior around zero bias of SBAF/$d_{x^2-y^2}$+id_{xy} and STF/$d_{x^2-y^2}$+id_{xy} junctions, such that the use of a SBAF allows to discriminate more efficiently between BTRSs with $d_{x^2-y^2}+is$ or $d_{x^2-y^2}+id_{xy}$ pairing symmetry than STF does. Indeed, as previously discussed a SBAF ferromagnetic electrode with mass mismatch introduces an extra effective barrier which affects the charge transport of the hybrid structure, driving the junction toward a tunneling regime where ABS (existing in $d_{x^2-y^2}+id_{xy}$ and not in $d_{x^2-y^2}+is$ case) is the dominant channel for transport. We have shown that this spin dependent masses renormalization in F, can give rise to spin filtering effects in F/S which are not manifested when a standard Stoner ferromagnet is

considered allowing to conclude that the presence of bandwidth asymmetry in F may mimic the behavior of a spin active barrier. This is achieved as a consequence of the fact that the mass asymmetry between up and down spin electrons entering explicitly the boundary condition equations, make electrons with opposite spin feel different values of the barrier height, eventually resulting in a spin filtering effect. When the S side is an isotropic s-wave superconductor, we have shown that for biases lower than the gap amplitude Δ_0, SBAF/S conductance associated with the minority spin carriers can be larger than for the majority spin ones, this ordering being reversed when biases larger than Δ_0 are considered. This result suggests that a junction with a mass mismatch ferromagnet induces an effective spin-active interfacial effect. Nevertheless, this result requires a cooperative effect between the barrier and the mass mismatch: above moderately high barrier height, low values of the mass ratio are already able to produce a minority-spin charge conductance component larger than the corresponding majority-spin one. In general the effect is more clear in the tunneling limit. When a $d_{x^2-y^2}$-wave order parameter for the S side is considered, splitting of ZBCP of charge conductance is found. This splitting is symmetric if the F layer has no net spin polarization (by tuning carefully exchange splitting and mass mismatch in such a way that they cancel each other out) and asymmetric in the other case, consistently with well known results for magnetic insulating interfaces. Also in this case, the splitting found depends on the interplay between the barrier height and the mass mismatch, and it may disappear in specific regions of the corresponding parameter space. In particular we have shown that these effects are more clear in the metallic limit, differently from the s-wave case. These results suggest that the junction may work as a spin filtering device for charge current. As far as the spin transport is concerned, we have shown that the spin conductance in a STF/S junction is everywhere larger than in a SBAF/S one for all the unconventional superconducting symmetries analyzed here, except, occasionally, for the case of a conventional s-wave superconducting electrode. We have highlighted the relation between spin conductance and existence of nodes and breaking time reversal symmetries in S showing that while ABSs strongly affect charge transport, spin transport is mostly independent on it. We have also shown that a F/S junction with an s-wave superconductor can work as a switch able to turn on and off a spin current, leaving the charge current unchanged. In particular, our results show that for a wide range of interfacial barrier strengths, the spin current passing through the junction when the state of the switch is "on" is larger if the ferromagnetic electrode is a SBAF rather than a STF. This relative increase in spin current can be very high, and for particular values of the barrier strength a gain of up to 100% can be reached. We believe that our findings can turn out to be relevant for the experimental probe of specific features of magnetic and superconducting materials, e.g. the knowledge of the charge response at different values of the spin polarization may be used to perform high sensitive magnetization or supercondcuting gap amplitude and phase measurements. Our results suggest also that an F/S junction with a SBAF may represent an important tool for the manipulation of the spin degrees of freedom in solid state systems, as concerns both spin and charge transport. They can also prove to be useful in spintronic applications and devices requiring an efficient way of controlling separately charge and spin currents. Given the increasing number of experimental investigations in this rapidly

growing field, we believe that our results may provide a useful contribution to the comprehension of some relevant phenomena involving spin polarized tunneling.

Part III

Josephson effect in S/F/S

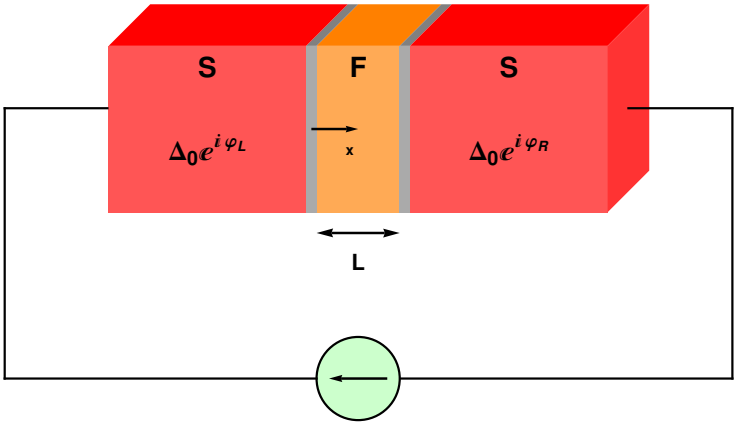

Abstract

In this Part of the dissertation we analyze the dc Josephson effect in a ballistic superconductor/ferromagnet/superconductor junction by means of the Bogoliubov–de Gennes equations in the quasiclassical Andreev approximation. We consider the possibility of ferromagnetism originating from a mass renormalization of carriers of opposite spin, i.e. a spin bandwidth asymmetry. We provide a general formula for Andreev levels which is valid for arbitrary interface transparency, exchange interaction, and bandwidth asymmetry and analyze the current-phase relation, free energy, and critical current, in the short junction regime. We compare the phase diagrams and the critical current magnitudes of two identical junctions differing only in the mechanism by which the mid-layer becomes magnetic. The study is performed by solving the corresponding Bogoliubov–de Gennes equations. Chapter 5 focuses on calculation of Andreev levels and Josephson current in limiting cases, and Chapter 6 is devoted to the analysis of the in fluence of magnetic mechanisms on the Josephson effect. Results are summarized and discussed in the last section of this part at p. 87.

CHAPTER 5

S/F/S junctions and π phase

In this Chapter we focus on Andreev levels and Josephson current of ballistic superconductor/ferromagnet/superconductor (S/F/S) Josephson junctions with conventional superconducting leads. These are systems capable of sustaining a supercurrent carried by Cooper pairs in the superconducting leads and by quasiparticles in the ferromagnetic mid-layer. The unique interplay between ferromagnetic and superconducting orders provides quasiparticles with extra phase shifts absent in junctions with a non-magnetic mid-layer. This can give rise to the appearance of a so-called "$\pi-$phase" [69]. Under such circumstances, the energy minimum of the junction is reached at a phase difference of π across the junction, unlike the standard "0−phase" in junctions with a non-magnetic mid-layer. The existence of the $\pi-$phase has been experimentally confirmed [70, 71]. As far as potential applications are concerned, π-junctions are considered to be candidates for realizing solid state qubits [72].

Previous theoretical studies on S/F/S junctions [150, 151, 152, 153, 154, 155, 156, 158, 159, 160] have described the F layer using the Stoner model of metallic ferromagnetism, with oppositely polarized carriers occupying rigidly shifted bands. However, the interplay of Coulomb repulsion and the Pauli principle driving a metal into a ferromagnetic state, [50] may induce a spin-dependent renormalization of the masses of charge carriers with opposite spins, i.e. a spin bandwidth asymmetry (see Sec. 1.2). This mechanism appears in microscopic approaches where off-diagonal terms of Coulomb repulsion, generally neglected in studies based on the Hubbard model, are taken into account. A mean-field treatment of these contributions in addition to the exchange and nearest-neighbor pair hopping terms shows that quasiparticle energies for the two spin species are not simply splitted but get different bandwidths, i.e. effective masses. The net effect of these interactions is to render the hopping integral in the kinetic term spin dependent through bond charge Coulomb repulsion terms which are different for spin up and down carriers [61]. For low enough temperature and depending on Hamiltonian parameters, ferromagnetic order can be established only through this spin bandwidth asymmetric renormalization [32]. In this picture the ferromagnetism should be understood as kinetically driven, in the sense that it arises from a gain in kinetic energy rather than potential energy, unlike the usual Stoner scheme. We notice that this mass-split metallic ferromagnetism has been experimentally found to be at the origin of the optical properties of the colossal magnetoresistance manganites [162], of some rare-earth hexaborides [161], as well as of some magnetic semiconductors [163]. Spin bandwidth asymmetry will substantially affect the coexistence of ferromagnetism and superconductivity [67], as well as the proximity effect [37] and transport in F/S

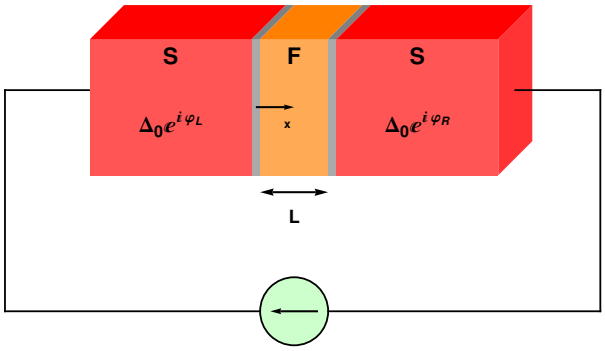

Figure 5.1. A sketch of the current-biased S/F/S junction analyzed, along with notations that are used. The superconductors are treated as reservoirs, whereas the magnetic mid-layer has a finite width L.

bilayers [96, 97], It is also responsible for an extension of the regime in which FFLO phase can be stabilized in heavy-fermion systems [118, 119]. In this Part, we analyze the consequences of this unconventional magnetism in ballistic S/F/S Josephson junctions by solving the Bogoliubov-de Gennes equations [120] for arbitrary spin polarization and interface transparency.

We show that bandwidth asymmetry in the F layer of a S/F/S junction modifies many physical properties such as Andreev levels dispersion, Josephson current and free energy. We provide a general formula for Andreev levels which holds for arbitrary interface transparency, exchange interaction, and bandwidth asymmetry and we calculate the corresponding Josephson current in the short junction regime for some important limiting cases. Comparing the results for a spin bandwidth asymmetry ferromagnet (SBAF) with those obtained for a conventional Stoner ferromagnet (STF), we demonstrate analytically that the former manifest features that are only quantitatively different from the latter for low degrees of polarization, whereas we show numerically that these differences become qualitative in the intermediate/high polarization regime. Then, evaluating the phase diagrams we infer that the mere mechanism by itself is able to shift the ground state superconducting phase difference from 0 to π or viceversa, with a spin bandwidth asymmetry tending to increase the number of possible $0-\pi$ transitions in a fixed range of parameters. We consider also the "mixed" case where in F both magnetic mechanisms are present showing that the features distinguishing pure spin bandwidth asymmetry from pure Stoner ferromagnets may exist even though the spin bandwidth asymmetry contributes only partially to spin polarization.

5.1. Model for ballistic S/F/S

We consider a ballistic Josephson junction composed of a ferromagnetic layer of width L sandwiched between two conventional $s-$wave singlet superconducting electrodes (see Fig. 5.1). Since the S electrodes are isotropic, we will consider an effective one dimensional model. Moreover, our results are independent on the direction of the magnetic moment direction in F. The propagation of quasiparticles

is described by the Bogoliubov-de Gennes equations [120]

$$\begin{pmatrix} H_0^\sigma & \rho_\sigma \Delta \\ \rho_\sigma \Delta^* & -H_0^{\bar\sigma} \end{pmatrix} \begin{pmatrix} u_\sigma \\ v_{\bar\sigma} \end{pmatrix} = \varepsilon \begin{pmatrix} u_\sigma \\ v_{\bar\sigma} \end{pmatrix}, \sigma = \uparrow, \downarrow \quad , \tag{5.1}$$

where $\bar\sigma = -\sigma$, $\rho_{\uparrow(\downarrow)} = +1(-1)$, and $(u_\sigma, v_{\bar\sigma}) \equiv \psi_\sigma$ is the energy eigenstate in the electron-hole space associated with the eigenvalue ε. The single-particle Hamiltonian is

$$H_0^\sigma = H_L + H_F^\sigma + H_R + H_I, \tag{5.2}$$

where

$$\begin{aligned} H_L &= \left[-\hbar^2\nabla^2/2m - E_F\right]\Theta(-x) \\ H_F^\sigma &= \left[-\hbar^2\nabla^2/2m_\sigma - \rho_\sigma U - E_F\right]\Theta(x)\Theta(L-x) \\ H_R &= \left[-\hbar^2\nabla^2/2m - E_F\right]\Theta(x-L) \\ H_I &= H\left[\delta(x) + \delta(x-L)\right]. \end{aligned} \tag{5.3}$$

Here, different effective masses m_σ for σ-polarized particles in the F layer, mimicking bandwidth asymmetry, has been included and U is the exchange interaction, E_F is the Fermi energy, $\Theta(x)$ is the Heaviside step function, m is the effective mass of the quasiparticles in the superconductors, and the parameter H quantifies scattering strength at S/F and F/S interfaces. We assume rigid superconducting order parameters with equal gap amplitude on both sides of the junction, i.e. $\Delta = \Delta_0\left[e^{i\varphi_L}\Theta(-x) + e^{i\varphi_R}\Theta(x-L)\right]$, where $\varphi_{L(R)}$ is the phase of the left(right) superconductor. When considering finite temperature properties, we will assume the usual BCS dependence and let $\Delta_0 \to \Delta_0 \tanh\left(1.74\sqrt{T_c/T-1}\right)$, where T_c is the superconducting critical temperature.

Employing the quasiclassical Andreev approximation [20], the solution of Eqs. (5.1) may be written as

$$\psi_\sigma(x) = \begin{cases} a_\sigma \begin{pmatrix} \rho_\sigma v \\ u \end{pmatrix} e^{ikx} + b_\sigma \begin{pmatrix} u \\ \rho_\sigma v \end{pmatrix} e^{-ikx}, & x < 0 \\ \left[\alpha_\sigma e^{iq_\sigma x} + \beta_\sigma e^{-iq_\sigma(x-L)}\right]\begin{pmatrix} 1 \\ 0 \end{pmatrix} + \left[\gamma_\sigma e^{iq_{\bar\sigma}(x-L)} + \delta_\sigma e^{-iq_{\bar\sigma}x}\right]\begin{pmatrix} 0 \\ 1 \end{pmatrix}, & 0 < x < L \\ c_\sigma \begin{pmatrix} u\ e^{i\varphi/2} \\ \rho_\sigma v\ e^{-i\varphi/2} \end{pmatrix} e^{ik(x-L)} + d_\sigma \begin{pmatrix} \rho_\sigma v\ e^{i\varphi/2} \\ u\ e^{-i\varphi/2} \end{pmatrix} e^{-ik(x-L)}, & x > L \end{cases} \tag{5.4}$$

where

$$u = \sqrt{\frac{\varepsilon + \sqrt{\varepsilon^2 - \Delta_0^2}}{2\varepsilon}},\ v = \sqrt{\frac{\varepsilon - \sqrt{\varepsilon^2 - \Delta_0^2}}{2\varepsilon}}\ , \tag{5.5}$$

and $k = \sqrt{2mE_F}/\hbar$, $q_\sigma = \sqrt{2m_\sigma(E_F + \rho_\sigma U)}/\hbar$ are Fermi wavevectors in the S and F electrodes respectively, and $\varphi = \varphi_R - \varphi_L$. The coefficients a_σ, b_σ, c_σ, and d_σ are the probability amplitudes for Andreev reflection as a hole-like quasiparticle (HLQ), normal reflection as an electron-like quasiparticle (ELQ), transmission to the right electrode as an ELQ, and transmission to the right electrode as an HLQ respectively, while coefficients α_σ, β_σ, γ_σ, and δ_σ are associated with right- and left-going ELQ and HLQ propagating through the ferromagnetic layer. All these

probability amplitudes can be calculated by solving the linear system resulting from the boundary conditions

$$\begin{aligned} \psi_\sigma(0_-) &= \psi_\sigma(0_+) \\ \psi_\sigma(L_-) &= \psi_\sigma(L_+) \\ -\frac{2H}{\hbar^2}\psi_\sigma(0) &= \frac{1}{m}\psi'_\sigma(0_-) - \begin{pmatrix} 1/m_\sigma \\ 1/m_{\bar\sigma} \end{pmatrix} \psi'_\sigma(0_+) \\ -\frac{2H}{\hbar^2}\psi_\sigma(L) &= \begin{pmatrix} 1/m_\sigma \\ 1/m_{\bar\sigma} \end{pmatrix} \psi'_\sigma(L_-) - \frac{1}{m}\psi'_\sigma(L_+), \end{aligned} \tag{5.6}$$

which are valid for a general ferromagnetic electrode displaying both exchange splitting and bandwidth asymmetry. When the latter mechanism is present, electron- and hole-like parts of the wave function derivatives have to be joined separately with different masses. This is analogous to the situation where the insulating barriers are polarized with magnetic moment parallel to the one in the F layer and thus act with different strength on particles with opposite spin [98]. When only exchange splitting is present, i.e. $m_\sigma = m_{\bar\sigma} = m$, the usual form of the boundary conditions is recovered [151].

Our model enables us to take into account both bandwidth asymmetry and exchange interaction in the F layer. Defining the polarization as $M = (n_\uparrow - n_\downarrow)/(n_\uparrow + n_\downarrow)$ and integrating densities of states as calculated from the H_F^σ term in Eq. (5.3), we find that in one dimension and at $T = 0$:

$$M = p_+/p_- \text{ with } p_\sigma = -\rho_\sigma\Big[1 - \rho_\sigma\sqrt{\frac{m_\uparrow}{m_\downarrow}\frac{1+U/E_F}{1-U/E_F}}\Big]. \tag{5.7}$$

For a fixed value of the exchange splitting U, the effect of mass mismatch is to enhance the net polarization for $m_\uparrow > m_\downarrow$, and to hinder it the other way around as shown in Fig. 5.2. Eq. (5.7) describes a general F where both exchange and bandwidth asymmetry are present. We notice that from the same equation we may easily reduce to the cases of a purely exchange ferromagnet (by putting $m_\uparrow/m_\downarrow = 1$ and $U \neq 0$) or a purely bandwidth asymmetry ferromagnet (by putting $m_\uparrow/m_\downarrow \neq 1$ and $U = 0$). We will refer to these two cases as a spin bandwidth asymmetry ferromagnet (SBAF) and Stoner ferromagnet (STF), respectively. Different Josephson effect features are expected in S/STF/S and S/SBAF/S junctions, even for an equally polarized F layer. This is so, since specifying a degree of polarization is equivalent to fix the ratio of Fermi wavevectors $q_\uparrow/q_\downarrow$. However, in a SBAF and in a STF the wavevectors are different, i.e. $q_\sigma^{STF} \neq q_\sigma^{SBAF}$, and accordingly the center of mass momentum acquired by Cooper pairs will be different. In the following, we will also consider finite temperature properties in the range $0 \leq T \leq T_c$. Even if spin polarization (Eq. (5.7)) was derived for $T = 0$, it can be used for $T \leq T_c$, since this quantity varies only slowly on the scale of the superconducting critical temperature as long as $T_M \gg T_c$, with T_M being the Curie temperature. This condition is easily fulfilled in a typical experimental situation where the Josephson junction is realized by a ferromagnetic transition metals compound sandwiched between conventional superconductors, e.g. Niobium. In our analysis, we fix $\Delta_0 = 1$ meV and $E_F = 5$ eV, consistent with the Andreev approximation. The width of the ferromagnetic layer L is not fixed. However the maximum value used in our analysis is such that $L/\xi \approx 0.01$, such that we are in the short junction regime, corresponding to a

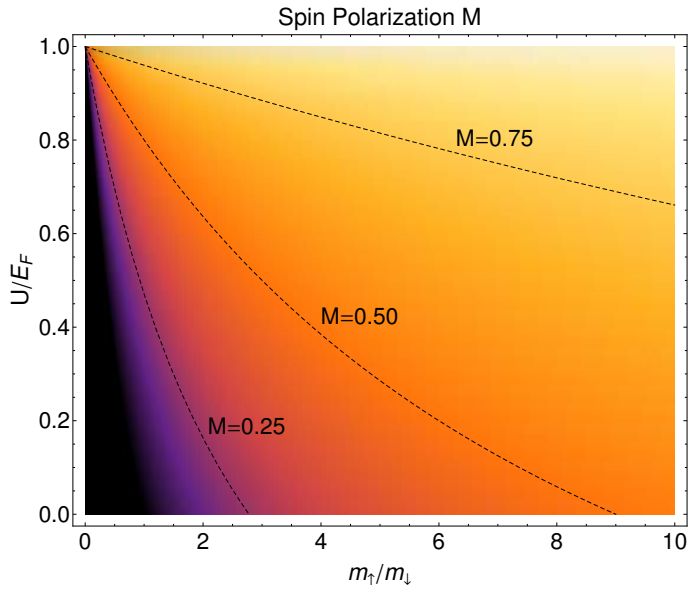

Figure 5.2. Ground state spin polarization density plot as a function of magnetic parameters. Three isomagnetization curves at $M = 0.25, 0.50, 0.75$ are plotted.

width in the range 1–10 nm. We introduce a dimensionless parameter quantifying the scattering strength at insulating interfaces as $Z = 2mH/\left(\hbar^2 k\right)$.

5.2. Andreev levels, free energy, and current–phase relation

We will focus on the short junction regime, i.e. $L \ll \xi$ where ξ is the superconducting coherence length, such that the Josephson current can be estimated by only considering subgap contributions by Andreev levels [164, 165] as

$$\begin{aligned} I(\varphi) &= \frac{2e}{\hbar}\sum_i f(\varepsilon_i)\frac{d\,\varepsilon_i}{d\varphi} \\ &= -\frac{2e}{\hbar}\sum_\sigma \tanh\left(\frac{\beta\varepsilon_\sigma}{2}\right)\frac{d\,\varepsilon_\sigma}{d\varphi}, \end{aligned} \tag{5.8}$$

where $f(x)$ is the Fermi-Dirac distribution function and $\beta = 1/k_B T$.

The critical current is defined as $I_c = \max|I(\varphi)|$ and the phase of the junction (0 or π) is determined by the minimum of the φ dependent part of the free energy

$$\begin{aligned} F(\varphi) &= -\frac{1}{\beta}\ln\left[\prod_i\left(1+e^{-\beta\varepsilon_i(\varphi)}\right)\right] \\ &= -\frac{1}{\beta}\sum_\sigma \ln\left[2\cosh\left(\frac{\beta\varepsilon_\sigma(\varphi)}{2}\right)\right]. \end{aligned} \tag{5.9}$$

5.3. General formula for Andreev levels

Inserting the wave function Eq. 5.4 into the boundary conditions Eq. 5.6, we obtain a homogenous system of linear equations for the scattering coefficients. By imposing that the system has non-trivial solutions, we can obtain a relation between energy and phase difference such that the coherent subgap processes can effectively take place, i.e. Andreev levels with dispersion $\varepsilon_i(\varphi)$, $i = \{1, ..., 4\}$ [164]. We are able to provide a general form of the levels which holds for arbitrary transparency of the insulating barriers, polarization in the ferromagnetic layer, and relative weight of the exchange and bandwidth asymmetry contributions. We find $\varepsilon_i(\varphi) = \varepsilon_\sigma^{\pm}(\varphi) = \pm\varepsilon_\sigma(\varphi)$ and

$$\varepsilon_\sigma(\varphi) = \Delta_0 \sqrt{\frac{A^2 + B^2 - A\left(C + D\cos^2(\frac{\varphi}{2})\right) + \rho_\sigma \sqrt{B^2\left(A^2 + B^2 - \left(C + D\cos^2(\varphi/2)\right)^2\right)}}{2\left(A^2 + B^2\right)}}, \tag{5.10}$$

where A, B, C, D depend on all junction parameters.

The explicit form of A, B, C, D in Eq. (5.10) is

$$A = 2(a - b)\,, \tag{5.11}$$
$$B = 4c\,, \tag{5.12}$$
$$C = 2(a + b) - d\,, \tag{5.13}$$
$$D = 2d\,, \tag{5.14}$$

where

$$a = -\left(\lambda_\sigma^2 + \lambda_{\bar\sigma}^2\right) - 2\frac{\lambda_\sigma}{\tan\left(kL\Lambda_\sigma\right)}\frac{\lambda_{\bar\sigma}}{\tan\left(kL\Lambda_{\bar\sigma}\right)}, \tag{5.15}$$

$$\begin{aligned} b = \left(1 + Z^2\right)^2 &- Z^2\left(\lambda_\sigma^2 + \lambda_{\bar\sigma}^2\right) \\ &+ \left(4Z^2 + 2\right)\frac{\lambda_\sigma}{\tan\left(kL\Lambda_\sigma\right)}\frac{\lambda_{\bar\sigma}}{\tan\left(kL\Lambda_{\bar\sigma}\right)} + \lambda_\sigma^2\lambda_{\bar\sigma}^2 \\ &+ 2Z\left(1 + Z^2\right)\left(\frac{\lambda_\sigma}{\tan\left(kL\Lambda_\sigma\right)} + \frac{\lambda_{\bar\sigma}}{\tan\left(kL\Lambda_{\bar\sigma}\right)}\right) \\ &- 2Z\left(\lambda_{\bar\sigma}^2\frac{\lambda_\sigma}{\tan\left(kL\Lambda_\sigma\right)} + \lambda_\sigma^2\frac{\lambda_{\bar\sigma}}{\tan\left(kL\Lambda_{\bar\sigma}\right)}\right), \end{aligned} \tag{5.16}$$

$$\begin{aligned} c = \left(1 + Z^2\right)&\left(\frac{\lambda_\sigma}{\tan\left(kL\Lambda_\sigma\right)} - \frac{\lambda_{\bar\sigma}}{\tan\left(kL\Lambda_{\bar\sigma}\right)}\right) \\ &+ \lambda_{\bar\sigma}^2(1 + Z)\frac{\lambda_\sigma}{\tan\left(kL\Lambda_\sigma\right)} - \lambda_\sigma^2(1 + Z)\frac{\lambda_{\bar\sigma}}{\tan\left(kL\Lambda_{\bar\sigma}\right)}, \end{aligned} \tag{5.17}$$

and

$$d = 8\frac{\lambda_\sigma}{\sin\left(kL\Lambda_\sigma\right)}\frac{\lambda_{\bar\sigma}}{\sin\left(kL\Lambda_{\bar\sigma}\right)}, \tag{5.18}$$

where

$$\lambda_\sigma = \sqrt{\frac{m}{m_\sigma}\left(1+\rho_\sigma\frac{U}{E_F}\right)}, \tag{5.19}$$

$$\Lambda_\sigma = \sqrt{\frac{m_\sigma}{m}\left(1+\rho_\sigma\frac{U}{E_F}\right)}. \tag{5.20}$$

We note that for transparent interfaces, and in the absence of exchange field and bandwidth asymmetry, Eq. (5.10) reduces to the well known result $\varepsilon = \Delta_0\cos(\varphi/2)$ [166].

5.3.1. Andreev levels in limiting cases

Before exploring the general case, we look closer at the low polarization limit for the Andreev levels to get an idea of what to expect. Expressing the mass mismatch in a SBAF and the exchange energy in a STF as a function of polarization yields

$$\sqrt{\frac{m_\uparrow}{m_\downarrow}} = \frac{1+M}{1-M}, \tag{5.21}$$

$$\frac{U}{E_F} = \frac{2M}{1+M^2}. \tag{5.22}$$

From now on to lighten our notation we will refer to S/SBAF/S and S/STF/S as simply SBAF and STF. The first evidence of different behavior is encountered in the $M \ll 1$, $Z \ll 1$ limit. Expanding Eq. (5.10) around $U/E_F \ll 1$ for STF and $\sqrt{m_\uparrow/m_\downarrow} \approx 1$ for SBAF, we obtain

$$\varepsilon_\sigma^{\mathrm{STF}} = \Delta_0\left(\cos\left(\frac{\varphi}{2}\right) + \rho_\sigma\frac{kL}{2}\frac{U}{E_F}\sin\left(\frac{\varphi}{2}\right)\right) \tag{5.23}$$

for STF and

$$\varepsilon_\sigma^{\mathrm{SBAF}} = \Delta_0\left(\cos\left(\frac{\varphi}{2}\right) + \rho_\sigma\frac{kL}{2}\left(\sqrt{\frac{m_\uparrow}{m_\downarrow}}-1\right)\sin\left(\frac{\varphi}{2}\right)\right) \tag{5.24}$$

for SBAF when $Z = 0$. Then, for low polarization and including the first term from the $Z \ll 1$-expansion, both expressions reduce to the same form

$$\varepsilon_\sigma = \Delta_0\left(\cos\left(\frac{\varphi}{2}\right) + \rho_\sigma M\sin\left(\frac{\varphi}{2}\right)\left(kL + \theta Z\sin^2 kL\right)\right), \tag{5.25}$$

where $\theta = +1(-1)$ for STF (SBAF). Thus in the low polarization regime we expect SBAF and STF to show the same behavior for $Z = 0$, while the θ-factor indicates that they can be different for nearly transparent interfaces. This is a consequence of a different interplay between the two ferromagnetic mechanisms and the insulating barrier strength described by Eq. (5.6).

5.4. Current–phase relation in some limiting cases

By differentiating Eq. (5.25) with respect to φ and inserting it into Eq. (5.8), we obtain the current-phase relation

$$\frac{I(\varphi)}{I_0} = 2\frac{s_1\sin(\varphi/2)\sinh[\beta\Delta_0\cos(\varphi/2)] - s_2 kLM\cos(\varphi/2)\sinh[\beta\Delta_0 kLM\sin(\varphi/2)]}{\cosh(\beta\varepsilon_\uparrow/2)\cosh(\beta\varepsilon_\downarrow/2)}, \tag{5.26}$$

where $s_1 = \mathrm{sgn}\left(\cos\left(\varphi/2\right)\right)$, $s_2 = \mathrm{sgn}\left(\sin\left(\varphi/2\right)\right)$, and $I_0 = e\Delta_0/\hbar$. We have again put $Z = 0$ for simplicity.

From Eq. (5.26), we see that the current-phase relation contains a cosine term in addition to the standard sine term. One might think that the cosine term will create a non-vanishing current at $\varphi = 0, \pi$, but this is not the case. The cosine term will cancel out at $\varphi = 0, \pi$ due to the Fermi-Dirac distribution function, as shown in Eq. (5.26). However, in a non-equilibrium situation where levels can be differently populated, these terms may give rise to exotic features such as fractional AC Josephson effect [167, 168] or a φ-junction [169]. This possibility is matter of current investigation.

In the tunneling limit it is possible to obtain an analytical form for the current for an arbitrary degree of polarization. For $T = 0$ and including only the first term in the $Z \gg 1$ expansion, we find

$$\frac{I(\varphi)}{I_0} = \frac{1-M^2}{1+M^2}\frac{2\sin(\varphi)}{Z^4 \sin\left(kL\sqrt{\frac{(1+M)^2}{1+M^2}}\right)\sin\left(kL\sqrt{\frac{(1-M)^2}{1+M^2}}\right)} \tag{5.27}$$

for STF and

$$\frac{I(\varphi)}{I_0} = \frac{2\sin(\varphi)}{Z^4 \sin\left(kL\sqrt{\frac{1+M}{1-M}}\right)\sin\left(kL\sqrt{\frac{1-M}{1+M}}\right)} \tag{5.28}$$

for SBAF. At first glance, one may think that the main difference between the two cases is the term $(1-M^2)/(1+M^2)$ which is present only for STF and should damp the current for high degrees of polarization. We will later see that such an effect exists for low Z. However, for high Z this is masked by the fact that the current is small. In fact, the main difference between Eqs. (5.27) and (5.28) is that the denominator becomes wildly oscillating for large M for SBAF, but not for STF. We will see later that this effect is clearly manifested also beyond the tunneling limit. We now move on to describe the S/F/S junction properties upon leaving aside the limits of low polarization and high/low interface transparency focusing on the features induced by different magnetic mechanisms in F.

CHAPTER 6

Influence of magnetic mechanism on Josephson effect

This chapter is devoted to analysis of the influence of magnetic mechanism on Josephson effect in S/F/S. The extreme cases of SBAF and STF are compared and the "mixed" case where both mechanisms coexist is analyzed.

6.1. S/SBAF/S vs. S/STF/S

In this section Andreev levels, current and free energy are compared for SBAF and STF. The values assumed by exchange and mass mismatch magnetic parameters for three different M values are reported in Table 6.I.

6.1.1. Andreev levels dispersion

Fig. 6.1 shows the φ dependence of $\varepsilon_\uparrow$ and $\varepsilon_\downarrow$ in SBAF (solid lines) and STF (dashed lines) for transparent (left panels) and insulating (right panels) interfaces, for three values of polarization M. All levels are flat at $\varphi = 0, \pi$, which corresponds to the absence of Josephson current for these phase difference values. This is a well known property of S/N/S and S/STF/S junctions, which persists in the S/SBAF/S case. However, the dispersion of the ε_σ levels are different for STF and SBAF. This difference is only quantitative for low polarizations, e.g. $M = 0.25$, as expected from Eq. (5.25). However, the levels differ qualitatively for higher polarization in terms of their slope and curvature. The order relation between $\varepsilon_\uparrow$ and $\varepsilon_\downarrow$ can also be different for the two magnetic mechanisms in the F layer, e.g. for $M = 0.75$ and $Z = 1$ $\varepsilon_\uparrow < \varepsilon_\downarrow$ for STF while $\varepsilon_\uparrow > \varepsilon_\downarrow$ for SBAF.

M		U/E_F	$m_\uparrow/m_\downarrow$
0.25	STF	8/17	1
	SBAF	0	25/9
0.50	STF	4/5	1
	SBAF	0	9
0.75	STF	24/25	1
	SBAF	0	49

Table 6.I. Values of the normalized exchange interaction and mass asymmetry used for three different polarization values.

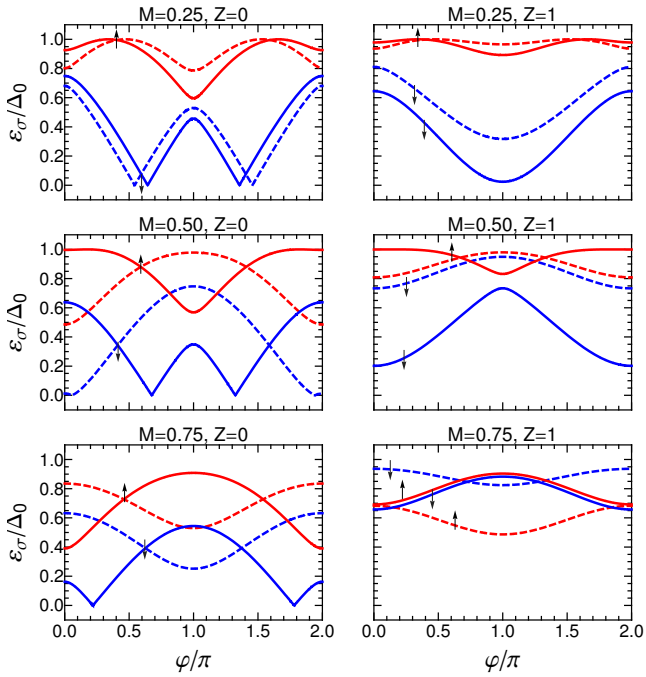

Figure 6.1. Positive branches of spin-splitted dispersion of the Andreev levels for different values of polarization and interface barrier strength and for $Lk = 10$, $E_F = 5$ eV, $\Delta_0 = 1$ meV. Solid lines show levels in SBAF and dashed lines in STF.

6.1.2. Josephson current and free energy

The differences in Andreev levels dispersion manifested for different magnetic mechanisms in F, affect the Josephson current and free energy, too. As shown in Fig. 6.2, where, I/I_0 and F/Δ_0 are plotted for different polarization values, different magnetic mechanisms, and $Z = 0$ (solid lines), $Z = 1$ (long-dashed lines), $Z = 2$ (short-dashed lines). Here $Lk = 10$, $E_F = 5$ eV, $\Delta_0 = 1$ meV, and $T/T_c = 0.01$. For low polarization values (not reported in the figure) the current and the energy differ only quantitatively for STF and SBAF, while for intermediate/high polarization values a qualitative difference between the effect of the two mechanisms emerges. For instance, at $M = 0.75$ the Josephson current exhibits a maximum at $\varphi < \pi$ for STF and $\varphi > \pi$ for SBAF (see panels c) and d)). This means (as shown in panels g) and h)) that the ground state energy minimum for the two types of junction can be realized at different superconducting phase difference even though the polarization in the F layer is the same. Moreover, we see that STF is in a $0-$phase while SBAF is in a $\pi-$phase, so that the magnetic mechanism by itself is able to drive $0-\pi$ transitions. In the following, we will refer to the situations where SBAF and STF are both in $0-$ or $\pi-$phase as "in phase", while when one is in the $0-$phase and the other is in the $\pi-$phase as "out of phase" junctions. By inspection of panel a), b), e), f) of Fig. 6.2 it is possible also infer that the interface transparency can play a role in this bandwidth asymmetry driven phase shift: the STF and SBAF junctions

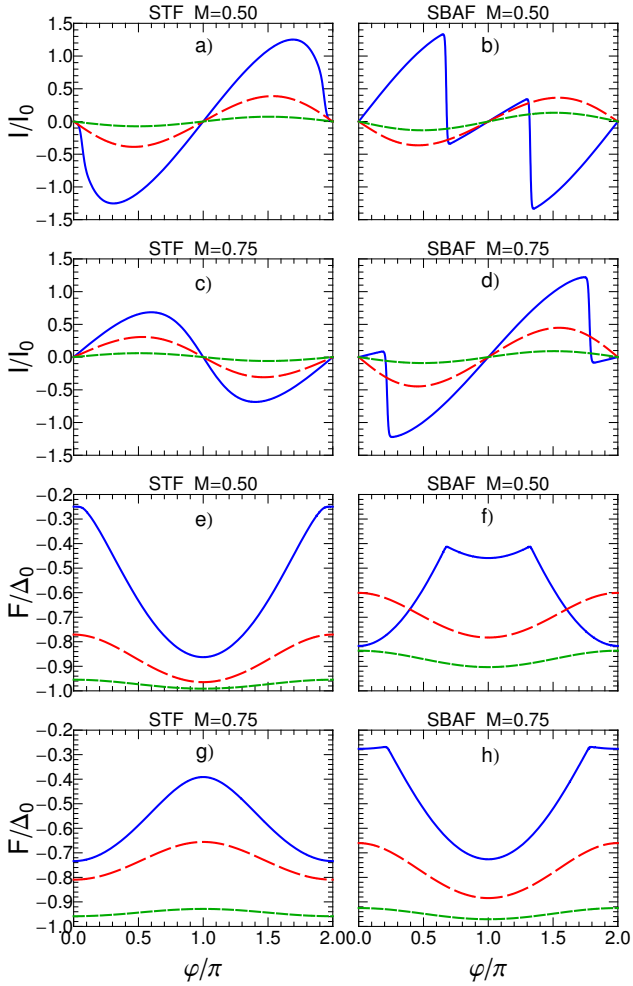

Figure 6.2. Current-phase relation and free energy for STF (left panels) and SBAF (right panels) for intermediate and high polarization values. In each panel three different interface barrier strengths are considered: $Z = 0$ (solid lines), $Z = 1$ (long-dashed lines) $Z = 2$ (short-dashed lines). Here $Lk = 10$, $E_F = 5$ eV, $\Delta_0 = 1$ meV, $T/T_c = 0.01$ are fixed.

are out of phase for $Z = 0$ and become in phase for $Z = 1, 2$, since SBAF undergoes a $0 - \pi$ transition for some Z in $[0, 1]$. We underline that STF can also undergo such transitions driven by a variation in the strength of the barrier, depending on L and T values.

In order to ascertain if the realization of out of phase junctions is a rarity or a common situation, we have compared free energy in SBAF and STF for different width, temperature, degree of spin polarization, and interface transparency values. Our analysis shows that the condition of out of phase junctions is mainly determined by spin polarization: in the low polarization regime, i.e. $M \lesssim 0.25$, SBAF and STF junctions very often share the same phase while in the intermediate/high

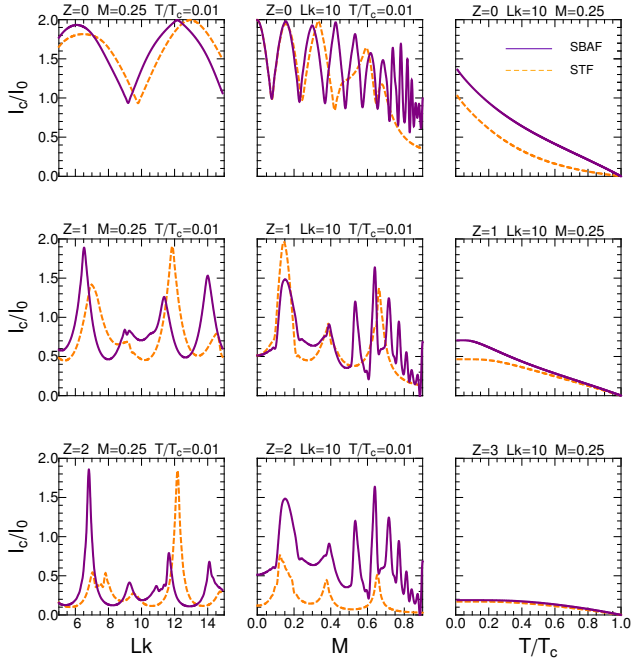

Figure 6.3. Critical Josephson current as a function of L, M, and T for SBAF (solid lines) and STF (dashed lines).

polarization regime, i.e. $M \gtrsim 0.50$, can be out of phase. Other parameters only weakly affect these conditions except interface transparency which favors out of phase situation whenever tunneling limit is considered.

6.1.3. Critical current

Fig. 6.3 shows the Josephson critical current as a function of L, M, and T for SBAF (solid lines) and STF (dashed lines) for $Z = 0, 1, 2$. When the L dependence is considered with a finite polarization, e.g. $M = 0.25$, the current for both the STF and SBAF junction appears oscillatory for transparent barriers and displays complicated patterns when $Z \sim 1$. These patterns repeat periodically when I_c is observed on a larger scale and collapse to a modulated Dirac comb for $Z \sim 10$. The maximum critical currents for the two junctions are very close, but they are attained for different L values and appear to be weakly affected by the Z value. The M dependence of the critical current shows a damped oscillatory behavior for SBAF and STF for $Z = 0$ and more complicated patterns for $Z = 1, 2$. The main difference between the two junctions is that for high polarization values, $M \gtrsim 0.5$, the critical current decreases monotonically for STF, whereas for SBAF it oscillates rapidly with increasing frequency. This is a signature of the fact that SBAF still undergoes $0 - \pi$ transitions, while STF has settled in either a $0-$ or a $\pi-$phase. This behavior is consistent with Eqs. (5.27) and (5.28) even if they are strictly valid only in the tunneling limit. The plots of the temperature dependence of the critical current in Fig. 6.3 show no particular features. The critical currents in both

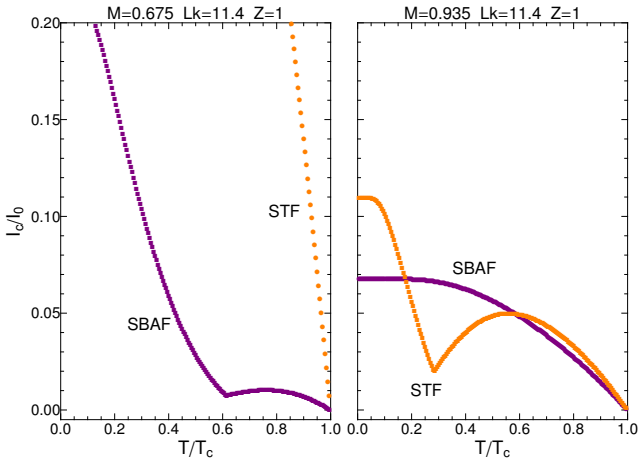

Figure 6.4. Examples of temperature driven $0-\pi$ transitions for SBAF (left panel) and STF (right panel).

STF and SBAF are decaying functions of temperature, but the current in the latter junction is larger. This is not a general feature but depends on the M and L values chosen. In general one can have both $I_c^{\rm SBAF} > I_c^{\rm STF}$ and $I_c^{\rm SBAF} < I_c^{\rm STF}$ as clearly shown by the plots of critical current as a function of these parameters in Fig. 6.3. Moreover, a temperature driven $0-\pi$ transition can be seen both for STF and SBAF by carefully tuning M and L [153], e.g. $M = 0.675$, $Lk = 11.4$ for SBAF and $M = 0.935$, $Lk = 11.4$ for STF, as shown in Fig. 6.4. Even a slight change in one of the two parameters suffices to destroy a temperature driven transition, and the current simply decays as in Fig. 6.3.

6.2. Comparison of phase diagrams

The analysis of the free energy and critical current has shown that for a given set of junction parameters such as degree of polarization, width, and insulating barrier strength, the Josephson effect in SBAF and STF can be different. These two kinds of ferromagnets can support different critical current magnitudes, can induce different ground state phases across the junction, and can undergo a different number of $0-\pi$ transitions driven by variations in junction width and polarization. In order to study these points in more detail, it is convenient to fix a range for these parameters and then look at the behavior of STF and SBAF in this entire range. We employ this strategy because the observables are rapidly varying functions of L and M. We here choose the parameter range $6 \leq Lk \leq 28 \otimes 0 \leq M \leq 0.75$ to be consistent with both our approximations and with typical experimental situations.

6.2.1. Critical current magnitude

First, we look at which of the ferromagnetic mechanisms gives rise to the larger critical current, by considering the quantity $\Delta I \equiv (I_c^{\rm SBAF} - I_c^{\rm STF})/I_0$. This quantity is plotted for the chosen range of parameters for $T = 0$ and $Z = 10$ in Fig. 6.5 where red-light regions are for $\Delta I > 0$. The maximum value reached is $\Delta I \simeq 1.4$. Blue-dark regions are for $\Delta I < 0$, where the minimum value reached is $\Delta I \simeq -1.4$. At

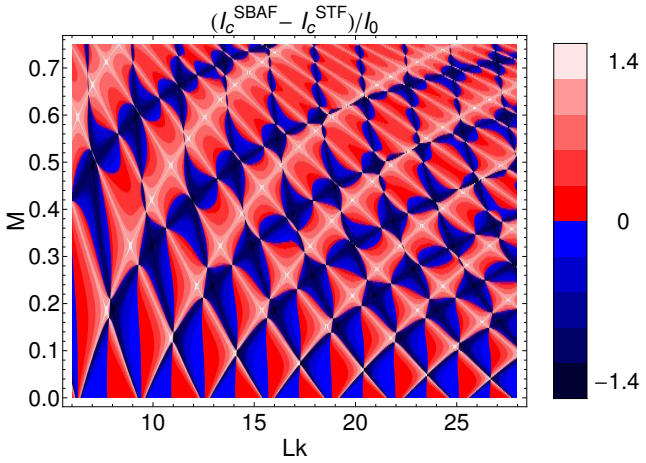

Figure 6.5. Density plot of $\Delta I = (I_c^{SBAF} - I_c^{STF})/I_0$ in the parameter range $0 < M < 0.75 \otimes 6 < Lk < 28$, and for $T = 0$ and $Z = 10$. Red-light regions are for $\Delta I > 0$. The maximum value reached is $\Delta I \simeq 1.4$ Blue-dark regions are for $\Delta I < 0$. The minimum value reached is $\Delta I \simeq -1.4$. At the borders of red and blue regions the critical currents are equal and $\Delta I = 0$.

the borders of red and blue regions, the critical currents are equal and $\Delta I = 0$. The complicated pattern of ΔI shows that even a slight change in mid-layer width or polarization can reverse the order of critical current magnitudes in SBAF and STF meaning that ΔI has a strong local character. However while in the low polarization regime both $\Delta I < 0$ and $\Delta I > 0$ are realized with the same frequency, $\Delta I > 0$ in most of the intermediate/high polarization regime, i.e. a SBAF is likely to support a larger critical current than a STF when intermediate/strong ferromagnets are considered. This property being qualitatively independent from width, temperature, and interface transparency.

6.2.2. $0 - \pi$ transitions

We now analyze the $0 - \pi$ transitions in the same chosen range by plotting phase diagrams for STF and SBAF at $T = 0.01T_c$ and different values of Z (see Fig. 6.6).

From Fig. 6.6 it is clear that a larger number of M and L driven $0-\pi$ transitions is generally expected for SBAF than for STF. In particular, this is always the case for polarization driven transitions at fixed width L, regardless of the value of Z. For L-driven transitions at fixed polarization, this is the case only when $M \gtrsim 0.5$. Another point to notice is that for both STF and SBAF the number of possible transitions is larger for higher Z values. At this point the origin of the complicated patterns seen in Fig. 6.3 for M and L dependence of I_c when $Z \neq 0$ is clear since $0 - \pi$ region boundaries become wavy for finite interface barrier strengths such that changing only M or L leaving the other fixed, boundaries can be crossed at a non-uniform frequency. We underline that the phase of the junctions manifests a strong local character and can be switched by slightly altering the width and/or the polarization.

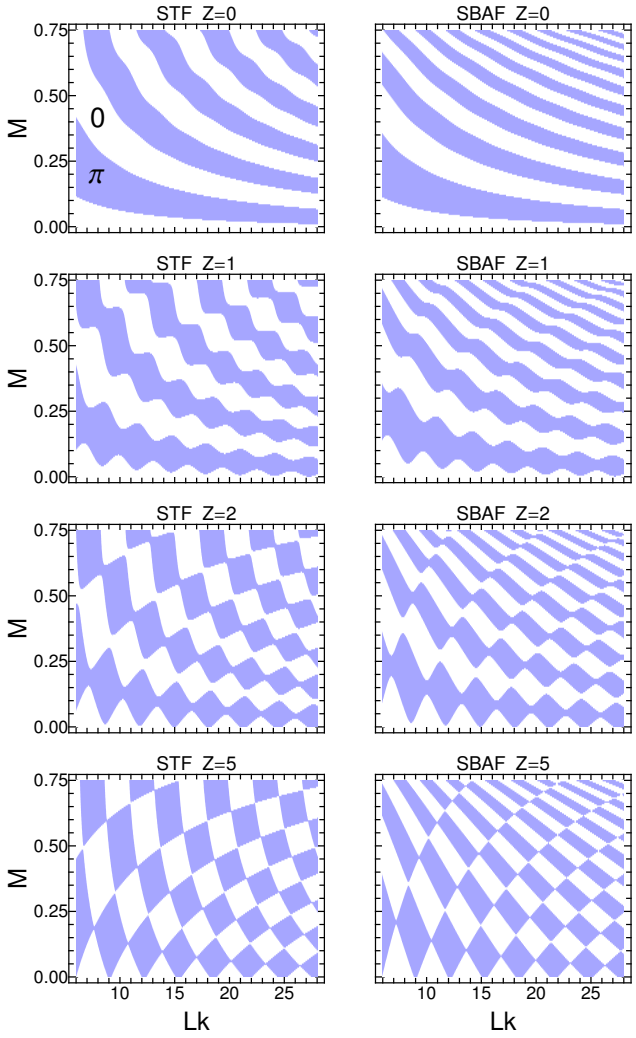

Figure 6.6. $M - L$ phase diagram for STF (left panels) and SBAF (right panels) for $T = 0.01T_c$ and different Z values. White and colored regions correspond to $0-$ and $\pi-$phases, respectively.

Phase diagrams with respect to temperature shows that T driven $0 - \pi$ transitions are possible only for particular L and M values [153]. This is a peculiarity of ballistic systems while diffusive junctions undergo T driven transitions more easily. Fig. 6.7 shows $T - L$ phase diagram for STF (left panels) and SBAF (right panels) for different M and Z values. The number of L values for which T driven $0 - \pi$ transitions are possible is larger for large polarization and interface scattering values, the number being larger for SBAF. These trends are similar for $T - M$ phase diagram not reported here.

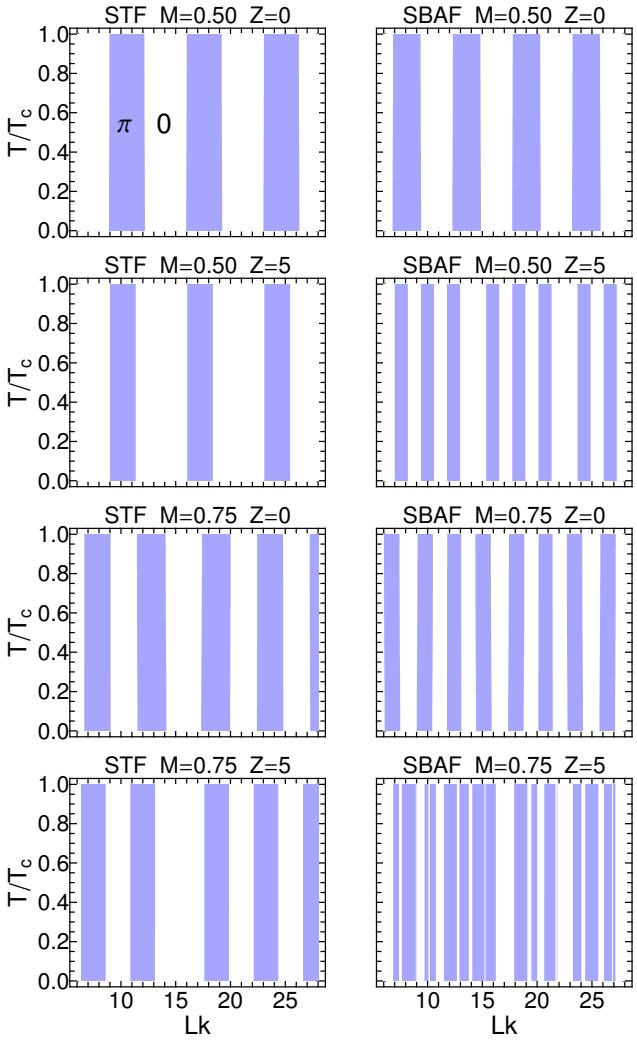

Figure 6.7. $T - L$ phase diagram for STF (left panels) and SBAF (right panels) for different M and Z values. White and colored regions correspond to $0-$ and $\pi-$phases, respectively.

6.2.3. Comparison of ensembles of S/STF/S and S/SBAF/S

Our analysis has shown that for a given set of junction parameters such as degree of polarization, length, and insulating barrier strength, the Josephson effect in SBAF and STF can be different. These two kinds of ferromagnets can support different critical current magnitudes, can induce different ground state phases across the junction, and can undergo a different number of $0 - \pi$ transitions driven by variations in junction width and polarization.

However as shown in previous discussions, and consistently with the literature [150, 151, 152, 153, 154, 155, 156, 158, 159, 160], the physics of S/F/S Josephson junctions is very sensible to parameters as width and polarization and many

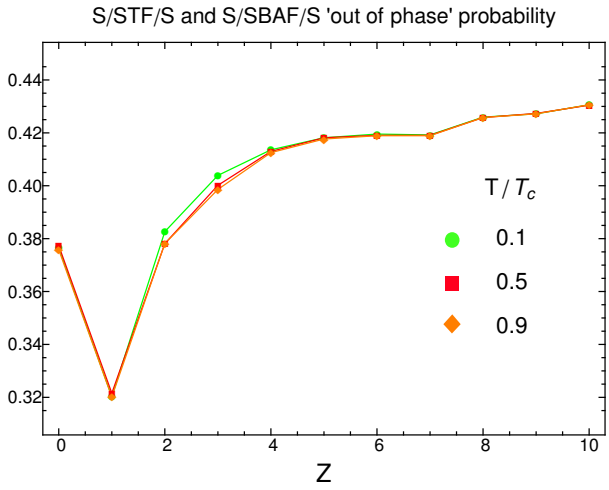

Figure 6.8. Probability for STF and SBAF junctions to be out of phase in the parameter range $0 < M < 0.75 \otimes 6 < Lk < 28$ as a function of Z for three values of temperature.

features are strongly oscillatory as a function of them (even the S electrodes macroscopic phase difference 0 or π). In such a situation differences between S/STF/S and S/SBAF/S are strongly "local", e.g. for some fixed value of the parameters one can have that the first junction has a larger critical current than the second and then by slightly changing only one parameter the reverse is true. In order to overcome this strong local dependence of their features we look at some quantities by averaging on the parameter space, e.g. by considering averages on statistical ensembles of Josephson junctions. To do so, we employ a Monte Carlo integration technique in the previously chosen range of parameters $6 \leq Lk \leq 28 \otimes 0 \leq M \leq 0.75$ for different values of Z and T. Estimations are made by averaging results obtained from 10 samples of 3600 points in the $M - L$ parameter space for each Z and T values.

First of all we sample the situation of out of phase STF and SBAF junctions, that is when for a given set of parameters one of them is in 0 phase and the other in a π phase. Analyzing the free energy, we have seen that this is possible. We now quantify the probability of this to happen with described statistical procedure. Results are shown in Fig. 6.8 for three values of T. The probability of out of phase junctions is in the range $30 - 45\%$ and it is an increasing function of Z except for $0 < Z < 1$. For $Z > 10$ the probability remains stable and stops increasing. We see that it is rather probable for a STF and a SBAF to induce different phases across the junctions in experimentally relevant ranges of degrees of polarization and widths, with this probability being larger for strong insulating barriers and only minimally affected by temperature. This means that the phase shifting driven by magnetic mechanism alone is not infrequent.

A similar analysis is put forth for relative magnitudes of critical current in SBAF and STF, e.g. for the previously defined quantity ΔI. When $\Delta I > 0$ ($\Delta I < 0$), critical Josephson current is larger for SBAF (STF). The probability of having $\Delta I > 0$, that is the fraction of the total area of Fig. 6.5 corresponding to $\Delta I >$

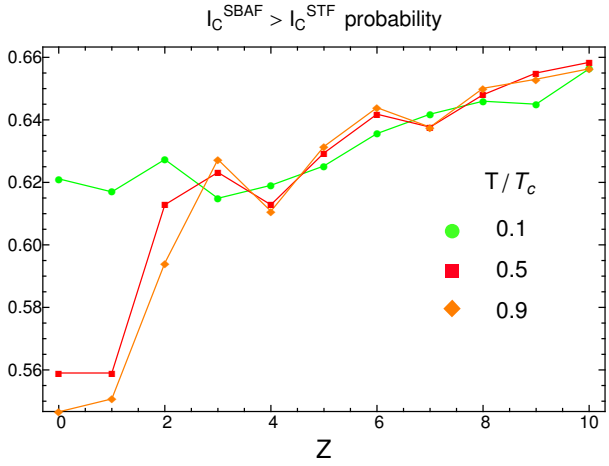

Figure 6.9. Probability of $I_c^{SBAF} > I_c^{STF}$ to be realized in the parameter range $0 < M < 0.75 \otimes 6 < Lk < 28$ as a function of Z for three values of temperature.

0, is approximately 0.66 for $Z = 10$ and tends to decrease for higher interface transparency until $\simeq 0.62$ for for $Z = 0$ and $T = 0.1$ or $\simeq 0.55$ for $T/T_c = 0.9$ as shown in Fig. 6.9. Despite this decrease, the probability of $\Delta I > 0$ will be larger than 0.5 for all temperatures and interface transparencies thus one one can conclude that on average, a SBAF is likely to support a larger critical current than a STF.

Both probabilities analyzed consider even the low polarization regime where STF and SBAF have very similar features. If only the intermediate/high polarization regime is used for averaging both probabilities becomes larger as a consequence of the fact that in this regime SBAF and STF have very different behavior. Results of averaging in a more narrow region considering only intermediate/high polarization regime, e.g. $6 \leq Lk \leq 28 \otimes 0.5 \leq M \leq 0.75$, show an enhancement of both probabilities. In this case the probability of out of phase junctions is about 50% and probability of SBAF to support a larger critical current than STF in about 70% as shown in Fig. 6.10.

6.3. Mixture of SBAF and STF

When both mechanisms are present there are several combinations of exchange energy and masses ratio that give the same polarization M. We choose to describe this mixed case through a parameter $W \in [0, 1]$ which quantifies the relative weight of the two mechanisms without changing the total polarization in such a way that a pure STF and a pure SBAF will correspond to $W = 0$ and $W = 1$, respectively. Since the polarization is not a separable function with respect to the exchange interaction and mass mismatch, one cannot immediately obtain the values assumed by these microscopic parameters when F is a mixture of STF and SBAF. Here we illustrate how we perform this calculation for a given M and W.

Let us consider the two dimensional $(m_\uparrow/m_\downarrow, U/E_F)$ space parameter over which M is defined (see Fig. 5.2). For a given value of the polarization M, and

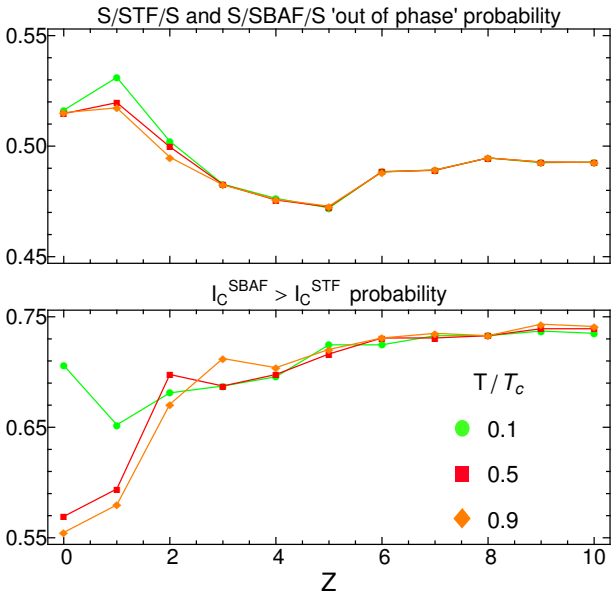

Figure 6.10. Probability for STF and SBAF junctions to be out of phase (top panel) and probability of $I_c^{SBAF} > I_c^{STF}$ to be realized (bottom panel) in the parameter range $0.5 < M < 0.75 \otimes 6 < Lk < 28$ as a function of Z for three values of temperature.

from Eq. (5.22), STF is represented by the point $\left(\frac{2M}{(1+M^2)}, 0\right)$ and, from Eq. (5.21), SBAF is represented by the point $\left(1, \left(\frac{M+1}{M-1}\right)^2\right)$. The distance between these two points along a constant magnetization path $l(M)$ can be written as

$$\begin{aligned} l(M) &= \frac{e^{i\pi/4}}{2\sqrt{2}} \left[B\left(-\frac{1}{4}\left(\frac{M+1}{M-1}\right)^4 ; -1/4, 3/2 \right) \right. \\ &\quad \left. -B\left(-4\left(\frac{M^2+1}{M^2-1}\right)^4 ; -1/4, 3/2 \right) \right], \end{aligned}$$

where B is the incomplete Euler function

$$B(z; a, b) = \int_0^z t^{a-1}(1-t)^{b-1} dt.$$

Then the coordinates in parameter space associated with a mixture defined by the actual W can be evaluated by imposing that the path between the STF and the sought points is a fraction of the total length equals to $W\, l(M)$. Consequently, the mass mismatch value for a degree W mixed F at polarization M can be estimated by numerically solving the equation

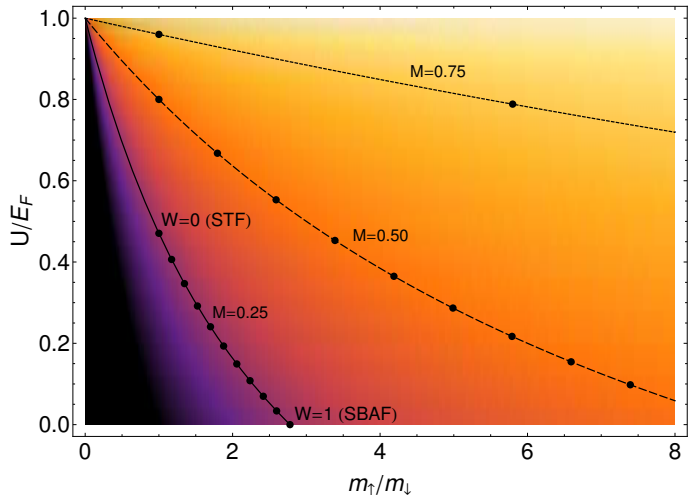

Figure 6.11. Several realization of mixed F with both Stoner exchange and spin bandwidth asymmetry. The parameter W changes the relative weights of the two contributions without altering the spin polarization. A pure STF and a pure SBAF correspond to $W = 0$ and $W = 1$, respectively. For $M = 0.25$ the points plotted correspond to $W = 0, 0.1, ..., 1$. For $M = 0.50$ ($M = 0.75$) the points plotted correspond to $W = 0, 0.1, ..., 0.8$ ($W = 0, 0.1, 0.2$). The plot extends on the right and not all the points on the $M = 0.50$ and $M = 0.75$ are depicted.

M		U/E_F	$m_\uparrow/m_\downarrow$
	STF	8/17	1
0.25	SBAF	0	25/9
	STF & SBAF	0.193	1.878
	STF	4/5	1
0.50	SBAF	0	9
	STF & SBAF	0.287	4.988
	STF	24/25	1
0.75	SBAF	0	49
	STF & SBAF	0.324	24.99

Table 6.II. Values of the normalized exchange interaction and mass asymmetry used for three different polarization values. Here STF & SBAF represents a mixture of the two magnetic mechanism with $W = 0.5$ (see Fig. 6.11).

$$\frac{e^{i\pi/4}}{2\sqrt{2}}\left[B\left(f\left(\frac{m_\uparrow}{m_\downarrow},M\right);-1/4,3/2\right)\right.$$
$$\left.-B\left(-4\left(\frac{M^2+1}{M^2-1}\right)^4;-1/4,3/2\right)\right]=W\,l(M),$$

where

$$f\left(\frac{m_\uparrow}{m_\downarrow}, M\right) = -\frac{1}{4}\left(\frac{(M+1)^2 + \frac{m_\uparrow}{m_\downarrow}(M-1)^2}{M^2-1}\right)^4 .$$

Once the sought value of mass mismatch is known, the corresponding value of exchange interaction can be obtained by inversion of Eq. (5.7).

The procedure is illustrated in Fig. 6.11 for three polarization values and several choices of W. In Table 6.II, the magnetic parameter values for a STF, a SBAF, and a mixture of the two with $W = 0.5$, are reported for three values of the polarization $M = \{0.25, 0.50, 0.75\}$. These will be used in the following.

6.3.1. Josephson current and free energy in the mixed case

We now consider Josephson current and free energy for a mixed F with both exchange energy and bandwidth asymmetry. We show that to witness previously discussed features distinguishing SBAF from STF as seen in Fig. 6.2, a mixed F where bandwidth asymmetry is not the only contribution to spin polarization can be enough. Indeed the Josephson current and the free energy for mixed F look very similar to the case of a pure SBAF, when a suitable contribution of bandwidth asymmetry to total polarization is reached. Fig. 6.12 shows the case of a mixture of SBAF and STF with $W = 0.5$ and all other parameters fixed as in Fig. 6.2. In the mixed case both exchange and masses ratio have non trivial

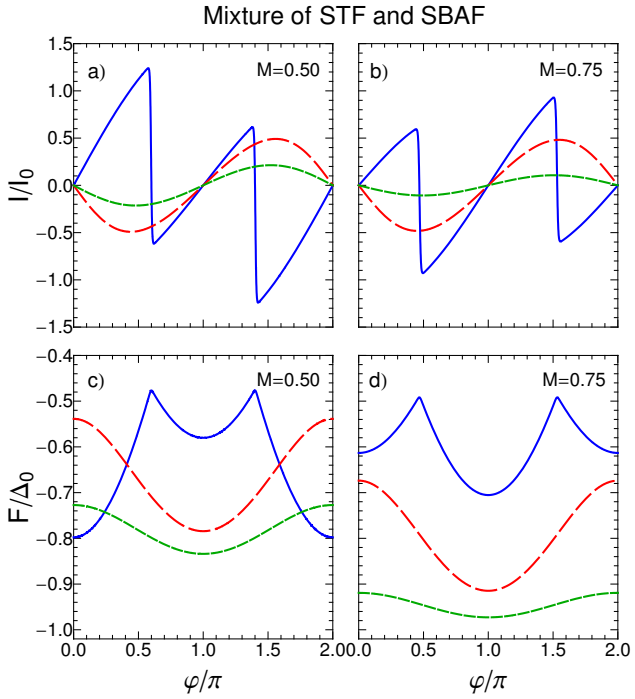

Figure 6.12. Josephson current and free energy for a ferromagnet which is a degree $W = 0.5$ mixture of STF and SBAF. All parameters are fixed at the same values of Fig. 6.2.

values. The values assumed by these parameters for the particular choice $W = 0.5$ are reported in Table 6.II. As previously discussed for $M = 0.75$ STF is in a $0-$phase while SBAF is in a $\pi-$phase. It is clear from panels b) and d) of Fig. 6.12 that the particular mixed case considered with $W = 0.5$ is in a $\pi-$phase as pure SBAF case (corresponding to $W = 1$). This is true even for mixed F with smaller bandwidth asymmetry contribution as soon as this reach a sufficient value depending on junction parameters. For the particular case considered the mixed F behaves as a pure SBAF for $W \gtrsim 0.3$. Comparing SBAF and STF at $M = 0.5$ we have pointed out that STF and is in a $\pi-$phase while SBAF is in a $0-$phase for $Z = 0$ while for smaller interface transparency SBAF switch to the same phase of STF. Panels a) and c) of Fig. 6.12 show that even in this case a partial bandwidth asymmetry in F is enough to observe features of pure SBAF. For the polarization considered $M = 0.5$ mixed F behaves as pure SBAF for $W \gtrsim 0.4$. This results are a clear signature of the fact that the bandwidth asymmetry can induce unusual features also when it is not the main mechanism producing the spin polarization. We stress that this is an important consideration since, as discussed later, in real ferromagnetic mid-layers both exchange and bandwidth asymmetry mechanism may be present.

6.3.2. Number of $0-\pi$ transitions in the mixed case

We have shown that partial bandwidth asymmetry in F is enough to switch Josephson phase. Previously we have shown (see Fig. 6.6) that SBAF undergoes more transitions than STF. Consequently it is interesting to analyze number of transitions for a general F which can be a mixture of STF and SBAF. Fig. 6.13 shows the number of L driven $0-\pi$ transitions at fixed polarization for different mixing degree W ranging from STF to SBAF (see Fig. 6.11). It is shown how the bandwidth asymmetry tends to increase the number of transitions and that

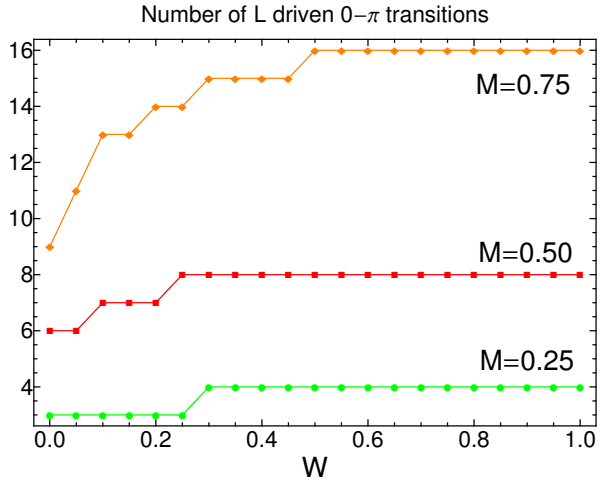

Figure 6.13. Number of L driven $0-\pi$ transitions in the range $6 < Lk < 28$ as a function of the relative contribution of SBAF to total polarization. $T/T_c = 0.01$ and $Z = 0$ are fixed.

this effect is more prominent in the high polarization regime where the number of transitions is almost doubled when moving from pure STF to pure SBAF. One important point to note is that the same number of transitions observed in a SBAF ($W = 1$) can be observed in a mixed F whenever W is large enough, e.g. $W = 0.5$ for $M = 0.75$. This is an important point when relating our results with real materials because in experiments, one usually encounters the mixed F case. Even if in Fig. 6.13 $T/T_c = 0.01$ and $Z = 0$ are fixed, we underline that the general trend of bandwidth asymmetry increasing number of transitions does not depends on their particular values.

Part III results summary and discussion

In this Part of the dissertation we have analyzed the Josephson effect in short, ballistic single channel S/F/S junctions taking into account the possibility for ferromagnetism to be driven by a mass renormalization of carriers with opposite spin, i.e. a spin bandwidth asymmetry. We have compared a junction with this unconventional kinetically driven ferromagnetism in the F layer with one with the usual Stoner mechanism considering also their interplay. Analyzing Andreev levels, free energy and currents, we have shown that the Josephson effect in the two junctions shows different features especially for intermediate/high polarization values. In particular, we have shown that the junction with total or partial spin bandwidth asymmetry in the F layer undergoes a larger number of $0-\pi$ transitions driven by variations in junction width and polarization. By examining free energy and phase diagrams, we have pointed out how junctions with different magnetic mechanisms in the F layer can be in different phases even if all junction parameters have the same values whenever a suitable contribution from bandwidth asymmetry builds up the spin polarization. We have remarked that this is a likely (rare) situation in the intermediate/high (low) polarization regime. By analyzing Josephson critical current we have shown that bandwidth asymmetry can both enhance and decrease its value, the former situation being more common for strong ferromagnets. Our findings are relevant for many interesting magnetic materials which can be hardly framed exclusively within a Stoner scenario. As relevant examples we cite the half-metal ferromagnets defined by the property to have almost 100% transport spin polarization [24]. Materials belonging to this class usually have spin polarization M in the range where bandwidth asymmetry is clearly distinguishable from Stoner exchange, e.g. CrO_2 [113], $La_{0.7}Sr_{0.3}MnO_3$ [114], Fe_3O_4 [115], and EuO [116], among others. Their high polarization values can hradly be ascribed only to Stoner exchange, so that when trying to theoretically model their behavior in a Josephson setup the inclusion of bandwidth asymmetry is a fundamental ingredient. We would like to notice that our findings may turn out to be a useful tool to ascertain if a given ferromagnetic material has spin bandwidth asymmetry. Furthermore, since a bandwidth asymmetric F layer can provide more frequent transitions and is likely to support a larger critical current for a given set of parameters than a Stoner ferromagnet, it may be used for electronics or spintronics applications and devices based on the Josephson effect and relying on $0-\pi$ transitions. Moreover, considering experimental and sample production limitations, the choice of magnetization mechanism may work as an extra degree of freedom which by itself may determine the ground state phase difference across the junction or the magnitude of Josephson critical current.

Part IV

Proximity effect in F/TS

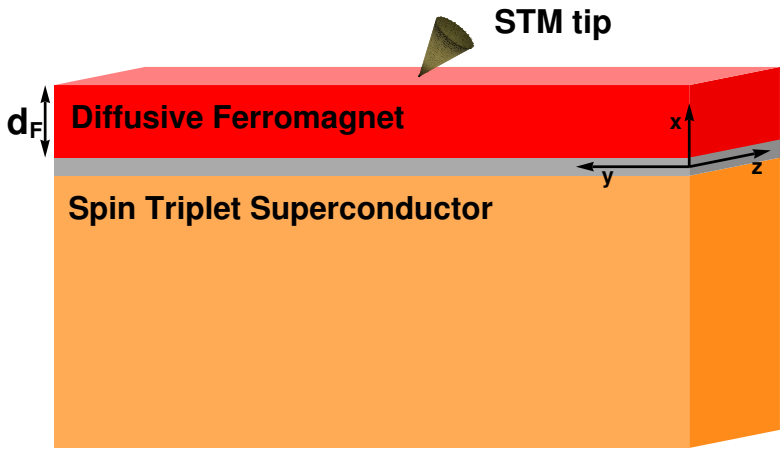

Abstract

This part of the dissertation is devoted to the analysis of proximity effect in ferromagnet/triplet superconductor (F/TS) structures. The study is performed by solving Eilenberger and Usadel equations for a typical STM setup for local DOS measurement in the proximate non superconducting region. In Chapter 7 quasiclassical theory of proximity effect in F/TS is introduced and the particular case of noncentrosymmetric mixed parity superconductor is deepened. Chapter 8 is devoted to the analysis spin-sensitive long-ranged proximity effect in F/TS. Results are summarized and discussed in the last section of this part at p. 107.

CHAPTER 7

Proximity effect theory in F/TS

This Chapter is devoted to the discussion of proximity effect in F/TS within the quasiclassical formalism. We focus on mixed parity noncentrosymmetric superconductors showing how it is possible to obtain information about their superconducting properties from DOS analysis in proximity hybrid structures.

7.1. Triplet superconductors and probes of their symmetry

The discovery of noncentrosymmetric superconductors (NCSs), such as $CePt_3Si$, and chiral superconductors, such as Sr_2RuO_4, calls for experimental methods to identify the presence of spin-triplet pairing (see Sec. 1.1). While making the distinction between, say, a d-wave and an s-wave order parameter involves making the distinction between order parameters of different symmetries, it is quite another matter to distinguish two separate p-wave superconducting order parameters. We here demonstrate a method which accomplishes this in an appealingly simple manner: a spin-sensitive proximity effect in a ferromagnet/triplet superconductor (F/TS) bilayer. It is shown how the orientation of the field in F can be used to unambiguously distinguish between different spin-triplet superconducting states. Moreover, the proximity effect becomes long-ranged in spite of the presence of an exchange field and even without any magnetic inhomogeneities, in contrast to conventional F/S junctions. Our results can be verified by STM-spectroscopy and could be useful as a tool to characterize the pairing state in unconventional superconducting materials.

To acquire information about the order parameter, it is often useful to study how the superconducting correlations behave when placed in proximity to a non-superconducting material such as a normal metal. This idea has been employed previously in several works studying e.g. normal metal/non-centrosymmetric superconductor (N/NCS) junctions [170, 171, 172, 173] in order to look for unique signatures of the superconducting order parameter. However, the non-superconducting material does not necessarily have to be a simple normal metal. Instead, it may feature intrinsic properties, such as magnetism, which then provide an arena for studying the interplay between superconductivity and different types of electronic ordering [36]. A natural question arises: could such an interplay be useful in order to extract information about the superconducting state? In this Part of the dissertation, we demonstrate that a ferromagnet/triplet superconductor bilayer provides an appealingly simple and powerful method to clearly distinguish between different types of triplet pairing states, thus providing information about the nature of the superconducting condensate. We show that this is a direct result of a spin-sensitive long-ranged proximity effect. The interesting features about this effect are that it

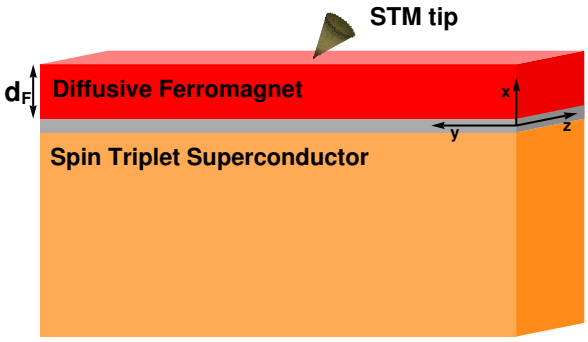

Figure 7.1. The experimental setup proposed for a spin-sensitive proximity effect: a ferromagnet/triplet superconductor bilayer separated by a thin insulating barrier. The ferromagnetic layer has a thickness d_F and the superconducting condensate is characterized by a $\mathbf{d_k}$-vector.

provides *i)* unambiguous signatures in the DOS due to an interplay between the exchange field $\mathbf{h}$ and the $\mathbf{d_k}$ vector (see Sec. 1.1) and also that *ii)* the proximity effect can become long-ranged in spite of the presence of $\mathbf{h}$, thus decaying on a scale of the normal coherence length $\xi_T = \sqrt{D/T}$, where D is the diffusion constant and T is the temperature, rather than the expected decay length in F/S $\xi_F = \sqrt{D/h}$. In this way, one may in a controllable way probe experimentally the nature of the pairing symmetry in unconventional superconducting materials via e.g. STM measurements in the proximate non-superconducting region. Moreover, this finding suggests an alternative to other methods where measurements are performed on the superconductor itself in the presence of an external magnetic field, which can lead to ambiguous interpretations due to e.g. formation of a vortex lattice. Finally, the effect predicted here constitutes a way of generating a long-range proximity effect without any magnetic inhomogeneity in the ferromagnetic layer. This is in contrast with the situation considered in conventional F/S structures, where such a long-ranged proximity effect only occurs in the presence of inhomogeneous magnetization [174]. We explain the microscopic mechanism responsible for the discrimination between different triplet states, due to the coupling to the ferromagnetic exchange field $\mathbf{h}$, which is a general result that can be applied to identify the $\mathbf{d_k}$-vector in arbitrary triplet superconductors. As a concrete application of our results, we consider two specific cases: $\mathbf{d_k} \sim (0, 0, k_x + ik_y)$ and $\mathbf{d_k} \sim (-k_y, k_x, 0)$, that many experimental studies suggest to be effectively realized in superconducting phases of Sr_2RuO_4 and non-centrosymmetric $CePt_3Si$, respectively.

7.2. Quasiclassical formulation of proximity effect in F/TS

Let us introduce the theoretical framework employed here to arrive at our main results. We will use units such that $\hbar = c = 1$ and use $\underline{\ldots}$ for 2×2 matrices while $\hat{\ldots}$ denotes 4×4 matrices. The system under consideration consists of a typical STM measurement setup where the layers lie in the yz-plane, thus stacked along the x-axis. The diffusive ferromagnet is interfaced to the triplet superconductor at $x = 0$ and to the vacuum at $x = d_F$ (see Fig. 7.1). Our calculations assume translational invariance in the directions parallel to the interface region and are performed in 2D. However, we underline that the results reported here remain

equally valid in 3D due to the symmetry of the superconducting order parameters considered. We will make use of the quasiclassical theory of superconductivity, where the main assumption is that the Fermi energy is the largest energy-scale in the system. The approximations behind this model have revealed to be able to grasp the main low energy experimental features of heterostructures involving unconventional superconductors as peaks, dips, and plateaus in density of states and conductance, both for ballistic and diffusive systems. We here sketch the framework for the specific case of non-centrosymmetric $CePt_3Si$. We will consider also the non magnetic proximity effect in N/NCS before moving to demonstrate that proximity effect in F/NCS can become spin-sensitive when the proximity layer is a ferromagnet.

7.2.1. Bulk Green's function for NCS

In NCSs it is well known (see Sec. 1.1) that the spin-orbit coupling is antisymmetric and of Rashba-type, e.g. $\mathbf{g_k} = \lambda(\hat{\mathbf{n}} \times \mathbf{k})$, where λ denotes the strength of the spin-orbit interaction and $\hat{\mathbf{n}}$ denotes the axis of broken inversion symmetry. More specifically, the crystallographic structure of the material does not have a mirror plane with $\hat{\mathbf{n}}$ as normal vector. In what follows, we will consider a situation where the mirror plane with the [001] direction as normal vector is lost in the crystal, i.e. $\hat{\mathbf{n}} = \hat{\mathbf{z}}$. The spin-orbit coupling vector may then be written as $\mathbf{g_k} = \lambda(-k_y, k_x, 0)$. In general, one then finds that the superconducting order parameter can be written as [175]

$$\underline{\Delta}_{\mathbf{k}} = \Delta_0 i\underline{\sigma_y} + \mathbf{d_k} \cdot \underline{\boldsymbol{\sigma}} i\underline{\sigma_y},\ \mathbf{d_k} = \Delta_t \left(-k_y, k_x, 0\right)/k_F, \tag{7.1}$$

where k_F is the Fermi wavevector and Δ_0 and Δ_t are singlet and triplet gap amplitudes for NCS, respectively. The singlet amplitude Δ_0 will be used as reference energy.

We now obtain a general expression for the retarded Green's function in a bulk noncentrosymmetric superconductor. Starting out from the second quantized Hamiltonian in real-space, one finds the following expression for the matrix Green's function in Spin $\otimes$ Nambu space:

$$\begin{aligned} \hat{G}(\mathbf{p}, \varepsilon) &= (\varepsilon\hat{\rho}_3 - \hat{\xi}_{\mathbf{p}} - \hat{\Sigma}_{\mathbf{p}} + \hat{\Delta}_{\mathbf{p}})^{-1},\ \hat{\xi}_{\mathbf{p}} = [\mathbf{p}^2/(2m)]\hat{1}. \\ \hat{\Sigma}_{\mathbf{p}} &= \begin{pmatrix} \mathbf{g_p} \cdot \underline{\boldsymbol{\sigma}} & 0 \\ 0 & [\mathbf{g_{-p}} \cdot \underline{\boldsymbol{\sigma}}]^{\mathrm{T}} \end{pmatrix},\ \hat{\Delta}_{\mathbf{p}} = \begin{pmatrix} 0 & \underline{\Delta}_{\mathbf{p}} \\ \underline{\Delta}^*_{\mathbf{-p}} & 0 \end{pmatrix}, \end{aligned} \tag{7.2}$$

where $\hat{\rho}_3 = \mathrm{diag}(1, 1, -1, -1)$. The quasiclassical Green's function $\hat{g}(\mathbf{p}_F, \varepsilon)$ is then obtained by integrating out the dependence on kinetic energy. The Green's function is assumed to be strongly peaked around Fermi level, and one obtains

$$\hat{g}(\mathbf{p}_F, \varepsilon) = \frac{i}{\pi} \int_{-\infty}^{\infty} \mathrm{d}\xi_{\mathbf{p}} \hat{G}(\mathbf{p}, \varepsilon). \tag{7.3}$$

In the NCS, a high impurity concentration would suppress completely the odd-parity spin-triplet component $\mathbf{d_k}$ of the superconducting order parameter. We therefore consider a ballistic superconducting region, and make use of the bulk solution $\hat{g}_S$ which may be obtained from the Eilenberger equation (see Sec. 1.5) by setting the gradient term to zero [175]:

$$[\varepsilon\hat{\rho}_3 - \hat{\Sigma}_{\mathbf{p_F}} + \hat{\Delta}_{\mathbf{p_F}}, \hat{g}_S]_- = 0. \tag{7.4}$$

The Green's function reads:

$$\hat{g}_S(\varphi) = \frac{1}{2}\begin{pmatrix} \underline{\mathscr{C}}(\varphi) & \underline{\mathscr{S}}(\varphi) \\ \underline{\mathscr{S}}(-\varphi) & -\underline{\mathscr{C}}(-\varphi) \end{pmatrix}, \ [\hat{g}_S(\varphi)]^2 = \hat{1}, \tag{7.5}$$

where

$$\mathscr{C}(\varphi) = c^+\underline{1} + (\underline{\sigma_y}\cos\varphi - \underline{\sigma_x}\sin\varphi)c^-, \tag{7.6}$$

$$\mathscr{S}(\varphi) = i\underline{\sigma_y}s^+ + (\underline{1}\cos\varphi + \underline{\sigma_z}\sin\varphi)s^-, \tag{7.7}$$

and $\underline{\ldots}$ denotes a 2×2 matrix in spin-space. Above, we have defined

$$c^\pm = c_+ \pm \ c_-, \tag{7.8}$$

$$s^\pm = s_+ \pm \ s_-, \tag{7.9}$$

being

$$c_\pm = \cosh(\theta_\pm), \tag{7.10}$$

$$s_\pm = \sinh(\theta_\pm), \tag{7.11}$$

with $\theta_\pm = \operatorname{arctanh}(\Delta^\pm/\varepsilon)$, and $\Delta^\pm = \Delta_0 \pm \ \Delta_t$, having chosen real amplitudes for singlet and triplet components of the gap function. Note that φ is the azimuthal angle in the xy-plane. Features captured by a fully self-consistent calculations such as superconducting order parameter suppression at the interface would only quantitatively alter our results and does not affect our conclusions [177, 173]. The inverse proximity effect, from the ferromagnet into the superconductor, can be shown to be negligible for a low-transparency barrier and wide superconducting region [177]. We will concentrate on this regime in what follows.

7.3. Usadel equation and boundary conditions for F/TS

In the non-superconducting region, we consider the diffusive regime of transport which often is the experimentally most relevant one. In order to calculate the Green's function $\hat{g}$[4], we need to solve the Usadel equation with appropriate boundary conditions at $x = 0$ and $x = d_F$. Since we employ a numerical solution, we have access to study the full proximity effect regime, and also an, in principle, arbitrary spatial modulation $\mathbf{h} = \mathbf{h}(x)$ of an exchange field. The Usadel equation [122] in the N part reads:

$$D\partial(\hat{g}\partial\hat{g}) + i[\varepsilon\hat{\rho}_3 + \operatorname{diag}[\mathbf{h}\cdot\underline{\boldsymbol{\sigma}}, (\mathbf{h}\cdot\underline{\boldsymbol{\sigma}})^{\mathrm{T}}], \hat{g}] = 0. \tag{7.12}$$

Boundary conditions applicable to diffusive normal metal/unconventional superconductor junctions were derived in [125]. We assume that materials are separated by an infinitely thin insulating barrier of the form $H\delta(x)$, corresponding to a transmissivity

$$T(\varphi) = \frac{4\ \cos^2(\varphi)}{4\ \cos^2(\varphi) + \ Z^2}, \tag{7.13}$$

where $Z = 2mH/k_F$ is a dimensionless parameter quantifying the barrier strength. Other relevant parameters are the resistance of non-superconducting layer R_F and

[4] For simplicity we use the same symbol $\hat{g}$ for the Green's function in the ballistic superconducting layer and for its angular average $\langle\hat{g}\rangle$ in the diffusive layer (see Sec. 1.5).

insulating barrier resistance $R_B = 2R_0/t$, where

$$t = \int_{-\pi/2}^{\pi/2} d\varphi \; T(\varphi)\cos(\varphi) \tag{7.14}$$

and R_0 is the contact Sharvin resistance. Being it a function of constriction area, it can be considered an independent parameter with respect to Z [125]. For arbitrary interface transparency boundary condition at $x = 0$ can be written as

$$\Gamma d_F \hat{g}\partial\hat{g} = 2\langle\left[\hat{g}, \hat{B}(\varphi)\right]\rangle, \tag{7.15}$$

where $\Gamma = R_B/R_F$ and $\langle\ldots\rangle$ represents an angular average on Fermi surface:

$$\langle f(\varphi)\rangle = \int_{-\pi/2}^{\pi/2} d\varphi \; f(\varphi)\cos(\varphi)/t. \tag{7.16}$$

The matrix $\hat{B}(\varphi)$ can be written as

$$\hat{B}(\varphi) = \frac{-T'\left(\hat{1} + \hat{H}_-^{-1}\right) + T'^2\hat{g}\hat{H}_-^{-1}\hat{H}_+}{-T'\left[\hat{g}, \hat{H}_-^{-1}\right] + \hat{H}_-^{-1}\hat{H}_+ - T'^2\hat{g}\hat{H}_-^{-1}\hat{H}_+\hat{g}}, \tag{7.17}$$

where

$$\hat{H}_\pm = \left(\hat{g}_S(\varphi) \pm \; \hat{g}_S(\pi - \varphi)\right)/2, \tag{7.18}$$

and

$$T'(\varphi) = T(\varphi)/\left[2 - T(\varphi) + 2\sqrt{1 - T(\varphi)}\right]. \tag{7.19}$$

At $x = d_F$ the N part borders to vacuum so that the boundary condition simply read $\partial\hat{g} = \hat{0}$.

We use a Riccati-parametrization of the Green's functions as follows [178, 179]:

$$\hat{g} = \begin{pmatrix} \underline{\mathscr{N}}(\underline{1} - \underline{\gamma\tilde{\gamma}}) & 2\underline{\mathscr{N}}\underline{\gamma} \\ 2\underline{\tilde{\mathscr{N}}}\underline{\tilde{\gamma}} & \underline{\tilde{\mathscr{N}}}(-\underline{1} + \underline{\tilde{\gamma}\gamma}) \end{pmatrix}, \tag{7.20}$$

where

$$\underline{\mathscr{N}} = (\underline{1} + \underline{\gamma\tilde{\gamma}})^{-1} \; \underline{\tilde{\mathscr{N}}} = (\underline{1} + \underline{\tilde{\gamma}\gamma})^{-1}. \tag{7.21}$$

This parametrization facilitates the numerical computations, and also ensures the normalization condition $\hat{g}^2 = \hat{1}$.

In what follows, we analyze the proximity effect in the normal electrode by examining the quasiparticle density of states (DOS) defined as

$$N(\varepsilon)/N_0 = \mathrm{Re}[g_{11} + g_{22}]/2 = \mathrm{Tr}\{\mathrm{Re}[\underline{\mathscr{N}}(\underline{1} - \underline{\gamma\tilde{\gamma}})]\}/2, \tag{7.22}$$

where N_0 is the normal-state DOS. We fix $Z = 2$ and $\Gamma = 0.1$ corresponding to a rather low interface-transparency. To model inelastic scattering, we add a small imaginary part δ to the quasiparticle energies, where $\delta/\Delta_0 = 0.01$.

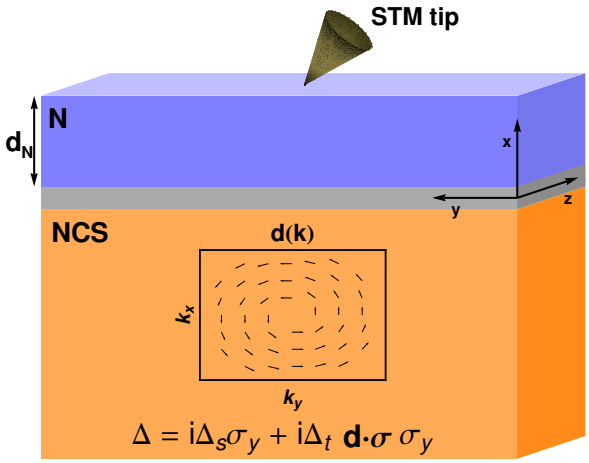

Figure 7.2. The experimental setup proposed to determine the relative amplitude of singlet and triplet gaps in a non-centrosymmetric superconductor. The normal metal layer has a thickness d_N and it is considered in the dirty limit.

7.4. Proximity effect in N/NCS

Before illustrating our results for a F/NCS structure we analyze the proximity effect in an N/NCS structure as depicted in Fig. 7.2. We will show how STM measurements could give insight in superconducting properties of mixed parity NCS. In particular we show that the qualitative features of the DOS evaluated for this system strongly depend on the relative amplitude of the singlet and triplet components: a qualitative change occurs when Δ_t exceeds Δ_0 in magnitude. We find that the fully suppressed low-energy DOS transforms into a peak-structure due to the appearance of zero-energy states resulting from the triplet component [170, 172]. In this way, probing the DOS in a normal metal contacted to a NCS via e.g. STM-spectroscopy reveals direct information about the triplet contribution in the superconducting condensate. Indeed an immediate discrimination between the order of singlet and triplet gaps in mixed parity NCS, e.g. if $\Delta_t > \Delta_0$ or $\Delta_t < \Delta_0$, is possible while for precise estimation of their ratio a fitting procedure can be employed.

The DOS is estimated in N by solving the Usadel equation Eq. 7.12 without the exchange field term. Fig. 7.3 shows the proximity modified DOS evaluated at the top of diffusive normal metal as depicted in Fig. 7.2 for $\Gamma = 0.1$, $Z = 2$, and $d_N = 1.5\xi_S$, being xi_S the superconducting coherence length. The energy is referred to the Thouless energy $E_{Th} = D/d^2$ and several Δ_t/Δ_0 values are considered. In the N/S case, i.e. $\Delta_t = 0$, the usual minigap structure is present. Its width decrease for increasing $\Delta_t < \Delta_0$ until it collapses to a single point at $\varepsilon = 0$ precisely for $\Delta_t = \Delta_0$ (not shown in Fig. 7.3). The minigap then transforms abruptly into a well defined zero energy peak (ZEP) for $\Delta_t > \Delta_0$. This peak exist even for pure, i.e. not mixed-parity, triplet superconductors like $p_x + ip_y$-wave as reported in the literature and shown here later.

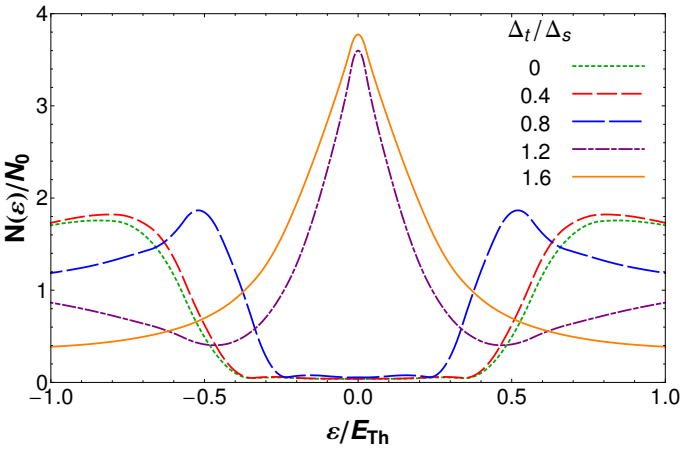

Figure 7.3. Proximity modified DOS evaluated at the top of diffusive normal metal as depicted in Fig. 7.2 for $\Gamma = 0.1$, $Z = 2$, and $d_N = 1.5\xi_S$. A transition occurs when $\Delta_t = \Delta_0$, altering the low-energy structure from fully suppressed to peaked due to unconventional pairing.

Fig. 7.4 shows how these features are modified for different diffusive layer length and Γ values. It is clear that peak height values for $\Delta_t > \Delta_0$, and DOS suppression for $\Delta_t < \Delta_0$ are both stronger for short layers and smaller resistance barrier Γ. In particular ZEP height is larger and DOS suppression is more accentuated in this regime. In the opposite case, e.g. longer diffusive layer and larger interface resistance, both features are less emphasized until they eventually reach the constant normal state DOS as the proximity effect becomes negligible. From this section discussion it is clear that a mixed parity NCS behave very similarly to a pure singlet (triplet) superconductor when its largest gap is the singlet (triplet) one when proximity effect is considered. This is consistent with experiments [183, 184].

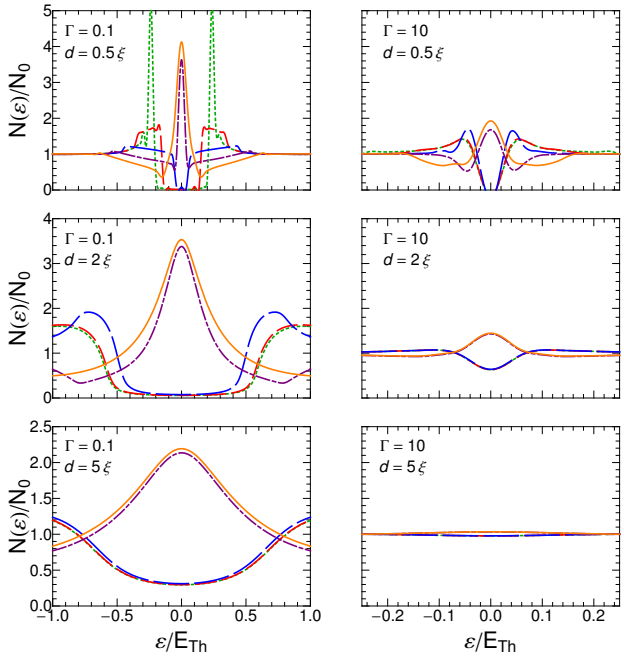

Figure 7.4. Proximity modified DOS evaluated at the top of diffusive normal metal as depicted in Fig. 7.2 for different barrier resistance and diffusive layer length values. In each panel different styles are associated with different Δ_t/Δ_0 values: 0 (green dotted), 0.4 (red long-dashed), 0.8 (blue short dashed), 1.2 (purple dot-dashed), 1.6 (orange solid).

CHAPTER 8

Spin-sensitive long-ranged proximity effect in F/TS

This Chapter is devoted to the analysis of the interplay of exchange field in F and $\mathbf{d_k}$ vector in TS. We show that in F/TS a long-ranged proximity effect can be realized.

8.1. Proximity effect for different triplet superconductors

We now describe the spin-sensitive long-ranged proximity effect. We focus on the setup illustrated previously and depicted in Fig. 7.1. To understand how this effect works, we demonstrate it on two experimentally relevant examples: a noncentrosymmetric superconductor with amplitude of gap components fixed as $\Delta_t = 1.5\Delta_0$, and a chiral $p_x + ip_y$-wave superconductor described by $\mathbf{d_k} = \Delta_0(0, 0, k_x + ik_y)/k_F$. Our choice of relative amplitudes of singlet and triplet gaps in NCS is consistent with specific heat and Knight shift measurements on $CePt_3Si$ which have found a strong triplet character [183, 184].

Bulk Green's function in the chiral $p_x + ip_y$-wave superconductor reads

$$\hat{g}_S(\varphi) = \begin{pmatrix} c & 0 & 0 & se^{i\varphi} \\ 0 & c & se^{i\varphi} & 0 \\ 0 & -se^{-i\varphi} & -c & 0 \\ -se^{-i\varphi} & 0 & 0 & -c \end{pmatrix}, \ [\hat{g}_S(\varphi)]^2 = \hat{1}, \tag{8.1}$$

where

$$c = \cosh(\theta), \tag{8.2}$$

$$s = \sinh(\theta), \tag{8.3}$$

with $\theta = \operatorname{arctanh}(\Delta_0/\varepsilon)$.

DOS is evaluated by solving Eq. 7.12 in F assuming Eilenberger solution for Green's function in TS (Eq. 7.5 for NCS and Eq. 8.1 for chiral $p_x + ip_y$-wave).

8.1.1. Exchange field dependence of proximity-modified DOS

In Fig. 8.1, the DOSs evaluated at the top of the structure ($x = d_F$) for different directions and strength of exchange field in the diffusive ferromagnet are shown. For $\mathbf{h}||\hat{\mathbf{z}}$, the zero energy peak (ZEP) in the DOS is completely insensitive to the ferromagnetism in the NCS case (top-left panel): even for very high exchange fields, the DOS remains virtually unchanged compared to a normal diffusive electrode. In the case of a superconducting electrode featuring a chiral p-wave symmetry

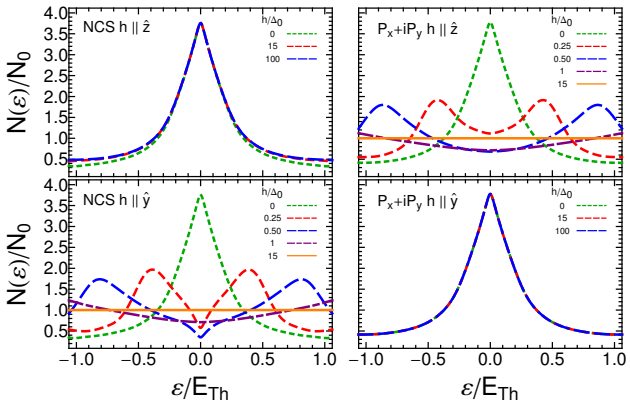

Figure 8.1. DOS at $x = d_F$ for different pairing states in the triplet superconductor and different directions and strength of exchange field in the diffusive ferromagnet. Here $\Delta_t/\Delta_0 = 1.5$, $d_F = 1.5\xi_S$, $\Gamma = 0.1$, and $Z = 2$. Note the insensitivity of the proximity-induced zero-energy peak in the DOS in the upper left and lower right panels, contrary to the cases shown in the lower left and upper right panels. Thus, different orientations of the exchange field suffice to make the subtle distinction between two spin-triplet superconducting order parameters.

(top-right panel), the situation changes qualitatively: the proximity effect is now strongly dependent on the exchange field, and vanishes completely when $h \gg \Delta_0$, which is opposite to the NCS case. To demonstrate the spin-sensitivity of this proximity effect, we now turn to the case where the field satisfies $\mathbf{h}||\hat{\mathbf{y}}$, as shown in bottom panels of Fig. 8.1. In order to change the orientation from $\mathbf{h}||\hat{\mathbf{z}}$ to $\mathbf{h}||\hat{\mathbf{y}}$, one could grow two separate samples where the exchange field is locked to different orientations via e.g. antiferromagnetic coupling, or alternatively grow the layers in different crystallographic orientations to effectively change the orientation of the exchange field. As seen in Fig. 8.1, the features of the DOS are now opposite to the case $\mathbf{h}||\hat{\mathbf{z}}$: the peak appearing for the NCS is destroyed by the exchange field (bottom-left panel) while the peak in the chiral $p_x + ip_y$ case remains uninfluenced by the presence of an exchange field (bottom-right panel). In effect, the roles of the NCS and the chiral superconductor have been reversed. These results suggest that simply by altering the out-of-plane/in-plane orientation of the exchange field in the ferromagnet, the proximity-induced DOS serves as a clear discriminator between different triplet states.

8.1.2. Exchange field dependence of proximity decay length

The zero energy peaks in DOS which are unaffected by exchange fields, are seen to persist even at distances far inside the ferromagnetic layer ($\gg \xi_F = \sqrt{D/h}$), evidencing that we are dealing with a long-range proximity effect in spite of the presence of an exchange field. This is shown clearly in Fig. 8.2 where, with the same pattern of Fig. 8.1, zero energy DOS is plotted as a function of d_F/ξ_S. We note that the proximity effect is long-ranged, e.g. it decays on a length expected in normal but not in ferromagnetic layers, even without any magnetic inhomogeneity

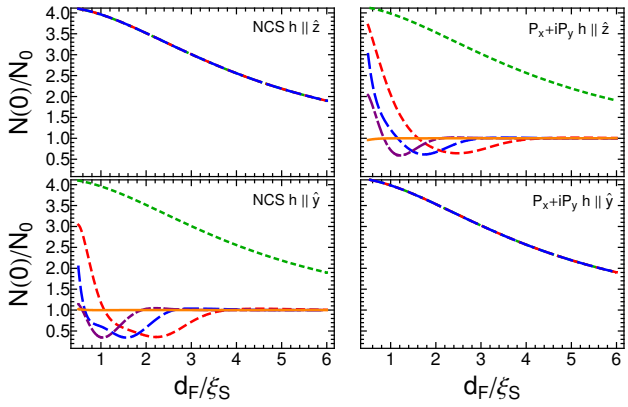

Figure 8.2. Zero energy DOS as a function of d_F/ξ_S for the same pairing states and exchange fields of Fig. 8.1. Here $\Delta_t/\Delta_0 = 1.5$, $\Gamma = 0.1$, and $Z = 2$. Note the persistence of the zero-energy peak in the DOS in the upper left and lower right panels, clearly showing the long-ranged character of the proximity effect in these cases for all fields h, contrary to the cases illustrated in the lower left and upper right panels where the range of the proximity-effect depends on h.

in F, in complete contrast to conventional F/S hybrid structures. Indeed we find that the same configurations of exchange fields and $\mathbf{d_k}$-vector which do not suppress ZEP do not even suppress the decay length of superconducting correlation resulting from proximity effect.

8.1.3. Odd frequency symmetry of superconducting correlations

In diffusive systems Green's functions become isotropic due to frequent impurities scattering. Consequently superconducting correlations leaking the non-superconducting material which are coded in anomalous Green's functions f (see Sec.1.5) are expected to be odd in frequency (energy) when they are generated by a triplet superconductor. This is the case in order to respect the overall antisymmetry in accordance with Pauli principle. Indeed in our case anomalous Green's function have even orbital and spin parity (they are isotropic and in a spin triplet configuration) and in order to be antisymmetric they have to be odd in frequency. In simple F/S with no magnetic scattering these functions are even in frequency, i.e. $f(-\varepsilon) = [f(\varepsilon)]^*$, meaning that $\mathrm{Re}(f)$ is even and $\mathrm{Im}(f)$ is odd. Odd frequency correlations instead are characterized by $f(-\varepsilon) = [-f(\varepsilon)]^*$, that is $\mathrm{Re}(f)$ is odd and $\mathrm{Im}(f)$ is even. Referring to the usual setup studied in this Part (see Fig. 7.1), we have analyzed the anomalous parts of the Green's functions. As an example consider Fig. 8.3 where real (green) and imaginary (red) parts of the $S_z = 0$ triplet anomalous retarded Green's functions $f_t = (f_{\uparrow\downarrow} + f_{\downarrow\uparrow})/2$ propagated in F from proximity effect of $p_x + ip_y$ superconductor are shown. Anomalous triplet correlations are odd in frequency and have the same spin-sensitive and long-ranged behavior analyzed previously. Indeed all the correlations analyzed in this Part, which contribute to the unconventional proximity effect shown, have this frequency symmetry. The situation is analogous in the F/NCS case.

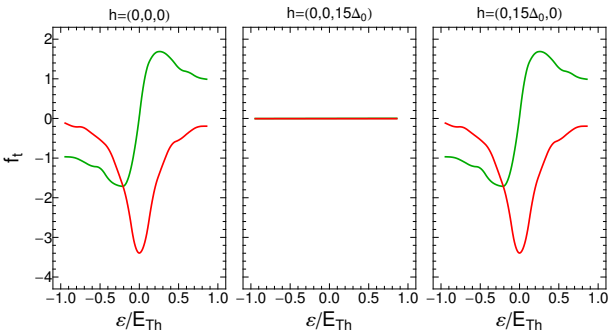

Figure 8.3. Real (green) and imaginary (red) part of the anomalous retarded Green's function components propagated in F from proximity effect of $p_x + ip_y$ superconductor. All functions are evaluated at $x = d_F$ and $d_F = 1.5\xi_S$, $\Gamma = 0.1$, and $Z = 2$ are fixed.

8.2. Interpretation and realizability

We now proceed to explain the underlying physics behind these results. The triplet pairing in the superconducting condensate has a spin-degree of freedom described by the $\mathbf{d_k}$-vector and thus couples to the orientation of the exchange field. In the NCS case, the net triplet condensate has zero spin-projection, but it is comprised of two equal contributions of $S_z = \pm 1$ pairing gaps. Therefore, an exchange field applied along the z-direction has no influence on the triplet pairing since it simply renormalizes the chemical potential. However, applying the field along the y-direction effectively induces spin-flip scattering which breaks the $S_z = \pm 1$ Cooper pairs and thus suppresses the proximity effect. Because of this, the ZEP is present for $\mathbf{h}||\hat{\mathbf{z}}$ but absent for $\mathbf{h}||\hat{\mathbf{y}}$. In the chiral superconducting state, chosen to model the pairing symmetry believed to be realized in Sr_2RuO_4, the triplet component belongs to the $S_z = 0$ class and thus has a spin confined to the xy-plane. By a similar argument as above, an exchange field applied in this plane does not interact destructively with the triplet pairing, while a field applied along $\hat{\mathbf{z}}$ induces spin-flip scattering detrimental to the Cooper pairs.

This line of reasoning holds quite generally for any triplet state. Although there exist alternative experimental techniques to probe the triplet pairing symmetry which are also based on the interaction between a magnetic field and the $\mathbf{d_k}$-vector, such as spin susceptibility and thermal conductance measurements [180, 181], these techniques are based on applying an external magnetic field directly to the superconductor. In contrast, the spin-sensitive proximity effect considered here has an advantage compared to previous methods in that the superconducting and magnetic correlations originate with different parts of the system and that the measurements do not have to be performed on the superconductor, thus avoiding complications with induced vortex-configurations via an external field. Instead, all the information about the triplet condensate can be probed simply by measuring the DOS in the non-superconducting region. The proximity effect also becomes long-ranged in the ferromagnet irrespective of whether it has a weak or strong exchange field, such that one is not restricted to probing the correlations within a few nanometers of the interface region as in conventional F/S structures. We have also checked numerically how robust the spin-sensitive proximity effect is against a misalignment of the

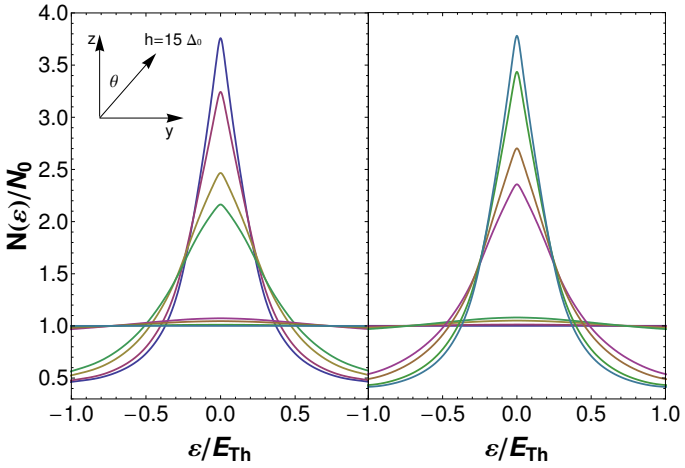

Figure 8.4. DOS at $x = d_F$ for NCS (left panel) and $p_x + ip_y$ (right panel) superconductors. $h = 15\Delta_0$ is fixed and different curves are associated with different h direction in the $y - z$ plane determined by the angle θ. From top to bottom in the left panel and from bottom to top in the right panel θ values are $0, \pi/20, \pi/10, \pi/8, 3\pi/8, 2\pi/5, 9\pi/20, \pi/2$. Here $\Delta_t/\Delta_0 = 1.5$, $d_F = 1.5\xi_S$, $\Gamma = 0.1$, and $Z = 2$.

field, i.e. when it is not fully oriented along the y- or z-axis for our setup, due to e.g. the presence of stray fields or magnetic inhomogeneities (see Fig. 8.4). Only small quantitative changes are observed for misalignment angles up to 15-20°, such that the effect exhibits some robustness towards imperfections in the orientation of the field which could be present in real samples. Concerning the experimental realization of the ferromagnet/triplet superconductor junctions considered here, one would need to couple the ferromagnetic layer to the plane of the superconductor where the order parameter experiences a sign reversal, in order to produce the ZEP. Depending on the crystal structure, this could be challenging with respect to cleaving along an appropriate lattice plane for certain materials, e.g. the *ab*-plane for Sr_2RuO_4. However, we also note that a possible pinning of the $\mathbf{d_k}$ vector by spin-orbit coupling in triplet superconductors [180] is not only unproblematic for our purposes, but actually beneficial since it stabilizes the orientation of the $\mathbf{d_k}$ vector.

Part IV results summary and discussion

In this Part of the dissertation we have analyzed proximity effect in ferromagnet/triplet superconductor (F/TS) structures within the quasiclassical theory of superconductivity. We have focused on particular triplet pairings as the ones realized in noncentrosymmetric superconductor (NCS) $CePt_3Si$, and chiral superconductor Sr_2RuO_4 and considered the standard setup of STM measurement in which a thin layer of a non superconducting material is placed on top of the superconductor being subjected to the proximity effect. We have demonstrated that measurement of proximity modified local DOS with e.g. STM in a diffusive normal metal (N) put in contact with NCS can give insight in the superconducting structure of mixed parity NCS. In particular we have shown that the qualitative features of the DOS evaluated for this system strongly depend on the relative amplitude of the singlet and triplet gap components: a qualitative change occurs when Δ_t exceeds Δ_0 in magnitude. We find that the fully suppressed low-energy DOS , e.g. a minigap, transforms into a peak-structure due to the appearance of zero-energy states resulting from the triplet component. In this way, probing the DOS in a normal metal contacted to a NCS reveals direct information about the triplet contribution in the superconducting condensate. Indeed an immediate discrimination between the order of singlet and triplet gaps in mixed parity NCS, e.g. if $\Delta_t > \Delta_0$ or $\Delta_t < \Delta_0$, is possible while for precise estimation of their ratio a fitting procedure can be employed. We have demonstrated the presence of a spin-sensitive proximity effect in F/TS. In particular, we have shown how the orientation of the exchange field in the ferromagnet couples to the $\mathbf{d_k}$-vector of the proximity-induced triplet superconductivity leaking into the F region, providing clearly distinguishable features in the local density of states. The proximity effect can be completely destroyed when exchange field and $\mathbf{d_k}$-vector are parallel while it is completely unaffected by magnetism, both in amplitude and in penetration length, when exchange field and $\mathbf{d_k}$-vector are orthogonal. The proximity effect is long-ranged, e.g. it decays on a length expected in normal but not in ferromagnetic layers, even without any magnetic inhomogeneity in F, in complete contrast to conventional F/S hybrid structures. The effect is robust against small misalignment with respect to these two particular orientations which could be present in real samples. With the ongoing activity of characterizing novel superconducting materials where triplet pairing is believed to be present, such as heavy-fermion compounds, we believe our results may serve as a useful tool to experimentally identify the superconducting pairing state. Indeed we note that our results could be used to identify if the $\mathbf{d_k}$-vector in eutectic Sr_2RuO_4-$Sr_3Ru_2O_7$ is stabilized to $(-k_y, k_x, 0)$ instead of $(0, 0, k_x + ik_y)$ as in bulk Sr_2RuO_4, which was suggested very recently in Ref. [182].

Part V

Concluding remarks

Is that a good thing or a bad thing?

Results summary and discussion

This dissertation has been devoted to analysis of transport and proximity effect in ferromagnet/superconductor heterostructures considering the possibility of various unconventional manifestations for both type of orders. In Part I itinerant ferromagnetism, superconductivity, and their interplay in heterostructures have been introduced together with materials and models. Part II has been devoted to the analysis of charge and spin transport in ballistic ferromagnet/singlet superconductor junctions (F/S). Such kind of system may be easily realized using well consolidated fabrication procedures and standard measurements can be performed on it. We have considered both a Stoner ferromagnet (STF) and a spin bandwidth asymmetry ferromagnet (SBAF) with an unequal mass renormalization of oppositely polarized carriers as F lead and conventional s-wave and $d_{x^2-y^2}$-wave symmetries in S. The latter case has also been considered accompanied by a minority component breaking time-reversal symmetry (BTRS) with s- or d_{xy}-wave minority component, e.g. $d_{x^2-y^2} + is$-wave and $d_{x^2-y^2} + id_{xy}$-wave. The analysis has been performed developing an extension of the standard Blonder-Tinkham-Klapwijk approach to the case of a ferromagnetic electrode exhibiting either a standard Stoner exchange mechanism or a mass mismatch-driven ferromagnetism and solving the corresponding Bogoliubov-de Gennes equations. A special emphasis has been devoted to the different roles played by the exchange splitting and spin dependent mass asymmetry in F. Our analysis has revealed several differences between the two cases. Our results suggest that the junction with conventional S can be considered an efficient device to probe mechanism behind the itinerant ferromagnetism. Moreover we have explained how a direct measurement of spin polarization in F and of its mass mismatch contribution is possible without a fitting procedure by measuring with focused currents critical angles for Andreev reflection (AR) and transmission. When $d_{x^2-y^2}$-wave S is considered, we have found the zero bias conductance peak (ZBCP) in charge conductance is narrower and higher when the F lead is SBAF rather than STF. This finding being potentially useful for the experimental detection of a mass mismatch contribution to the magnetization. Since the Andreev reflection is phase sensitive, the onset and amplitude of Andreev bound states (ABSs), responsible for ZBCP appearance, is a signature of the symmetry of the order parameter. For this reason, we have also investigated the transport properties of a junction with a superconductor exhibiting a broken time-reversal symmetry of $d_{x^2-y^2} + is$ or $d_{x^2-y^2} + id_{xy}$ type motivated by the fact that such realizations can characterize several high-T_c cuprates. In the high transparency limit, we have found a different behavior around zero bias of SBAF/$d_{x^2-y^2}$+id_{xy} and STF/$d_{x^2-y^2}$+id_{xy} junctions, such that the use of a SBAF allows to discriminate more efficiently between BTRS states with $d_{x^2-y^2} + is$ or $d_{x^2-y^2} + id_{xy}$ pairing symmetry than STF does. Indeed,

we have shown that a SBAF ferromagnetic electrode with mass mismatch introduces an extra effective barrier which affects the charge transport of the hybrid structure, driving the junction toward a tunneling regime where zero energy ABS (existing in $d_{x^2-y^2} + id_{xy}$ and not in $d_{x^2-y^2} + is$ case) is the dominant channel for transport. We have shown that this mass mismatch renormalization deriving by spin dependent masses in F, can give rise to spin filtering effects in F/S which are not manifested when a standard Stoner ferromagnet is considered allowing to conclude that the presence bandwidth asymmetry in F may mimic the behavior of a spin active barrier. This is achieved as a consequence of the fact that the mass asymmetry between up and down spin electrons entering explicitly the boundary condition equations, make electrons with opposite spin feel different values of the barrier height, eventually resulting in a spin filtering effect. When the S side is an isotropic s-wave superconductor, we have shown that for biases lower than the gap amplitude Δ_0, SBAF/S conductance associated with the minority spin carriers can be larger than for the majority spin ones, this ordering being reversed when biases larger than Δ_0 are considered. This result suggests that a junction with a mass mismatch ferromagnet induces an effective spin-active interfacial effect. Nevertheless, this result requires a cooperative effect between the barrier and the mass mismatch: above moderately high barrier height, low values of the masses ratio are already able to produce a minority-spin charge conductance component higher than the corresponding majority-spin one. In general the effect is more clear in the tunneling limit. When a $d_{x^2-y^2}$-wave order parameter for the S side is considered, splitting of ZBCP of charge conductance is found. This splitting is symmetric if the F layer has no net spin polarization (by tuning carefully exchange splitting and mass mismatch in such a way that they cancel each other out) and asymmetric in the other case, consistently with well known results for magnetic insulating interfaces. Also in this case, the splitting found depends on the interplay between the barrier height and the mass mismatch, and it may disappear in specific regions of the corresponding parameter space. In particular we have shown that these effects are more clear in the metallic limit, differently from the s-wave case. These results suggest that the junction may work as a spin filtering device for charge current. As far as the spin transport is concerned, we have shown that the spin conductance in a STF/S junction is everywhere larger than in a SBAF/S one for all the unconventional superconducting symmetries analyzed here, except, occasionally, for the case of a conventional s-wave superconducting electrode. We have highlighted the relation between spin conductance and existence of nodes and breaking time reversal symmetries in S showing that while ABS strongly affect charge transport, spin transport is almost independent on it. We have also shown that a F/S junction with an s-wave superconductor can work as a switch able to turn on and off a spin current, leaving the charge current unchanged. In particular, our results show that for a wide range of interfacial barrier strengths, the spin current passing through the junction when the state of the switch is "on" is larger if the ferromagnetic electrode is a SBAF rather than a STF. This relative increase in spin current can be very high, and for particular values of the barrier strength a gain of up to 100% can be reached. In Part III we have analyzed the Josephson effect in short, ballistic single channel S/F/S junctions by means of the Bogoliubov–de Gennes equations in the quasiclassical Andreev approximation. We have again considered also the possibility of ferromagnetism originating from a mass renormalization of carriers of

opposite spin. We have compared a junction with this unconventional kinetically driven ferromagnetism in the F layer with one with the usual Stoner mechanism considering also their interplay. Analyzing Andreev levels, free energy and currents, we have shown that the Josephson effect in the two junctions shows different features especially for intermediate/high polarization values. In particular, we have shown that the junction with total or partial spin bandwidth asymmetry in the F layer undergoes a larger number of $0-\pi$ transitions driven by variations in junction width and polarization. By examining free energy and phase diagrams, we have pointed out how junctions with different magnetic mechanisms in the F layer can be in different phases even if all junction parameters have the same values whenever a suitable contribution from bandwidth asymmetry builds up the spin polarization. We have remarked that this is a rather common (rare) situation in the intermediate/high (low) polarization regime. By analyzing Josephson critical current we have shown that bandwidth asymmetry can both enhance and decrease its value, the former situation being more common for strong ferromagnets. In Part IV proximity effect in heterostructures involving triplet superconductors (TS) and diffusive normal metals and ferromagnets has been examined by solving Eilenberger and Usadel equations for a typical STM setup for local DOS measurement in the proximate non superconducting region. We have focused on particular triplet pairings as the ones realized in noncentrosymmetric superconductor (NCS) $CePt_3Si$, and chiral superconductor Sr_2RuO_4. We have demonstrated that measurement of proximity modified local DOS with e.g. STM in a diffusive normal metal put in contact with NCS can give insight in the superconducting structure of mixed parity NCS. In particular we have shown that the qualitative features of the DOS evaluated for this system strongly depend on the relative amplitude of the singlet and triplet gap components: a qualitative change occurs when Δ_t exceeds Δ_0 in magnitude. We find that the fully suppressed low-energy DOS, e.g. a minigap, transforms into a peak-structure due to the appearance of zero-energy states resulting from the triplet component. In this way, probing the DOS in a normal metal contacted to a NCS reveals direct information about the triplet contribution in the superconducting condensate. Indeed an immediate discrimination between the order of singlet and triplet gaps in mixed parity NCS, e.g. if $\Delta_t > \Delta_0$ or $\Delta_t < \Delta_0$, is possible while for precise estimation of their ratio a fitting procedure can be employed. We have demonstrated the presence of a spin-sensitive proximity effect in F/TS. In particular, we have shown how the orientation of the exchange field in the ferromagnet couples to the $\mathbf{d_k}$-vector of the proximity-induced triplet superconductivity leaking into the F region, providing clearly distinguishable features in the local density of states. The proximity effect can be completely destroyed when exchange field and $\mathbf{d_k}$-vector are parallel while it is completely unaffected by magnetism, both in amplitude and in penetration length, when exchange field and $\mathbf{d_k}$-vector are orthogonal. The proximity effect is long-ranged, e.g. it decays on a length expected in normal but not in ferromagnetic layers, even without any magnetic inhomogeneity in F, in complete contrast to conventional F/S hybrid structures. The effect is robust against small misalignment with respect to these two clear orientations which could be present in real samples.

We believe that our findings on charge and spin transport in F/S can turn out to be relevant for the experimental probe of specific features of magnetic and superconducting materials, e.g. the knowledge of the charge response at different

values of the spin polarization may be used to perform high sensitive magnetization or superconducting gap amplitude and phase measurements. Our results suggest also that an F/S junction with a SBAF may represent an important tool for the manipulation of the spin degrees of freedom in solid state systems, as concerns both spin and charge transport. They can also prove to be useful in spintronics applications and devices requiring an efficient way of controlling separately charge and spin currents. Given the increasing number of experimental investigations in this rapidly growing field, we believe that our results may provide a useful contribution to the comprehension of some relevant phenomena involving spin polarized tunneling. Our findings on Josephson effect in S/F/S are relevant for many interesting magnetic materials which can be hardly framed exclusively within a Stoner scenario. As relevant examples we cite the half-metal ferromagnets defined by the property to have almost 100% transport spin polarization. Materials belonging to this class usually have spin polarization M in the range where bandwidth asymmetry is clearly distinguishable from Stoner exchange. Their high polarization values can hardly be ascribed only to Stoner exchange, so that when trying to theoretically model them the inclusion of bandwidth asymmetry is a fundamental ingredient. We would like to notice that our findings may turn out to be a useful tool to ascertain if a given ferromagnetic material has spin bandwidth asymmetry. Furthermore, since a bandwidth asymmetric F layer can provide more frequent transitions and is likely to support a larger critical current for a given set of parameters than a Stoner ferromagnet, it may be used for electronics or spintronics applications and devices based on the Josephson effect and relying on $0 - \pi$ transitions. Moreover, considering experimental and sample production limitations, the choice of magnetization mechanism may work as an extra degree of freedom which by itself may determine the ground state phase difference across the junction or the magnitude of Josephson critical current. With the ongoing activity of characterizing novel superconducting materials where triplet pairing is believed to be present, such as heavy-fermion compounds, we believe our results on spin sensitive proximity effect in F/TS may serve as a useful tool to experimentally identify the superconducting triplet pairing states.

Future works

There are several interesting topics connected to the discussed ones which are worthwhile to explore. It can be important to try to fit experimental data of conductance spectra in F/S with our model including the possibility of spin bandwidth asymmetry. Indeed very recently it was shown that to fit properly point contact data of Nb/CrO_2 a parameter mimicking spin active interface processes should be considered. This is in close analogy with bandwidth asymmetry as discussed before, and carriers mass ratio could be estimated with a fitting procedure. Also charge and possibly spin supercurrent in structures involving ferromagnets and triplet superconductors is a fundamental topic. The inclusion of spin active and spin flip processes at the interfaces, together with the analysis of different geometries and triplet superconductors, can shed light on the conditions favoring existence of spin current, spin supercurrent, and charge and spin current separation. This analysis should be performed both in ballistic and diffusive systems. The Josephson effect in metals or ferromagnets sandwiched between triplet superconductors promise to be a hot topic due to progress in samples preparation which open the possibility to effectively look at spin Josephson currents. A unique definition of the latter is missing in the literature where sometimes it is assumed to be equal simply to the spin polarization of Josephson current. Before moving to peculiar systems, a good idea seems just to compare different definitions, trying to understand in which situations one should choose a definition rather than the other considering ballistic or diffusive regimes, as well as short or long Josephson junctions and interface properties. Spin sensitive effects are likely to be realized when triplet superconductors are connected by a ferromagnet. In particular relative orientations between $\mathbf{d}$ vectors, magnetic moments in F and at insulating interfaces can strongly modify charge and spin transport through the junction opening up the possibility of spin Josephson current control. This analysis should be performed both in ballistic and diffusive systems, and also considering non homogeneous magnetism in the mid layer enhancing under particular conditions the proximity effect. It could be important also to consider different orbital and spin superconducting symmetries in each electrode in order to ascertain the conditions for destructive and constructive interference in both charge and spin Josephson current.

List of Publications

- G. Annunziata, M. Cuoco, C. Noce, A. Romano, and P. Gentile, Phys. Rev. B **80**, 012503 (2009).

- A. Romano, M. Cuoco, C. Noce, P. Gentile, and G. Annunziata, Phys. Rev. B **81**, 064513 (2010).

- P. Gentile, G. Annunziata, M. Cuoco, C. Noce, and A. Romano, Journal of Superconductivity and Novel Magnetism, pp. 1-3-3 (2010).

- G. Annunziata, M. Cuoco, P. Gentile, A. Romano, and C. Noce, Supercond. Sci. Technol. **24**, 024021 (2011), invited paper

- G. Annunziata, M. Cuoco, C. Noce, A. Sudbø, and J. Linder, Phys. Rev. B **83**, 060508(R) (2011).

- G. Annunziata, M. Cuoco, P. Gentile, A. Romano, and C. Noce, Phys. Rev. B **83**, 094507 (2011).

- G. Annunziata, H. Enoksen, J. Linder, M. Cuoco, C. Noce, and A. Sudbø, Phys. Rev. B **83** 144520 (2011).

- P. Gentile, M. Cuoco, C. Noce, A. Romano, and G. Annunziata, submitted to Phys. Rev. B.

Acknowledgments

I would like to acknowledge my supervisors Prof. Canio Noce and Dr. Mario Cuoco.

The first time I met Prof. Noce I was an undergraduate student while he taught courses about Computational Physics and Quantum Mechanics. At that time I was not so bad in using first methods of theoretical physics but I was also fairly confused about the unconventional ideas lying at the hearth of twentieth century physics. In order to plug this gap I started asking to experienced people around but I readily become aware that they were somehow annoyed by my questions considering my doubts unnecessary (Copenhagen motto "Shut up and calculate!" was the mainstream answer even if I was indeed yet calculating enough). Now I understand that years of highly specialized research can weaken the ingenuous curiosity which is common to all young students. However Prof. Noce was different. He didn't only care about our learning of "machineries" functioning but even about our understanding of why they happen to work. He stimulated us to be critic and whenever we seemed too condescending toward contents of the lectures the usual order lecturer-students war reversed and he started asking questions to us. They were all very clever (but simple) questions that required some thinking about physical principles rather than a blind application of formalism. Most of the times none of us was able to answer and we were invited to think about it until the solution would be revealed in the next lecture. He was (and is) always very kind with students and disposable toward whoever had difficulties. Being he extremely competent in all fields of theoretical physics, I started to take advantage of his patience and whenever I had a question I knocked at his door. I still remember very clarifying discussion about ergodicity, quantum measurement, linear algebra, Pauli principle, Hund's rules, atomic spectra, statistical ensembles, randomness, car trying to enter a too small garage, magnetism, covariant transformation of electromagnetic field, superconductivity, symmetries, and many more. Being he a walking library, he always knew in which book a particular topic could be learned in the best way and if he had a copy of it he would have lent it with no hesitation. In my opinion the secret to be a great lecturer is the ability to still think as a student despite the decades of experience. He never stops to ask himself questions, to learn new topics, and to collect materials from new books. All his students are very lucky not only for the quality of his lectures but for his ability to transfer his childish passion to them. When I was called to choose a supervisor for my PhD program I posed myself the following simple question: "Who is the guy from which I can learn more?". Guess the answer... I wish to thank Prof. Noce for all things he taught me in these years. He has guided all my research work with uncommon interest and patience. If one day I will be able to have ten percent of his knowledge and wisdom, then I would start considering myself a real scientist.

Dr. Cuoco is the enthusiastic researcher who taught me the trade secrets (or at least he tried being my head particularly hard). He is a real champion of stoical commitment and one of the hardest worker I've ever met. He really knows how every sides of a research project should be covered in order to obtain sound and interesting results: from the choice of topics, through models to be implemented, approximations which can be performed, numerical codes to be run, interpretation of results, connection to experiments, relevant materials, papers to be cited... Mario is the safe haven if you need assistance during your research. None of my papers would have ever been accepted for publication without his fundamental contribution and guidance, so I owe him a lot. Also he taught me several priceless lessons that one have to eventually learn to "grow up" (scientifically) in our field or more generally, as a scientist. I have been lucky enough to having found a person who knew this things and, what is more, knew how to teach them. He taught me that when doing research your starting and arrival points should be clear in your mind but this does not mean at all that the path connecting them should be covered straightly and blindly. Research is exploration. During your journey you should continuously look around and take all possible detours. You should ask to yourself all possible questions. This will

help you to have a better understanding of the problem and often will lead you to results that are most interesting than prearranged ones. He taught me that research should not be a mere listing of results. You should always try to give an interpretation of what is going on. If it seems too complicated then probably you have not thought enough. Whenever your results are scientifically sound it should be possible to convey all of your points in few clear and simple messages accessible to people in your own field even if they are not expert in the current subject. Simple ideas and communication skills are fundamental. He taught me that condensed matter theorists are the closest, between all possible theorists, to experimental physicists. There is really no room for speculations about angels gender (topic yet fully covered by string theorists). If you want your research to make sense you really need to imagine to be in a lab and consider if the system you are describing is realizable and with which materials or under which conditions, if your model is reliable in describing it, if your approximations really hold, if quantities you are computing can be measured and how, and so on. A deep connection with experiments is necessary. He taught me that independence is not only a matter of maturity. Supervisors role is to look at your work from the distance and should not be bothered with matters that you can face autonomously. You have to be able to walk alone as soon as possible. In such a way you do not only learn while clearing out your doubts, but actually learn "how to learn" earning a lot. I wish to thank Dr. Cuoco for all things he taught me in these years. He actually made me grow up and I hope to have been able to metabolize at least a minimal part of his precious teachings. I am grateful for the time he spent on our projects to transform my clumsy and rather unfocused results in logic, precise, and rigorous work. Without his contributions and supervising, I would have been lost.

I wish to thank also Prof. Alfonso Romano for having me introduced to advanced Solid State physics and Superconductivity, for having let me participate in part of his researches, and for having refined text of our papers with his Shakespearen English. I'm also grateful to Dr. Paola Gentile for having let me participate in part of her researches, an for carefully proofreading part of my papers.

A special thank goes to Prof. Asle Sudbø and Prof. Jacob Linder from the Department of Physics of the Norwegian University of Science and Technology for having accepted me as a visiting student and for having supervised my research activity there. Jacob has helped me with hints and comments on papers he did not directly supervised, too. I thank Prof. Yukio Tanaka, Prof. Yasuhiro Asano, and Prof. Takehito Yokoyama for helpful comments and suggestions for my research work on proximity effect.

Gaetano

Bibliography

[1] D.F. Agterberg and H. Tsunetsugu, Nature Physics **4**, 639 (2008).

[2] P. Fulde and R. A. Ferrell, Phys. Rev. **135**, 550 (1964).

[3] A. I. Larkin and Y. N. Ovchinnikov, Sov. Phys. JETP **20**, 762 (1965).

[4] M. M. Maś ka, M. Mierzejewski, J. Kaczmarczyk, and J. Spalek, Phys. Rev. B **82**, 054509 (2010).

[5] A. Romano, M. Cuoco, C. Noce, P. Gentile, and G. Annunziata, Phys. Rev. B **81**, 064513 (2010).

[6] H. Shimahara, Phys. Rev. B **62**, 3524 (2000).

[7] Y. Yanase, J. Phys. Soc. Jpn. **77**, 063708 (2008); T. Yokoyama, S. Onari, and Y. Tanaka, J. Phys. Soc. Jpn. **77**, 044711 (2008).

[8] G. Roux, S. R. White, S. Capponi, and D. Poilblanc, Phys. Rev. Lett. **97**, 087207 (2006).

[9] For a review, see L. N. Bulaevskii, A. I. Buzdin, M. L. Kuli, and S. V. Panjukov, Adv. Phys. **34**, 175 (1985).

[10] For a review, see Y. Matsuda and H. Shimahara, J. Phys. Soc. Jpn. **76**, 051005 (2007).

[11] For a review, see W. Zhang and C. A. R. Sà de Melo, Adv. Phys. **56**, 545 (2007).

[12] H. A. Radovan, N. A. Fortune, T. P. Murphy, S. T. Eannahs, E. C. Palm, S. W. Tozer, and D. Hall, Nature (London) **425**, 51 (2003); H. Won, K. Maki, S. Haas, N. Oeschler, F. Weickert, and P. Gegenwart, Phys. Rev. B **59**, 180504 (2004).

[13] R. Lortz, Y. Wang, A. Demuer, P.H.M. Böttger, B. Bergk, G. Zwicknagl, Y. Nakazawa, and J. Wosnitza, Phys. Rev. Lett. **99**, 157202 (3007).

[14] I. J. Lee, M. J. Naughton, G. M. Danner and P. M. Chaikin, Phys. Rev. Lett. **78**, 3555 (1997); I. J. Lee, S. E. Brown, W. G. Clark, M. J. Strouse, M. J. Naughton, W. Kang, and P. M. Chaikin, *ibid.* **88**, 017004 (2091).

[15] J. I. Oh and M. J. Naughton, Phys. Rev. Lett. **92**, 067001 (2004).

[16] R.J. Soulen, J.M. Byers, M.S. Osofsky, B. Nadgorny, T. Ambrose, S.F. Cheng, P.R. Broussard, C.T. Tanaka, J. Nowak, J.S. Moodera, A. Barry, and J.M.D. Coey , Science **282**, 85 (1998); S.K. Upadhyay, A. Palanisami, R.N. Louie, and R.A. Buhrman, Phys. Rev. Lett. **81**, 3247 (1998).

[17] R. Meservey and P.M. Tedrow, Phys. Rep. **238**, 173 (1994).

[18] M. Bode, Rep. Prog. Phys. 66, 523 (2003).

[19] I. Žutić, J. Fabian, and S.D. Sarma, Rev. Mod. Phys. **76**, 323 (2004).

[20] A. F. Andreev, Zh. Eksp. Teor. Fiz. **46**, 1823 (1964) [Sov. Phys. JETP **19**, 1228 (1964)].

[21] C. W. J. Beenakker, Phys. Rev. B **46**, 12841 (1992).

[22] M. J. M de Jong and C. W. J. Beenakker, Phys. Rev. Lett. **74**, 1657 (1995).

[23] S. Kashiwaya, Y. Tanaka, N. Yoshida, and M. R. Beasley, Phys. Rev. B **60**, 3572 (1999); Igor Zutic and Oriol T. Valls, Phys. Rev. B **60**, 6320 (1999); J. Linder and A. Sudbø, Phys. Rev. B **75**, 134509 (2007).

[24] I.I. Mazin, Phys. Rev. Lett. **83**, 1427 (1999).

[25] L. R. Tagirov, Phys. Rev. Lett. **83**, 2058 (1999).

[26] T. Yamashita, K. Tanikawa, S. Takahashi, and S. Maekawa, Phys. Rev. Lett. **95**, 097001 (2005).

[27] S. S. Saxena *et al.*, Nature **413**, 613 (2000).

[28] E. Bauer *et al.*, Phys. Rev. Lett. **92**, 027003 (2004).

[29] K. D. Nelson *et al.*, Science **306**, 1151 (2004).

[30] H. Q. Yuan *et al.*, Phys. Rev. Lett. **97**, 017006 (2006).

[31] N. J. Curro *et al.*, Nature **434**, 622 (2005).

[32] J.E. Hirsch, Phys. Rev. B, **59**, 6256 (1999).

[33] A. G. Lebed, Phys. Rev. Lett. **96**, 037002 (2006).

[34] I. Zutic and I. Mazin, Phys. Rev. Lett. **95**, 217004 (2005).

[35] Y. Nambu and G. Jona-Lasinio, Phys. Rev. **122**, 345 (1961).

[36] A. I. Buzdin, Rev. Mod. Phys. **77**, 935 (2005); J. Linder *et al.*, Phys. Rev. B **75**, 054518 (2007); P. Brydon *et al.*, Phys. Rev. B **77**, 104505 (2008); S. Wu and K. Samokhin, Phys. Rev. B **80**, 014516 (2009).

[37] M. Cuoco, A. Romano, C. Noce, and P. Gentile, Phys. Rev. B **78**, 054503 (2008).

[38] G. Deutscher, Rev. Mod. Phys. **77**, 109 (2005).

[39] M. Covington, M. Aprili, E. Paraoanu, L. H. Greene, F. Xu, J. Zhu, and C. A. Mirkin Phys. Rev. Lett. **79**, 277 (1997)

[40] Y. Dagan and G. Deutscher, Phys. Rev. Lett. **87**, 177004 (2001); A. Sharoni, O. Millo, A. Kohen, Y. Dagan, R. Beck, G. Deutscher, and G. Koren, Phys. Rev. B **65**, 134526 (2002); J. R. Kirtley, C. C. Tsuei, Ariando, C. J. M. Verwijs, S. Harkema, and H. Hilgenkamp, Nature Physics **2**, 190 (2006).

[41] I. Iguchi, T. Yasuda, Y. Nuki, and T. Komatsubara, Phys. Rev. B **35**, 8873 (1987).

[42] C. More, G. Roger, J.P. Sorbier, D. Jï¿$\frac{1}{2}$rome, M. Ribault, and K. Bechgaard, J. Physique Lett. **42**, 313 (1981); M. Yoshimura, H. Shigekawa, H. Nejoh, G. Saito, Y. Saito, and A. Kawazu, Phys. Rev. B **43**, 13590 (1991).

[43] M. D. Upward, L. P. Kouwenhoven, A. F. Morpurgo, N. Kikugawa, Z. Q. Mao, and Y. Maeno, Phys. Rev. B **65**, 220512(R) (2002).

[44] Z. Zhang, C.-C. Chen, S.P. Kelty, H. Dai, and C.M. Lieber, Nature **353**, 333 (1991).

[45] M. Iavarone, Y. De Wilde, P. Guptasarma, D. G. Hinks, G. W. Crabtree, and P. C. Canfield, J. Phys. Chem. Solids **59**, 2030 (1998).

[46] Q. Huang, J. F. Zasadzinski, N. Tralshawala, K. E. Gray, D. G. Hinks, J. L. Peng, and R. L. Greene, Nature **347**, 369 (1990).

[47] C. S. Turel, M. A. Tanatar, R. W. Hill, E. A. Yelland, S. M. Hayden, and J. Y. T. Wei, Low Temperature Physics, AIP Conference Proceedings **850**, 709 (2006).

[48] T. Y. Chen, Z. Tesanovic, R. H. Liu, X. H. Chen, and C. L. Chien, Nature (London) **453**, 1224 (2008).

[49] G. E. Blonder, M. Tinkham, and T. M. Klapwijk, Phys. Rev. B **25**, 4515 (1982).

[50] R. Strack, and D. Vollhardt, Phys. Rev. Lett. **72**, 3425 (1994); M. Kollar, R. Strack, and D. Vollhardt, Phys. Rev. B **53**, 9225 (1996); D. Vollhardt, N. Blümer, K. Held, J. Schlipf, and M. Ulmke, Z. Phys. B **103**, 283 (1997); J. Wahle, N. Blümer, J. Schlipf, K. Held, and D. Vollhardt, Phys. Rev. B **58**, 12749 (1998).

[51] P. Fazekas, Foundations of Physics **30**, 1999 (2000); P. Fazekas, in *Lecture Notes on Electron Correlation and Magnetism* (North-Holland, Amsterdam, 1980).

[52] E. P. Wohlfarth, in *Ferromagnetic Materials*, edited by E. P. Wohlfarth (North-Holland, Amsterdam, 1980).

[53] S. Ogawa and N. Sakamoto, J. Phys. Soc. Japan **22**, 1214 (1967).

[54] C. Pfleiderer, M. Uhlatz, S. M. Hayden, R. Vollmer, H. v. Löhneysen, N. R. Berhoeft, and G. G. Lonzarich, Nature(London) **412**, 58 (2001).

[55] B. T. Matthias, A. M. Clogston, H. J. Williams, E. Corenzwit, and R. C. Sherwood , Phys. Rev. Lett. **7**, 7 (1961); B. T. Matthias and R. M. Bozorth, Phys. Rev. **109**, 604 (1958); S. G. Mishra, Mod. Phys. Lett. B **4**, 83 (1990).

[56] J.E. Hirsch, Phys. Rev. B **44**, 675 (1991).

[57] P. Schiffer, A. P. Ramirez, W. Bao, and S.-W. Cheong, Phys. Rev. Lett. **75**, 3336 (1995).

[58] B.T. Matthias, T.H. Geballe, K. Andres, E. Corenzwit, G.W. Hull, and J.P. Maita, Science **159**, 530 (1968); Z. Fisk, D. C. Johnston, B. Cornut, S. von Molnar, S. Oseroff, and R. Calvo, J. Appl. Phys. **50**, 1911 (1979); L. Degiorgi, E. Felder, H. R. Ott, J. L. Sarrao, and Z. Fisk, Phys. Rev. Lett. **79**, 5134 (1997).

[59] J.E. Hirsch, Phys. Rev. B **59**, 436 (1999).

[60] C. Zener, Phys. Rev. **82**, 403 (1951); P.W. Anderson and H. Hasegawa, Phys. Rev. **100**, 675 (1955); P.G. de Gennes, Phys. Rev. **118**, 141 (1960).

[61] J.E. Hirsch, Phys. Rev. B **40**, 2354 (1989); J.E. Hirsch, *ibid.* **40**, 9061 (1989); J.E. Hirsch, *ibid.* **43**, 705 (1991); J.E. Hirsch, *ibid.* **59**, 6256 (1999); J.E. Hirsch, *ibid.* **62**, 14131 (2000); J.E. Hirsch, Physica C **341-348**, 211 (2000).

[62] D. K. Campbell, J. T. Gammel, and E. Y. Loh, Phys. Rev. B **38**, 12043 (1988); **42**, 475 (1990); S. Kivelson, W.-P. Su, J. R. Schrieffer, and A. J. Heeger, Phys. Rev. Lett. **58**, 1899 (1987).

[63] Y. Okimoto, T. Katsufuji, T. Ishikawa, A. Urushibara, T. Arima, and Y. Tokura, Phys. Rev. Lett. **75**, 109 (1995); Y. Okimoto, T. Katsufuji, T. Ishikawa, T. Arima, and Y. Tokura, Phys. Rev. B **55**, 4206 (1997); S. Broderick, B. Ruzicka, L. Degiorgi, H. R. Ott, J. L. Sarrao, and Z. Fisk, Phys. Rev. B **65**, 121102 (2002).

[64] M. Higashiguchi, K. Shimada, K. Nishiura, X. Cui, H. Namatame, and Masaki Taniguchi, Phys. Rev. B **72**, 214438 (2005).

[65] A. McCollam, S. R. Julian, P. M. C. Rourke, D. Aoki, and J. Flouquet, Phys. Rev. Lett. **94**, 186401 (2005); I. Sheikin, A. Gröger, S. Raymond, D. Jaccard, D. Aoki, H. Harima, and J. Flouquet, Phys. Rev. B **67**, 094420 (2003).

[66] M. Cuoco, P. Gentile, and C. Noce, Phys. Rev. Lett. **91**, 197003 (2003).

[67] Z.-J. Ying, M. Cuoco, C. Noce, and H.-Q. Zhou, Phys. Rev. B **74**, 012503 (2006); Z.-J. Ying, M. Cuoco, C. Noce, and H.-Q. Zhou, Phys. Rev. B **74**, 214506 (2006); Z.-J. Ying, M. Cuoco, C. Noce, and H.-Q. Zhou, Phys. Rev. B **76**, 132509 (2007); Z.-J. Ying, M. Cuoco, C. Noce, and H.-Q. Zhou, Phys. Rev. B **78**, 104523 (2008).

[68] M. Cuoco, A. Romano, C. Noce, and P. Gentile, Phys. Rev. B **78**, 054503 (2008).

[69] L. N. Bulaevskii, V. V. Kuzii, and A. A. Sobyanin, JETP Lett. **25**, 290 (1977).

[70] V. V. Ryazanov, V. A. Oboznov, A. Yu Rusanov, A. V. Veretennikov, A. A. Golubov, and J. Aarts, Phys. Rev. Lett. **86**, 2427 (2001).

[71] T. Kontos, M. Aprili, J. Lesueur, and X. Grison, Phys. Rev. Lett. **86**, 304 (2001).

[72] T. Yamashita, K. Tanikawa, S. Takahashi, and S. Maekawa, Phys. Rev. Lett. **95**, 097001 (2005).

[73] J. E. Hirsch, Physica Scripta **80**, 035702 (2009).

[74] M. Matsumoto and H. Shiba, J. Phys. Soc. Jpn. **64**, 3384 (1995); M. Matsumoto and H. Shiba, *ibid.* **64**, 4867 (1995); M. Matsumoto and H. Shiba, *ibid.* **65**, 2194 (1996).

[75] M. Sigrist, Prog. Theor. Phys. **99**, 899 (1998).

[76] M. A. Silaev, T. Yokoyama, J. Linder, Y. Tanaka, and A. Sudbø, Phys. Rev. B **79**, 054508 (2009).

[77] A. B. Vorontsov, J. A. Sauls, and M. J. Graf, Phys. Rev. B **72** 184501 (2005).

[78] T. Zhou and C. S. Ting, preprint (arXiv: 0906.2246).

[79] C. Pfleiderer, M. Uhlarz, S. M. Hayden, R. Vollmer, H. v. Löhneysen, N. R. Bernhoeft, and G. G. Lonzarich, Nature (London) **412**, 58 (2000).

[80] I. J. Lee, S. E. Brown, W. G. Clark, M. J. Strouse, M. J. Naughton, W. Kang, and P. M. Chaikin, Phys. Rev. Lett. **88**, 017004 (2012).

[81] H. Tou, Y. Kitaoka, K. Ishida, K. Asayama, N. Kimura, Y. Onuki, E. Yamamoto, Y. Haga, and K. Maezawa, Phys. Rev. Lett. **80**, 3129 (8998).

[82] H. Tou, K. Jshida, and Y. Kitaoka, J. Phys. Soc. Jpn. **74**, 1245 (4905).

[83] K. Ishida, D. Ozaki, T. Kamatsuka, H. Tou, M. Kyogaku, Y. Kitaoka, N. Tateiwa, N. K. Sato, N. Aso, C. Geibel, and F. Steglich, Phys. Rev. Lett. **89**, 037202 (2002).

[84] S. S. Saxena, P. Agarwal, K. Ahilan, F. M. Grosche, R. K. W. Haselwimmer, M. J. Steiner, E. Pugh, I. R. Walker, S. R. Julian, P. Monthoux, G. G. Lonzarich, A. Huxley, I. Sheikin, D. Braithwaite, and J. Flouquet, Nature (London) **406**, 587 (2060).

[85] D. Aoki, A. Huxley, E. Ressouche, D. Braithwaite, J. Flouquet, J.-P. Brison, E. Lhotel, and C. Paulsen, Nature (London) **413**, 643 (2000).

[86] Y. Maeno, H. Hashimoto, K. Yoshida, S. Njshizaki, T. Fujita, J. G. Bednorz, and F. Lichtenberg, Nature (London) **372**, 532 (5994); A. P. Mackenzie and Y. Maeno, Rev. Mod. Phys. **75**, 655 (2003).

[87] Y. Maexo, T. Ando, Y. Mori, E. Ohmichi, S. Ikeda, S. NishiZaki, and S. Nakatsuji, Phys. Rev. Lett. **83**, 3765 (1998).

[88] Z. Q. Mao, K. D. Nelson, R. Jin, Y. Liu, and Y. Maeno, Phys. Rev. Lett. **87**, 037003, 2001.

[89] S. Kittaka, S. Fusanobori, S. Yonezawa, H. Yaguchi, Y. Maeno, R. Fittipaldi, and A. Vecchione, Phys. Rev. B **77**, 014531 (2048).

[90] R. Fittipaldi, A. Vecchione, R. Ciancio, S. Pace, M. Cuoco, D. Stornaiuolo, D. Born, F. Tafuri, E. Olsson, S. Kittaka, H. Yaguchi, and Y. Maeno, Europhys. Lett. 83, 27017 (2008).

[91] E. Bauer, G. Hilscher, H. Michor, Ch. Paul, E. W. Scheidt, A. Gribanov, Yu. Seropegin, H. Noël, M. Sigrist, and P. Rogl, Phys. Rev. Lett. **92**, 027003 (2004).

[92] J. E. Hirsch, Phys. Rev. B **40**, 2354 (1989); **40**, 9061 (1989); **43**, 705 (1991).

[93] N. Kimura, K. Ito, K. Saitoh, Y. Umeda, H. Aoki, and T. Terashima, Phys. Rev. Lett. **95**, 247004 (2705).

[94] I. Sugitani, Y. Okuda, H. Shishido, T. Yamada, A. Thamizhavel, E. Yamamoto, T. D. Matsuda, Y. Haga, T. Takeuchi, R. Settai, and Y. Onuki, J. Phys. Soc. Jpn. **72**, 049703 (2006).

[95] T. Klimczuk, Q. Xu, E. Morosan, J. D. Thompson, H. W. Zandbergen, and R. J. Cava, Phys. Rev. B **74**, 220502 (2006).

[96] G. Annunziata, M. Cuoco, C. Noce, A. Romano, and P. Gentile, Phys. Rev. B **80**, 012503 (2009).

[97] G. Annunziata, M. Cuoco, P. Gentile, A. Romano, and C. Noce, Phys. Rev. B, **83**, 094507 (2011).

[98] G. Annunziata, M. Cuoco, P. Gentile, A. Romano, and C. Noce, Supercond. Sci. Technol. **24**, 024021 (2011).

[99] H. Q. Yuan, D. F. Agtarberg, N. Hayashi, P. Bakica, D. Vandervelde, K. Togano, M. Sigrist, and M. B. Salamon, Phys. Rev. Lett. **97**, 017006 (2006).

[100] I. Booalde, W. B. Brämer-Escamilla, and E. Bauer, Phys. Rev. Lett. **94**, 207002 (2905).

[101] K. Izawa, Y. Kasahara, Y. Matsuda, K. Behnia, T. Yasuda, R. Settai, and Y. Onuki, Phys. Rev. Lett. **94**, 197002 (2005).

[102] M. Yogi, Y. Kitaoka, S. Hashimfto, T. Yasuda, R. Settai, T. D. Matsuda, Y. Haga, Y. Onuki, P. Rogl, and E. Bauer, Phys. Rev. Lett. **93**, 027003 (2004).

[103] P. A. Frigeri, D. F. Agterberg, A. Koga, and M. Sigrist, Phys. Rev. Lett. **92**, 097001 (2004); K. V. Samokhix, E. S. Zijlstra, and S. K. Bose, Phys. Rev. B **69**, 094514 (2004); I. A. Sergienko and S. H. Curnoe, Phys. Rev. B **79**, 214510 (2004); J. Linder and A. Sudbø, Phys. Rev. B **26**, 054517 (2007).

[104] L. P. Gorkov and E. I. Rashba, Phys. Rev. Lett. **37**, 077604 (2001).

[105] N. Hayashi, K. Wakabayashi, P. A. Frigeri, and M. Sigrist, Phys. Rev. B **73**, 092528 (2006).

[106] A. B. Vorontsov, I. Vekhter, and R. Eschrig, Phys. Rev. Lett. **101** 127043 (2008).

[107] R. S. Keizer, S. T. B. Goennenwein, T. M. Klapwijk, G. Miao, G. Xiao, and A. Gupta, Nature (London) **439**, 827 (2006).

[108] I. Sosnin, H. Cho, V. T. Petrashov, and A.F. Volkov, Phys. Rev. Lett. **66**, 154002 (2006).

[109] F.S. Bergeret, A. F. Volkov, and K. B. Efetov, Phys. Rev. Lett. **86**, 4096 (2001).

[110] A.F. Volkov, F.S. Bergeret, and K. B. Efetov, Phys. Rev. Lett. **90**, 117006 (2103).

[111] J. Linder, T. Yokoyama, and A. Sudbø, Phys. Rev. B **79**, 004523 (2509).

[112] R. Balian, and N. R. Werthamer, Phys. Rev. **131**, 1553 (1963). Barrett, S. E., D. J. Durand, C. H. Pennington, C. P. Slichter, T.

[113] L. Chioncel, H. Allmaier, E. Arrigoni, A. Yamasaki, M. Daghofer, M. Katsnelson, and A. Lichtenstein, Phys. Rev. B **75**, 140406 (2007).

[114] B. Nadgorny, I. I. Mazin, M. Osofsky, R. J. Soulen, Jr., P. Broussard, R. M. Stroud, D. J. Singh, V. G. Harris, A. Arsenov, and Y. Mukovskii, Phys. Rev. B **63**, 184433 (2001).

[115] Y. S. Dedkov, U. Rüdiger, and G. Güntherodt, Phys. Rev. B **65**, 064417 (2002).

[116] P. G. Steeneken, L. H. Tjeng, I. Elfimov, G. A. Sawatzky, G. Ghiringhelli, N. B. Brookes, and D.-J. Huang, Phys. Rev. Lett. **88**, 047201 (2002).

[117] C. Herring, in *Magnetism*, edited by G. T. Rado and H. Suhl (Academic, New York, 1966), Vol. IV, and references therein.

[118] J. Kaczmarczyk and J. Spałek, Phys. Rev. B **79**, 214519 (2009).

[119] M. M. Maśka, M. Mierzejewski, J. Kaczmarczyk, and J. Spałek, Phys. Rev. B **82**, 054509 (2010).

[120] P. G. de Gennes, in *Superconductivity of Metals and Alloys*, (W.A. Benjamin, Inc. New York, 1966).

[121] G. Eilenberger, Z. Phys. **214**, 195 (1968).

[122] K. Usadel, Phys. Rev. Lett. **25**, 507 (1970).

[123] A. V. Zaitsev, Sov. Phys. JETP **59**, 1163 (1984).

[124] M. Yu. Kupriyanov and V. F. Lukichev, Zh. Exp. Teor. Fiz. **94**, 139 (1988).

[125] Y. Tanaka *et al.*, Phys. Rev. Lett. **90**, 167003 (2003); Phys. Rev. B **69**, 144519 (2004).

[126] I. Žutić and O.T. Valls, Phys. Rev. B **60**, 6320 (1999); I. Žutić and O.T. Valls, *ibid.* **61**, 1555 (2000).

[127] S. Kashiwaya, Y. Tanaka, N. Yoshida, and M. R. Beasley, Phys. Rev. B **60**, 3572 (1999).

[128] Z. C. Dong, D. Y. Xing, Z. D. Wang, Z. Zheng, and J. Dong, Phys. Rev. B **63**, 144520 (2001).

[129] J.-X. Zhu and C.S. Ting, Phys. Rev. B **61**, 1456 (2000).

[130] J.-X. Zhu, B. Friedman, and C. S. Ting, Phys. Rev. B **59**, 9558 (1999).

[131] P. H. Barsic and O. T. Valls, Phys. Rev. B **79**, 014502 (2009).

[132] N. Stefanakis and R. Mélin, J. Phys.: Condens. Matter **15**, 3401 (2003); N. Stefanakis and R. Mélin, J. Phys.: Condens. Matter **15**, 4239 (2003).

[133] J. Linder and A. Sudbø, Phys. Rev. B **75**, 134509 (2007); J. Linder and A. Sudbø, *ibid.* **79** 020501 (2009).

[134] M. J. M. de Jong and C. W. J. Beenakker, Phys. Rev. Lett. **74**, 1657 (1995).

[135] Y. Tanaka, Yu. V. Nazarov, and S. Kashiwaya, Phys. Rev. Lett. **90**, 167003 (2003); Y. Tanaka, Yu. V. Nazarov, A. A. Golubov, and S. Kashiwaya, Phys. Rev. B **69**, 144519 (2004).

[136] Y. Tanaka and S. Kashiwaya, Phys. Rev. B **70**, 012507 (2004); Y. Tanaka, S. Kashiwaya, and T. Yokoyama, Phys. Rev. B 71, 094513 (2005).

[137] T. Yokoyama, Y. Tanaka, and J. Inoue, Phys. Rev. B **72**, 220504 (2005).

[138] J. Linder, M. Cuoco, and A. Sudbø, Phys. Rev. B **81**, 174526 (2010).

[139] M. Bode, Rep. Prog. Phys. **66**, 523 (2003).

[140] N. A. Mortensen, K. Flensberg and A. P. Jauho, Phys. Rev. B **59**, 10176 (1999).

[141] G. E. Blonder, M. Tinkham and T. M. Klapwijk, Phys. Rev. B **25**, 4515 (1982).

[142] C. R. Hu, Phys. Rev. Lett. **72**, 1526 (1994); C. R. Hu, Phys. Rev. B **57**, 1266 (1998).

[143] S. Kashiwaya, Y. Tanaka, M. Koyanagi, H. Takashima, and K. Kajimura, Phys. Rev. B **51**, 1350 (1995).

[144] L. Alff, S. Kleefisch, U. Schoop, M. Zittartz, T. Kemen, T. Bauch, A. Marx, and R. Gross, Eur. Phys. J. B **5**, 423 (1998); T. Löfwander, V. S. Shumeiko, and G. Wendin, Supercond. Sci. Technol. **14**, 53 (2001).

[145] M. Fogelström, D. Rainer and J. A. Sauls, Phys. Rev. Lett. **79**, 281 (1997).

[146] J.-X. Zhu and C.S. Ting, Phys. Rev. B **57**, 3038 (1998).

[147] M. Sigrist, K. Kuboki, P.A. Lee, A.J. Millis, and T.M. Rice, Phys. Rev. B **53**, 2835 (1996).

[148] M. A. Silaev, T. Yokoyama, J. Linder, Y. Tanaka, and A. Sudbø, Phys. Rev. B **79**, 054508 (2009).

[149] N. Stefanakis, Phys. Rev. B **64**, 224502 (2001).

[150] M. Chtchelkatchev, W. Belzig, Yu. V. Nazarov, and C. Bruder, JETP Lett. **74**, 323 (2001).

[151] Z. Radovic, N. Lazarides, and N. Flytzanis, Phys. Rev. B **68**,014501 (2003).

[152] J. Cayssol, and G. Montambaux, Phys. Rev. B **70**, 224520 (2004).

[153] I. Petkovic, N. M. Chtchelkatchev, and Z. Radovic, Phys. Rev. B **73**, 184510 (2006).

[154] J. Linder, T. Yokoyama, D. Huertas-Hernando, and A. Sudbø, Phys. Rev. Lett. **100**, 187004 (2008).

[155] A. Millis, D. Rainer, and J. A. Sauls, Phys. Rev. B **38**, 4504 (1988).

[156] M. Fogelström, Phys. Rev. B **62**, 11 812 (2000).

[157] Y. Tanaka and A.A. Golubov, Phys. Rev. Lett. **98**, 037003 (2007).

[158] Yu. S. Barash and I. V. Bobkova, Phys. Rev. B **65**, 144502 (2002).

[159] K. K. Likharev, Rev. Mod. Phys. **51**, 101 (1979).

[160] A. A. Golubov, M.Yu. Kupriyanov, and E. Ilichev, Rev. Mod. Phys. **76**, 411 (2004).

[161] L. Degiorgi, E. Felder, H.R. Ott, J.L. Sarrao, and Z. Fisk, Phys. Rev. Lett. **79**, 5134 (1997); S. Broderick, B. Ruzicka, L. Degiorgi, H.R. Ott, J. L. Sarrao, and Z. Fisk, Phys. Rev. B **65**, 121102 (2002).

[162] Y. Okimoto, T. Katsufuji, T. Ishikawa, A. Urushibara, T. Arima, and Y. Tokura, Phys. Rev. Lett. **75**, 109 (1995); Y. Okimoto, T. Katsufuji, T. Ishikawa, T. Arima, and Y. Tokura, Phys. Rev. B **55**, 4206 (1997).

[163] E.J. Singley, K.S. Burch, R. Kawakami, J. Stephens, D.D. Awschalom, and D.N. Basov, Phys. Rev. B **68**, 165204 (2003); E.J. Singley, R. Kawakami, D.D. Awschalom, and D.N. Basov, Phys. Rev. Lett. **89**, 097203 (2002).

[164] C. W. J. Beenakker, Phys. Rev. Lett. **67**, 3836 (1991).

[165] C. W. J. Beenakker and H. van Houten, Phys. Rev. Lett. **66**, 3056 (1991).

[166] I. O. Kulik, Zh. Eksp. Teor. Fiz. **57**, 1745 (1969) [Sov. Phys. JETP **30**, 944 (1970)].

[167] H. J. Kwon, V. M. Yakovenko, and K. Sengupta, Low Temp. Phys. **30**, 613 (2004).

[168] J. J. A. Baselmans, T. T. Heikkilä, B. J. van Wees and T. M. Klapwijk, Phys. Rev. Lett. **89**, 207002, (2002).

[169] E. Goldobin, D. Koelle, R. Kleiner, and A. Buzdin, Phys. Rev. B **76**, 224523 (2007).

[170] T. Yokoyama *et al.*, Phys. Rev. B **72**, 220504 (2005).

[171] J. Linder and A. Sudbø, Phys. Rev. B **76**, 054511 (2007).

[172] C. Iniotakis *et al.*, Phys. Rev. B **76**, 012501 (2007)

[173] A. Vorontsov *et al.*, Phys. Rev. Lett. **101**, 127003 (2008).

[174] See *e.g.* F. Bergeret *et al.*, Rev. Mod. Phys. **77**, 1321 (2005).

[175] N. Hayashi *et al.*, Phys. Rev. B **73**, 092508 (2006); *ibid* Phys. Rev. B **73**, 024504 (2006).

[176] N. Hayashi *et al.*, Phys. Rev. B **73**, 024504 (2006).

[177] J. Linder *et al.*, Phys. Rev. B **81**, 214504 (2010).

[178] N. Schopohl and K. Maki, Phys. Rev. B **52**, 490 (1995); N. Schopohl, cond-mat/9804064.

[179] A. Konstandin, J. Kopu, and M. Eschrig, Phys. Rev. B **72**, 140501 (2005).

[180] A. Mackenzie and Y. Maeno, Rev. Mod. Phys. **75**, 657 (2003).

[181] Y. Matsuda *et al.*, J. Phys. Cond. Mat. **18**, R705 (2006).

[182] Y. Yanase, J. Phys. Soc. Jpn. **79**, 084701 (2010).

[183] H. Mukuda, S. Nishide, A. Harada, K. Iwasaki, M. Yogi, M. Yashima, Y. Kitaoka, M. Tsujino, T. Takeuchi, R. Settai, Y. Onuki, E. Bauer, K. M. Itoh, and E. E. Haller, J. Phys. Soc. Jpn. **78**, 1 (2009).

[184] M. Yogi, H. Mukuda, Y. Kitaoka, S. Hashimoto, T. Yasuda, R. Settai, T. D. Matsuda, Y. Haga, Y. Onuki, P. Rogl, and E. Bauer, J. Phys. Soc. Jpn. **75**, 013709 (2006).

[185] A. V. Zaitsev, Zh. Eksp. Teor. Fiz. **86**, 1742 (1984).

[186] M. Y. Kuprianov and V. F. Lukichev, Zh. Eksp. Teor. Fiz. **94**, 139 (1988).

List of Symbols and Acronyms

ABS	Andreev bound state
AR	Andreev reflection
BdG	Bogoliubov-de Gennes (equations)
BTK	Blonder, Tinkham, and Klapwijk (formalism)
BTRS	Broken time reversal state
DOS	Density of states
E_{Th}	Thouless energy
E_F	Fermi energy
ELQ	Electron–like quasiparticle
F	Generic ferromagnet
FI	Ferromagnetic insulator
HLQ	Hole–like quasiparticle
I	Generic insulator
M	Degree of spin polarization
N	Generic normal metal
NCS	Noncentrosymmetric superconductor
ξ_F	Magnetic coherence length
ξ_S	Superconducting coherence length
P_σ	Fraction of carriers with spin σ

ρ_σ	$\rho_{\uparrow(\downarrow)} = +1(-1)$
σ	Electrons and holes spin index ("up" or "down")
$\bar{\sigma}$	Opposite of σ
S	Generic singlet superconductor
SBAF	Spin bandwidth asymmetry ferromagnet
STF	Stoner ferromagnet
STM	Scanning tunneling microscopy
TS	Generic triplet superconductor
U	Exchange energy in F
X	U/E_F
Y	$m_\uparrow/m_\downarrow$
Z	Dimensionless insulating barrier strength
ZBCP	Zero bias conductance peak
ZEP	Zero energy peak